



The Iby and Aladar Fleischman Faculty of Engineering
The Zandman – Slaner School of Graduate Studies

On the Coverage and Reconstructability of 2D Functions Sampled by Arbitrary Line Projections with an Application to Rain Field Mapping

A thesis submitted toward the degree of
Master of Science in Electrical and Electronic Engineering

by
Omry Sendik

July 2013



The Iby and Aladar Fleischman Faculty of Engineering
The Zandman – Slaner School of Graduate Studies

On the Coverage and Reconstructability of 2D Functions Sampled by Arbitrary Line Projections with an Application to Rain Field Mapping

A thesis submitted toward the degree of
Master of Science in Electrical and Electronic Engineering

by
Omry Sendik

This research was carried out in the Department of Electrical Engineering –
Systems, under the supervision of Prof. Hagit Messer-Yaron

July 2013

Acknowledgments

First and foremost I would like to express my gratitude to **Prof. Hagit Messer**. I believe Hagit found the singular point which constitutes an optimal balance between supervision and freedom. Functioning both as a shepherd, knowing when to keep me out of dead-end directions and as a support vector which only showed me the general direction and let me go my own way while making the mistakes I most definitely needed to make.

I would like to thank my buddies from the TAU research group for a handful of fruitful discussions and mind boggling suggestions. I endlessly thank **Yoav Liberman, Dani Cherkassky, Noam David, Oz Harel, Elad Heiman, Ori Ausländer and Yonatan Ostromesky**. Thanks for patiently putting up with my infinite lectures on my research trials and tribulations.

A special thank you goes to **Artem Zinevich** which drew me into my research question, an interdisciplinary field which finely merges between environmental phenomena and applied mathematics.

Finally, I would like to thank my second half, **Tsefi**, for her relentless ability to push me towards pursuing my dreams and her patience to put up with the endless hours which I sat in front of my computer with a trashcan filled with crumpled drafts.

Tsefi, thanks for tolerating what I put you through, for keeping my goals no matter what they were and mostly for simply being yourself.

Abstract

Signals received by microwave systems are inherently path averages since they are the result of an integrated sample of the signal along the microwave's path. A novel method, suggested by Messer *et al* at 2006 followed by Leijnse *et al* at 2007, involving existing commercial wireless networks (CWN) suggested the usage of the backhaul communication links for the sake of environmental monitoring. Put simply, Messer *et al* suggested using existing cellular networks' equipment for the sake of meteorological monitoring of rainfall.

In the CWN system as suggested by Messer *et al* the links' geometry is for any means arbitrary. Location of communication links, as performed by network technicians, is an intricate task. Execution of this task usually balances between the attempt to minimize the number of calls which will be lost due to a lack of reception while maximizing the distance between links in an attempt to minimize the number of links (and by such minimize network establishment costs). Such an optimization target unsurprisingly generates a completely undefined geometry of a spatial distribution of links.

In this thesis I treat two central problems which arise from the arbitrary topology which describes the links' distribution. The first is the question of coverage. I answer the question regarding under what circumstances is a rain cloud detectable. By applying our approach to the coverage problem we are able to generate coverage maps which depict the exact coverage of rain events in Israel, when employing the newly suggested rain fall monitoring system.

The second answer which I attempt to answer is the question of reconstructability. If one is to reconstruct the rain map from the samples of added attenuation, it is first to examine whether the geometry of links enables so. I address the issue of sampling a general two dimensional function, an image perhaps, by collecting the values of its projections along lines. By projections I mean the sum or integration of its values along a line. I do not impose any geometrical/topographical constraints on the nature of the lines. The lines may differ one from another by its angle, length and the distances between them may be uneven.

Our contribution is a procedure for determining whether a given links realization yields a reconstructable function and if so, what is the maximal non-aliased spatial frequency which is properly sampled.

I apply our solutions to the coverage and reconstructability on actual links of the Israeli Cellular Service Provider Cellcom.

Table Of Contents

| | | |
|----------|--|-----------|
| 1 | Introduction | 10 |
| 1.1 | Problem Motivation & Background..... | 10 |
| 1.2 | Problem Statement..... | 12 |
| 1.3 | The Nature of the Links' Topology..... | 13 |
| 1.4 | Sampling Literature Survey | 14 |
| 1.5 | Mathematical Preliminaries..... | 18 |
| 1.5.1 | The Dirac Comb and the Poisson Summation | 18 |
| 1.5.2 | The Whittaker-Shannon-Kotelnikov Theorem | 18 |
| 1.5.3 | The Papoulis Generalized Sampling Expansion | 19 |
| 1.5.3.1 | Proof for 1D functions | 20 |
| 1.5.3.2 | The 1D Papoulis Generalized Sampling Expansion – An Example | 23 |
| 1.5.3.3 | Proof for 2D signals..... | 24 |
| 2 | Coverage..... | 28 |
| 2.1 | Coverage of detecting Rain..... | 28 |
| 3 | Reconstruction | 33 |
| 3.1 | Reconstruction of a Sampled Function..... | 33 |
| 3.1.1 | Solution Overview | 33 |
| 3.1.2 | Sampling with a single line type..... | 34 |
| 3.1.3 | Usage of the Papoulis Generalized Sampling Expansion for our solution..... | 35 |
| 3.1.4 | Usage of the Papoulis Generalized Sampling Expansion for our solution – An Example | 37 |
| 3.1.5 | Coping with an irregular grid..... | 39 |
| 3.1.6 | Coping with an irregular grid – An Example | 42 |
| 3.1.7 | Missing Samples | 44 |
| 3.1.7.1 | Missing Samples in the classical sampling scheme | 44 |
| 3.1.7.2 | Missing Samples in the Arbitrary Line Projections sampling scheme..... | 45 |
| 3.1.8 | Missing Samples - An Example | 48 |
| 3.1.9 | Integrating the 3 Phases | 54 |
| 3.1.10 | Computational Complexity of the Solution | 54 |
| 3.1.10.1 | Definitions and Notations | 54 |
| 3.1.10.2 | Complexity of Coping with an irregular grid..... | 55 |
| 3.1.10.3 | Complexity of the Generalized Sampling Expansion Usage | 55 |
| 3.1.10.4 | Complexity of coping with Missing Samples | 56 |
| 3.2 | Non Reconstructable Geometries..... | 57 |
| 3.2.1 | Two Equally lengthed Sampling Functionals with Different Angles | 57 |
| 3.2.2 | Two Different lengthed Sampling Functionals with 90 deg appart | 59 |
| 4 | Application..... | 61 |
| 4.1 | Coverage..... | 61 |
| 4.1.1 | Sensitivity to Network Parameters | 67 |
| 4.2 | Reconstructability | 71 |
| 4.2.1 | Example 1..... | 71 |
| 4.2.2 | Example 2..... | 73 |
| 4.2.3 | Example 3..... | 75 |
| 4.2.4 | Example 4..... | 78 |

| | |
|---|-----------|
| 5 Discussion | 81 |
| 5.1 A Discussion on our Simplifications and Future Directions | 81 |
| 5.2 Adding Rain Gauges | 84 |
| 5.2.1 Sampling with both Rain Gauges and Lines | 85 |
| 5.3 Coverage of other than Rain | 87 |
| 6 Appendix..... | 89 |
| 6.1 Correlation Function of the Sampling Process..... | 89 |
| 6.1.1 Modeling the Sampling Process | 89 |
| 6.1.2 Choice of the Random Variables Probability Distribution Functions | 90 |
| 6.1.3 The Sampling Process's Autocorrelation Function and Spectrum | 91 |
| 7 References..... | 95 |
| 8 תקציר | 98 |
| 9 תודות | 99 |

Figure List

| | |
|--|----|
| FIGURE 1 – WIRELESS CELLULAR LINKS IN ISRAEL VS. THE GIULI MONITORING SYSTEM [15]..... | 12 |
| FIGURE 2 – THE LINK DISTRIBUTION IN ISRAEL; ANGLES, LENGTHS AND LOCATIONS..... | 14 |
| FIGURE 3 – THE PAPOULIS GENERALIZED SAMPLING EXPANSION | 20 |
| FIGURE 4 – SAMPLING WITH UP TO FIRST ORDER DERIVATIVES | 23 |
| FIGURE 5 – ATMOSPHERE AND WEATHER EFFECTS ON PERFORMANCE OF MM-WAVE COMMUNICATION LINK [14]..... | 29 |
| FIGURE 6 – THE BACKHAUL LINK LENGTHS AS A FUNCTION OF TRANSMISSION FREQUENCIES..... | 29 |
| FIGURE 7 – CLOUD INTERSECTING WITH VARIOUS LINKS | 30 |
| FIGURE 8 – THE "CLASSICAL" SAMPLING VS. THE ARBITRARY LINE PROJECTIONS SAMPLING | 34 |
| FIGURE 9 – SAMPLING SCHEME WITH PROJECTIONS ON ARBITRARY LINES WITH A REGULAR GRID..... | 36 |
| FIGURE 10 – GSE USAGE FOR TWO LINES WITH EQUAL LENGTHS AND ANGLES $\pi/4$ AND $3\pi/4$ | 38 |
| FIGURE 11 – GSE USAGE FOR TWO LINES WITH EQUAL LENGTHS – DETERMINANT EVALUATION | 39 |
| FIGURE 12 – THE REGULARIZATION OF THE SAMPLING GRID | 40 |
| FIGURE 13 – MISSING SAMPLES EXAMPLE | 49 |
| FIGURE 14 – COVERAGE MAP I | 62 |
| FIGURE 15 – COVERAGE THRESHOLD MAP I | 63 |
| FIGURE 16 – COVERAGE MAP II | 64 |
| FIGURE 17 – COVERAGE THRESHOLD MAP II | 64 |
| FIGURE 18 – COVERAGE MAP III..... | 65 |
| FIGURE 19 – COVERAGE THRESHOLD MAP III..... | 66 |
| FIGURE 20 – IMPROVING THE COVERAGE – LINKS OPERATIONAL FREQUENCY..... | 68 |
| FIGURE 21 – IMPROVING THE COVERAGE – LINKS OPERATIONAL QUANTIZATION..... | 68 |
| FIGURE 22 – IMPROVING THE COVERAGE – LINKS QUANTIZATION TRESHOLDED | 69 |
| FIGURE 23 – IMPROVING THE COVERAGE – LINKS QUANTIZATION TRESHOLDED | 70 |
| FIGURE 24 – THE MICROWAVE LINKS IN RAMOT-MENASHE..... | 71 |
| FIGURE 25 – THE GSE DETERMINANT - EXAMPLE I | 72 |
| FIGURE 26 – THE ARBITRARY LINES – EXAMPLE II..... | 73 |
| FIGURE 27 – THE ARBITRARY LINES – EXAMPLE II – THE GSE DETERMINANT | 74 |
| FIGURE 28 – THE GIULI LINKS [15] | 75 |
| FIGURE 29 – THE GIULI RAIN EVENTS [15] | 76 |
| FIGURE 30 – THE GIULI LINES REGULARIZED– EXAMPLE III | 77 |
| FIGURE 31 – THE GIULI LINES – EXAMPLE III – THE GSE DETERMINANT | 78 |
| FIGURE 32 – ISRAEL LINKS – EXAMPLE III..... | 80 |
| FIGURE 33 – RAIN GAUGE SAMPLING SCHEME | 85 |
| FIGURE 34 – THE DEFINITION OF THE INTEGRATION AREA $\Gamma_{n,m}$ | 92 |

Table List

| | |
|--|----|
| TABLE 1 – NOTATIONS AND NOMENCLATURE..... | 9 |
| TABLE 2 – POWER LAW COEFFICIENTS | 32 |
| TABLE 3 – DISTINCT FUNCTIONAL IDENTIFICATION PROCESS | 41 |
| TABLE 4 – EVALUATION OF THE REGULARIZATION ALGORITHM | 44 |
| TABLE 5 – MISSING SAMPLES AN EXAMPLE | 50 |
| TABLE 6 – COMPUTATIONAL COMPLEXITY TERMS | 55 |

Notations and Nomenclature

| Mark | Explanation | Misc |
|------------------------|--|---|
| $f(t)$ | Continuous time signal | |
| $f[n]$ | Discrete time signal | |
| $f_I(t)$ | Continuous time signal after a integration | |
| $F(\omega)$ | Continuous Frequency Fourier Transform of $f(t)$ | |
| $F(k)$ | Continuous Frequency Fourier Transform of $f[n]$ | |
| $\mathcal{F}\{\cdot\}$ | Continuous time Fourier Transform | $\mathcal{F}\{f(t)\} = \frac{1}{2\pi} \int_{-\infty}^{\infty} f(t) e^{-jut} dt \Rightarrow \mathcal{F}^{-1}\{F(u)\} = \int_{-\infty}^{\infty} F(u) e^{jut} du$ |
| T_s | Sample Time | |
| u_s | Sample Frequency | $u_s = 1/T_s$ |
| Rect(t) | Rectangular function | $\text{Rect}(t) = \begin{cases} 1, & t \in [-0.5, 0.5] \\ 0, & \text{else} \end{cases}$ |
| Sinc(u) | Sinc function | $\begin{aligned} \mathcal{F}\{\text{Rect}(t)\} &= \frac{1}{2\pi} \int_{-\infty}^{\infty} \text{Rect}(t) e^{-jut} dt = \frac{1}{2\pi} \int_{-1/2}^{1/2} e^{-jut} dt = \\ &= \frac{1}{2\pi} \frac{1}{-ju} \left(e^{-\frac{ju}{2}} - e^{\frac{ju}{2}} \right) = \frac{1}{2\pi} \frac{\sin(u/2)}{u/2} = \frac{1}{2\pi} \text{sinc}(u/2) \end{aligned}$ |
| $f_{W,\theta}(x, y)$ | 2D line function | $f_{W,\theta}(x, y) = \begin{cases} 1, & -\frac{W}{2} \cos \theta \leq x \leq \frac{W}{2} \cos \theta \\ & y = x \tan \theta \\ 0, & \text{else} \end{cases}$ |
| CWN | Commercial Wireless Networks | |
| LTI | Linear Time Invariant | |
| LSI | Linear Space Invariant | |
| CT | Continuous Time | |
| DT | Discrete Time | |
| FT | Fourier Transform | |

Table 1 – Notations and Nomenclature

1 Introduction

1.1 Problem Motivation & Background

Recently a new paradigm has pervaded the discipline of environmental monitoring. Using microwave attenuation measurements for the reconstruction of rainfall fields, which was initially suggested by Giuli *et al*[15][16] The latter suggested a proprietary design of microwave links with a specifically chosen geometry which was designed to ensure proper reconstruction of rain fields.

Though Giuli's proposition dates back about 20 years it seemed not to gain rise. This is most probably due to the price of deploying such a microwave based system. A project named MANTISSA[17], or Microwave Attenuation as a New Tool for Improving Stormwater Supervision Administration, set out to test the feasibility of using microwave signals to estimate rainfall estimates.

These signals are inherently path averages since they are the result of an integrated sample of the signal along the microwave's path. MANTISSA aspired to use these averaged rainfall estimates as a complement to radar data and by such improve the available input data to hydrological models for forecasting urban and rural drainage systems' response.

A novel method, suggested by Messer *et al* [21] at 2006 followed by Leijnse *et al* [18] at 2007, involving *existing* commercial wireless networks (CWN) suggested the usage of the backhaul communication links for the sake of environmental monitoring. Put simply, Messer *et al* suggested using *existing* cellular networks' equipment for the sake of meteorological monitoring of rainfall. This suggestion alleviated the problem of the costs of the microwave based systems by using the *existing* links, which changed their high deployment price to zero. This constituted the first major step towards the new approach for Environmental Monitoring.

Evidently, the received signal strength at which each antenna receives its pair's transmitted signal may be stored. Moreover, it is indeed often stored and kept for offline inspection. Messer *et al* have proposed the usage of these cellular networks' built-in monitoring facilities. Being a "widely distributed observation network, operating in real-time with minimum supervision and without additional cost" [21] motivated the attempt to use this data from the CWN with the theoretical justification for such attempts being a power law which related the signal *attenuation* to the rain rate [23]. The power law relating the attenuation to the rain rate was shown to be an

approximation which holds in convective rains and in communication systems operating in mid range frequencies (above 1GHz and below the optical range). The exact relation between the attenuation and rain rate is given by a series relation in the frequency and the rain rate –

$$A = a' R^b \left[1 + \sum_{n=2}^{\infty} c_n f^n R^{n\beta/q} \right] \quad (1.1)$$

where c_n, β and q are constants which are frequency, temperature and DSD (drop size distribution) dependant. A is the logarithmic attenuation per km $A[\text{dB / km}]$ and $R[\text{mm / hr}]$ is the rain rate. Later, Olsen *et al* [23] also showed that using the approximation of –

$$A = aR^b \quad (1.2)$$

is a good one and evaluated its usage with experimental results. The $A - R$ relation is often considered as a completely linear one, approximating the power coefficient b to 1, when operating at around 1cm wavelengths. And indeed, in the dedicated microwave links which were suggested by Giuli *et al* [15][16] the frequencies were chosen to ensure a linear $A - R$ relation.

If we were to properly measure the rain induced attenuation we would apply a relation which integrates the rain along the path which connects between two links, rather than assuming that the rain is constant along such a line. This implicitly suggests that the rain along such a path isn't necessarily constant. This is shown in the relation below –

$$A = a \int R(x)^b dx \quad (1.3)$$

In the system devised by Giuli *et al* [15] the geometry of links was designed to attempt to yield a proper reconstruction of rain maps inside an area of 400km^2 . In the CWN system as suggested by Messer *et al* the links geometry was for any means arbitrary. Location of communication links, as performed by network technicians, is an intricate task. Execution of this task usually balances between the attempt to minimize the number of calls which will be lost due to a lack of reception while maximizing the distance between links in attempt to minimize the number of links (and by such minimize network establishment costs). Such an optimization target

unsurprisingly generates a completely undefined geometry of a spatial distribution of links. Figure 1 depicts the Giuli link system geometry compared with the link distribution in Israel.

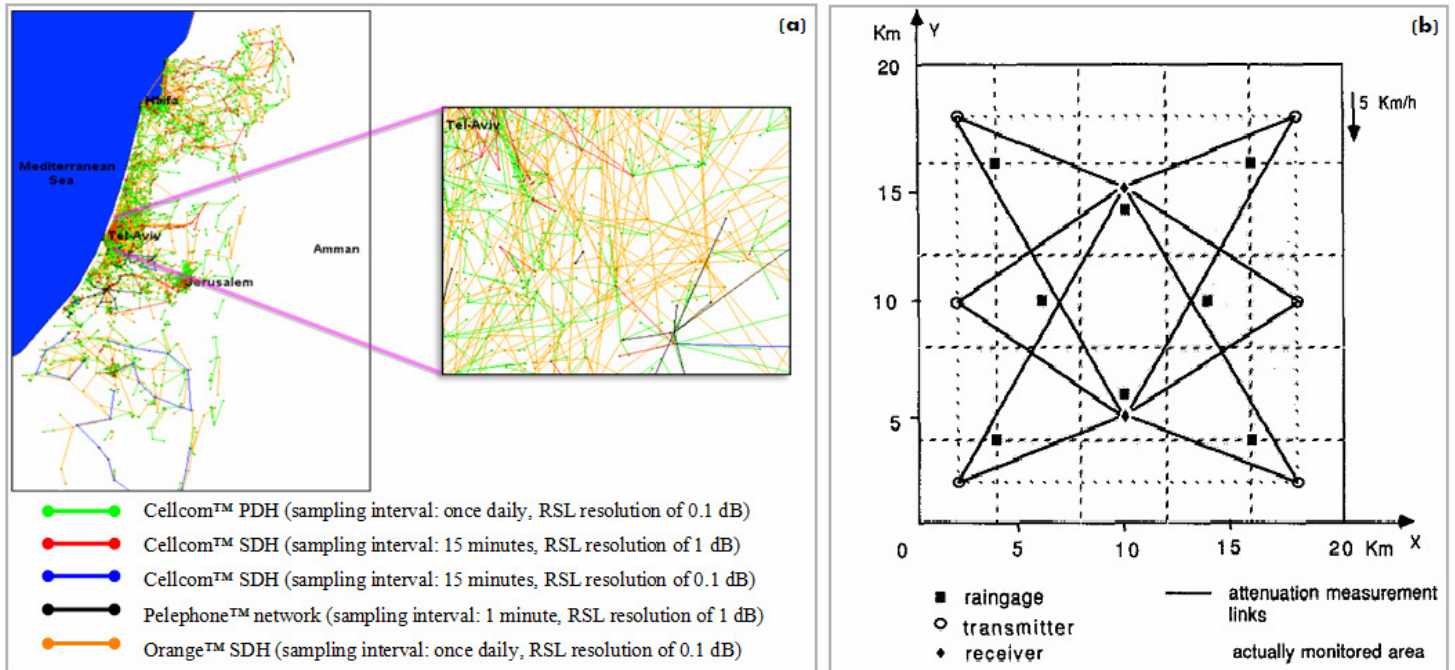


Figure 1 – Wireless Cellular Links in Israel vs. the Giuli monitoring system [15]

1.2 Problem Statement

The measurements of the attenuation of the microwave signal are the result of the path-integrated rainfall [3][4] along the wireless links. Each pair of antennas communicates one with the other and experiences an added attenuation in case of rain fall. If one is to reconstruct the rain map from the samples of added attenuation, it is first to examine whether the geometry of antennas enables so.

I address the issue of sampling a two dimensional function, an image perhaps, by collecting the values of its projections along lines. By projections I mean the sum or integration of its values along the lines or links. I do not impose any geometrical constraints on the nature of the lines. The lines may differ one from another by its angle, length and the distances between them may be uneven. Our intent is to answer the question regarding the *ability* to reconstruct a function from such a sampling scheme.

We broaden the theoretical discussion by applying the suggested method on a practical example, the problem of reconstructing rain-fall maps by commercial wireless communication networks [18][21][22][31].

I also discuss a method for generating coverage. These are maps which present the minimal detectable rain rate given a predetermined set of links operating at a known frequency.

1.3 The Nature of the Links' Topology

The motivation to the problem of sampling a two dimensional function by integrations along lines with arbitrary geometry is mainly due to the newly suggested method for environmental monitoring [21][18].

In this section I present an insight into what typical sampling sets appear like. For this purpose, I analysed roughly 8400 links of three Israeli cellular service providers, namely Cellcom, Telephone and Orange.

I plot the histograms of the links' lengths, angles and distance one from the other for Israel, having divided it into four quarters, from North to South. I also analyse the histogram of the entire set of links.

The centre of Figure 2 depicts the Israeli map of links. On the left hand side of the map, the histograms of the link distances one from the other are depicted for each quarter of Israel (e.g. the upper left most histogram is the histogram of distances of the upper quarter of Israel). On the right hand side of the map, the histograms of the link angles and lengths are depicted for each quarter of Israel.

The histograms emphasize the fact that urban, sub-urban and rural areas have different sampling sets, not only in terms of the link densities but also in terms of the nature of lines (their typical lengths and angles). One may notice that the maximal lengths, which may be found by considering the maximal value in the histogram of link lengths on the entirety of the data, appears only in the most rural part of Israel. These parts are the southern parts of Israel. The histogram of angles shows that more urban areas display a more uniform distribution of angles compared to areas which link's density isn't as high.

The definition of the distance between links is tough to state because the grid of links which I have in hand is far from regular. Hence, the distance between links was chosen to be the shortest distance between two links. The distance presented is in units of longitude and latitude. The histograms below show that if we consider a small area and discard the values in the histogram

with low probability, we may consider this as a relatively uniform distribution. However, if one requires considering the low probability tail of the distribution, a fast decaying probability density function must be used.

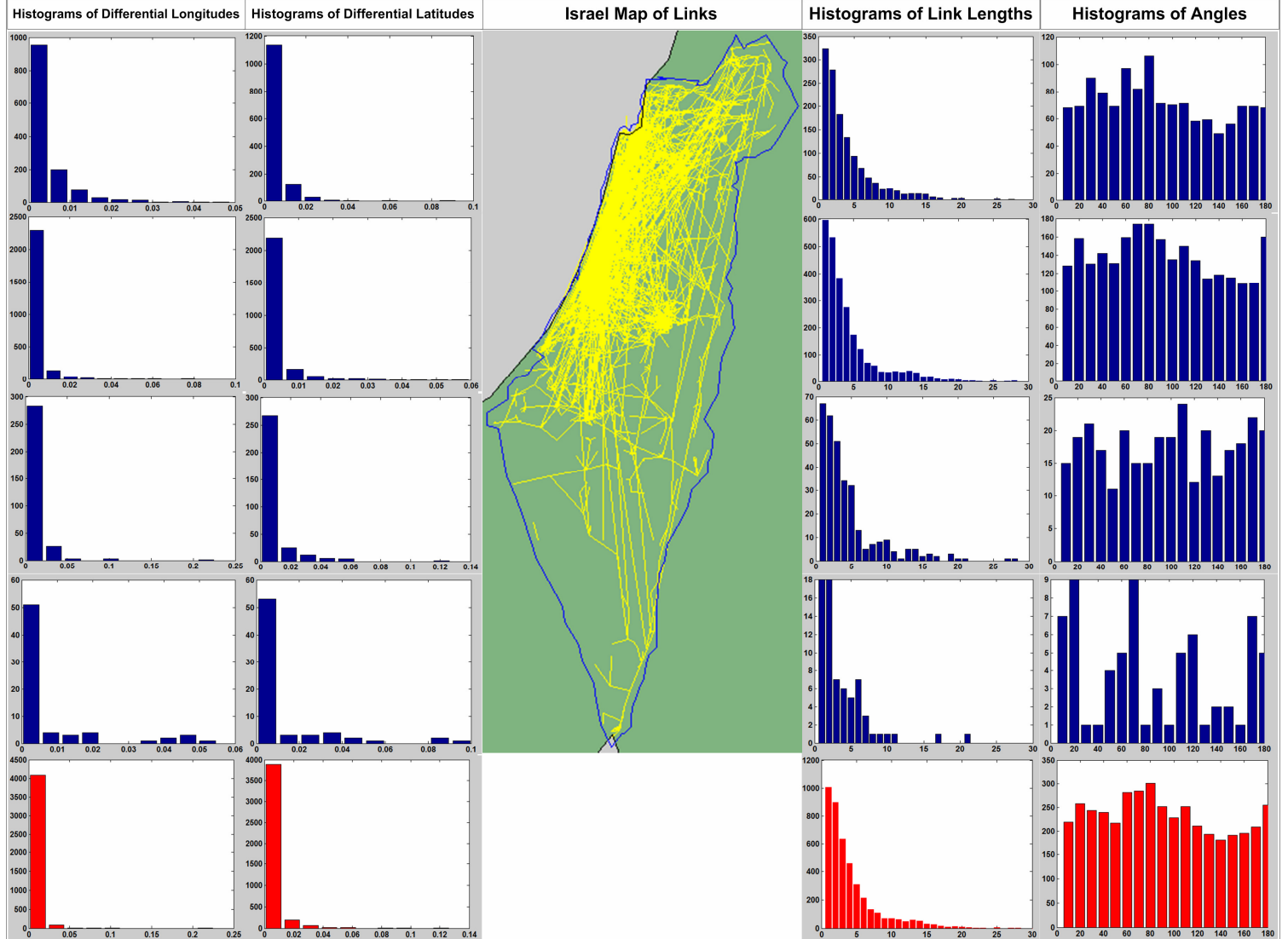


Figure 2 – The Link Distribution in Israel; Angles, Lengths and Locations

1.4 Sampling Literature Survey

The reconstruction of a sampled signal, as proved by Whittaker, Kotelnikov and Nyquist and which was discussed by Claude E. Shannon [27] has been well studied and is classically considered to be one of the most cardinal results on the subject of sampling. The Nyquist theorem states the terms under which a *perfect* reconstruction of a band limited function can be

reconstructed from its *point samples*. Moreover, the Nyquist theorem states exactly how to reconstruct the sampled function by presenting the exact interpolation kernel, which is no other than the sinc kernel.

Many variances of the sampling problem have been introduced since. Many of such variances have been motivated by real-life applications. E.g., the problem of sampling in the presence of Jitter is a common case. Any realistic sampling device cannot be of infinite sample rate precision. Hence, the sample instance is usually presented as a delta function with probability density function of deviating from its nominal location [5]. Jitter is known to be equivalent to a phase noise in the frequency domain which is the reason it creates a spread of the spectrum around the nominal one, which is the reasoning for suggesting a linear band pass filtering for the spread mitigation.

An interesting perspective on the problem of Jitter is to consider it as a problem of irregular sampling. In other words, different than the sampling manner which was discussed in the paper by Shannon[27], we may consider the problem of sampling with an other-than constant grid. Margolis and Eldar discussed the problem of Nonuniform Sampling of Periodic Bandlimited Signals[20]. They treated the problem of reconstructing a periodic band limited signal from a finite number of its non uniform samples. By extending the samples periodically, and assuming that the underlying continuous time signal is band limited, they showed a simple way to deal with a reconstruction from a finite amount of samples on an irregular grid. They also presented two algorithms for reconstructing such a periodic band limited signal (for an even or odd amount of samples). Feuer and Goodwin [13] addressed the problem of the reconstruction of a multidimensional signal reconstruction sampled on an irregular grid. However, typical solutions usually suggest a linear filtering approach for this problem (as stated above). Feuer and Goodwin presented an interpolation identity which establishes the equivalence of two multidimensional processing operations, one which uses continuous domain filters, whereas the other uses discrete processing. An excellent survey discussing non uniform Sampling and Reconstruction in Shift-Invariant Spaces is given by Aldroubi and Grochenig [1] in which they discuss modern techniques and provide a unified framework for uniform and non uniform sampling and reconstruction in shift-invariant spaces by bringing together wavelet theory , frame theory and sampling.

Another well studied problem is the problem of sampling via a generalized function. In other words, one may want to sample with other than the Dirac comb point process. A pragmatic

motivator for this need is the fact that any real life device suffers from inertia and simply cannot properly evaluate the point value of a function. Hence, many papers discuss the problem of sampling via a local average, which is the manifestation of inertia. E.g., Sun [28] discusses the Non-Uniform Average Sampling and Reconstruction of band limited functions which he terms "signals with finite rate of innovation". Sun and Zhou [29] discussed the Reconstruction of Band-Limited Signals from Local Averages and showed that the reconstruction of such band-limited signals from local averages with symmetric averaging functions have an explicit error bound. Considering the "point sampling" as a limit case of the average sampling they showed aliasing error bounds for such average sampling. The problem of sampling with a general functional may be expanded to many directions. However, the generalization of the problem to any linear functional was beautifully treated by Papoulis [24]. Papoulis showed that a simple evaluation of a determinant can be applied for the sake of determining whether the sampling functionals are proper for the sake of sampling a band limited function. The Papoulis Generalized Sampling Expansion (GSE) is used as a central tool in our work.

Yet another interesting aspect of the sampling problem is the ability to cope with missing samples. The simplest case of treatment of missing samples was treated by many. An example of such is given by Ferreira [12]. An extension to the problem of coping with missing samples in the case of point values and point derivatives via the Papoulis Generalized Sampling Expansion was proposed by Dorabella and Ferreira [10]. The conceptual approach to this problem is the inspiration to our use of the missing samples problem for the case of the arbitrary line sampling case.

An excellent survey discussing a multitude of sampling problems since the innovative paper which was published by Shannon was written by Unser and is given in [30].

The papers above show the vast interest in sampling problems. However, to the best of our knowledge, the problem of sampling via local averages along a one-dimensional line in the case of a two-dimensional function (an image) where the lines are spread arbitrarily (and non uniformly) hasn't been treated.

An innovative paper by Candes and Tao [6] discusses Near Optimal Signal Recovery From Random Projections. At first this paper seemed like the exact application to our problem of sampling via a local projection. Their paper showed that if the objects of interest are sparse in a fixed basis, or compressible, then it is possible to reconstruct the sampled function to within a very high accuracy from a small number of random measurements by solving a simple linear

program. However, the central assumption in their problem is the presence of sparsity in a given basis. We wouldn't want to assume so, due to the highly irregular spectral nature of rain. In case a sparse basis would be a probable assumption, then any signal made with a sparse frequency representation may be recovered by convex programming from almost every set of frequencies and the reconstruction is nearly optimal in the sense that the method will succeed with probability which approaches unity.

Another paper which seemed highly related is a work by Leneman [19] which discusses the correlation function and power spectrum of randomly shaped pulse trains. However, when attempting to generalize this treatment to the case of the two dimensional function with varying angles and lengths the complexity becomes clear. In our work I extend this result and show the correlation function of randomly placed and rotated lines/rectangles placed on a two dimensional space.

Due to the fact that many medical applications sample via projections along lines, many treatments of such sampling scenarios may be found in the scientific literature. Beginning with the prominent work by Radon [25] which showed the ability to properly reconstruct a sampled two-dimensional function from Fourier Slices. In medical applications such as a CT imager, an image is captured by the local cross sections of an object. The Radon transform represents the scattering data captured by the tomographic device and the Inverse Radon transform may be used for the purpose of reconstructing the volume density function. The crucial difference between this tomographic application and ours is the fact that the cross sections are well organized in space and by such ease the modelling and enable the relation to the Fourier Slices. As stated previously, our sampling case employs projections (or Slices) along lines with arbitrary lengths, angles or locations. A heuristic approach to the reconstruction of such a sampled image was discussed by Marchi *et al* [9] where a kernel based Image reconstruction from scattered radon data was presented. However, no thorough discussion regarding the precision at which the reconstruction is achieved is discussed.

In this work I present a procedure which input is a set of lines of arbitrary lengths, angles and locations and output is a binary answer regarding the ability to reconstruct a band limited function from such a set of lines. This solution is formalized as a deterministic one as the line coordinates are treated explicitly and no underlying probability density function describing the lines characteristics are required.

In an extension to this result I also show a derivation of the correlation function of a process which describes sampling with randomly placed and rotated lines/rectangles placed on a two dimensional space.

I apply the set of tools which I developed hereby on the problem of reconstructing rain maps from a set of links which represent projections along arbitrary lines.

1.5 Mathematical Preliminaries

In the following section I mention some equations and theorems which I will often use along this dissertation

1.5.1 The Dirac Comb and the Poisson Summation

The Dirac Comb and its Fourier transform is given by –

$$\mathcal{F} \left\{ \sum_{n=-\infty}^{\infty} \delta(t-nT) \right\} = \frac{1}{T} \sum_{n=-\infty}^{\infty} \delta \left(u - \frac{2\pi n}{T} \right) \quad (1.4)$$

The Poisson Summation is given by –

$$\sum_{n=-\infty}^{\infty} \delta(t-nT) = \frac{1}{T} \sum_{n=-\infty}^{\infty} e^{2\pi jnt/T} \quad (1.5)$$

Another form of the Poisson Summation is given by –

$$\sum_{n=-\infty}^{\infty} f(n) = \frac{1}{2\pi} \sum_{n=-\infty}^{\infty} F(2\pi n) \quad (1.6)$$

1.5.2 The Whittaker-Shannon-Kotelnikov Theorem

The sampling theorem, more commonly referred to as the Nyquist sampling theorem is a fundamental result in the field of information and sampling theory.

The Whittaker-Shannon theorem states that if a continuous time function $f(t)$ contains no frequencies higher than ω_m it may be completely determined by its samples spaced no less than $1/2u_m$ apart.

We make a use of the Poisson summation formula and prove the Nyquist sampling theorem –

$$f_s(t) = f(t) \sum_{n=-\infty}^{n=\infty} \delta(t - nT) \quad (1.7)$$

We apply a Fourier Transform to both sides of the equation –

$$\mathcal{F}\{f_s(t)\} = \mathcal{F}\left\{f(t) \sum_{n=-\infty}^{n=\infty} \delta(t - nT)\right\} = \frac{1}{T} \left[F(u) * \sum_{n=-\infty}^{n=\infty} \delta(u - nu_s) \right] = \frac{1}{T} \sum_{n=-\infty}^{n=\infty} F(u - nu_s) \quad (1.8)$$

We assume the signal is band limited with a maximal frequency of u_m . Hence, we must sample at a sample rate $2u_m \leq u_s$.

1.5.3 The Papoulis Generalized Sampling Expansion

Let us consider $f(t)$ as a σ band limited function if –

$$f \in L^2 \text{ and } F(u) = 0 \quad |u| \geq \sigma \quad (1.9)$$

The Whittaker-Shannon sampling theorem states that –

$$f(t) = \sum_{n=-\infty}^{\infty} f(nT) \operatorname{sinc}\left(\frac{\pi}{T}(t - nT)\right) \quad (1.10)$$

The Papoulis Generalized Sampling Expansion states when $f(t)$ can be expressed in terms of the samples $g_k(nT)$ of m linear functionals $g_k(t)$ of $f(t)$ each of which samples at a slower rate –

$$T_g = mT = 2\pi m / \sigma \quad c = 2\sigma / m \quad (1.11)$$

We stress that linear functionals are in essence LTI systems $H_k(u)$ $k \in [1, \dots, m]$.

These systems are all fed by the σ band limited function $f(t)$

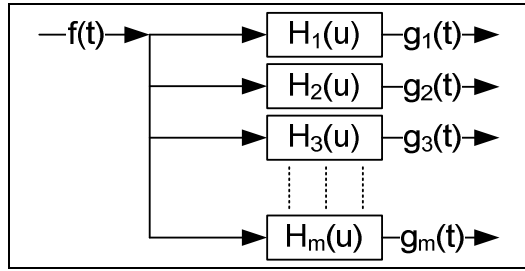


Figure 3 – The Papoulis Generalized Sampling Expansion

1.5.3.1 Proof for 1D functions

We now attempt to show that $f(t)$ can be expressed in terms of the samples $g_k(nT)$ of m linear functionals $g_k(t)$ of $f(t)$ each of which samples at a slower rate. We do so by following the result given by [24]

$$T_g = mT = 2\pi m / \sigma \quad c = 2\sigma / m \quad (1.12)$$

We stress that linear functionals are in essence LTI systems, hence the motivation to show so. Let us assume we are given m linear systems with transfer functions –

$$H_k(u) \quad k \in [1, \dots, m] \quad (1.13)$$

These systems are all fed by the σ band limited function $f(t)$

Each $g_k(t)$ is given by –

$$g_k(t) = \int_{-\sigma}^{\sigma} F(u) H_k(u) e^{jut} du \quad (1.14)$$

We shall attempt to express $f(t)$ in terms of the samples $g_k(nT_g)$ of these functions. i.e. – we wish to find $y_k(t)$ such that –

$$f(t) = \sum_{n=-\infty}^{\infty} [g_1(nT_g) y_1(t-nT_g) + \dots + g_m(nT_g) y_m(t-nT_g)] = \sum_{n=-\infty}^{\infty} \sum_{k=1}^m g_k(nT_g) y_k(t-nT_g) \quad (1.15)$$

We begin by forming the following set of equations –

$$\begin{aligned}
 H_1(u)Y_1(u,t) + \dots + H_m(u)Y_m(u,t) &= 1 \\
 H_1(u+c)Y_1(u,t) + \dots + H_m(u+c)Y_m(u,t) &= e^{jct} \\
 H_1(u+2c)Y_1(u,t) + \dots + H_m(u+2c)Y_m(u,t) &= e^{j2ct} \\
 &\vdots \\
 H_m(u+(m-1)c)Y_1(u,t) + \dots + H_m(u+(m-1)c)Y_m(u,t) &= e^{j(m-1)ct}
 \end{aligned} \tag{1.16}$$

where –

$$y_k(t) = \frac{1}{c} \int_{-\sigma}^{-\sigma+c} Y_k(u,t) e^{jut} du \tag{1.17}$$

The coefficients of the linear system of equations (1.16) $H_k(u+lc)$ are independent of t , and the right side consists of periodic functions of t with a period of T_g (note that $lc(t+T_g) = lct + 2\pi l$). Hence, the solutions $Y_k(u,t)$ must be periodic –

$$Y_k(u,t) = Y_k(u, t + T_g) \tag{1.18}$$

Using (1.17) and (1.18) we may write –

$$y_k(t-nT_g) = \frac{1}{c} \int_{-\sigma}^{-\sigma+c} Y_k(u, t-nT_g) e^{ju(t-nT_g)} du = \frac{1}{c} \int_{-\sigma}^{-\sigma+c} Y_k(u, t) e^{jut} e^{-jnT_g u} du \tag{1.19}$$

We notice that (1.19) implies that $y_k(t-nT_g)$ is the n^{th} Fourier series coefficient of the function $Y_k(u,t)e^{jut}$ in the interval $(-\sigma, -\sigma+c)$. Hence –

$$Y_k(u,t)e^{jut} = \sum_{n=-\infty}^{\infty} y_k(t-nT_g) e^{jnT_g u} \quad u \in (-\sigma, -\sigma+c) \tag{1.20}$$

By multiplying the first equation in (1.16) by e^{jut} we have –

$$H_1(u)e^{jut}Y_1(u,t) + \dots + H_m(u)e^{jut}Y_m(u,t) = e^{jut} \tag{1.21}$$

Plugging (1.20) into (1.21) we yield -

$$H_1(u) \sum_{n=-\infty}^{\infty} y_1(t - nT_g) e^{jnT_g u} + \dots + H_m(u) \sum_{n=-\infty}^{\infty} y_m(t - nT_g) e^{jnT_g u} = e^{jut} \quad (1.22)$$

which is true for every $u \in (-\sigma, \sigma + c)$.

We now multiply the second equation in (1.16) by e^{jut} and similarly yield -

$$H_1(u+c) \sum_{n=-\infty}^{\infty} y_1(t - nT_g) e^{jnT_g(u+c)} + \dots + H_m(u+c) \sum_{n=-\infty}^{\infty} y_m(t - nT_g) e^{jnT_g(u+c)} = e^{j(u+c)t} \quad (1.23)$$

Which is also true for every $(u+c) \in (-\sigma, -\sigma + c)$. However, due to the fact that

$e^{jnT_g(u+c)} = e^{jnT_g u}$ we may write (1.23) as -

$$H_1(u) \sum_{n=-\infty}^{\infty} y_1(t - nT_g) e^{jnT_g u} + \dots + H_m(u) \sum_{n=-\infty}^{\infty} y_m(t - nT_g) e^{jnT_g u} = e^{jut} \quad (1.24)$$

which is also true for every $\omega \in (-\sigma + c, \sigma + 2c)$.

In the same manner we may prove that (1.22) holds for every $\omega \in (-\sigma, \sigma)$.

Finally, we multiply (1.22) by $F(u)$ and integrate according to u . In other words we calculate the inverse Fourier transform -

$$\int_{-\sigma}^{\sigma} F(u) \left(H_1(u) \sum_{n=-\infty}^{\infty} y_1(t - nT_g) e^{jnT_g u} + \dots + H_m(u) \sum_{n=-\infty}^{\infty} y_m(t - nT_g) e^{jnT_g u} \right) du = \int_{-\sigma}^{\sigma} F(u) e^{jut} du \quad (1.25)$$

By using (1.14) we may write -

$$f(t) = \sum_{n=-\infty}^{\infty} g_1(nT_g) y_1(t - nT_g) + \dots + \sum_{n=-\infty}^{\infty} g_m(nT_g) y_m(t - nT_g) \quad (1.26)$$

which is what we wanted to prove.

We stress that the determinant of the linear system in (1.16) must be different than zero in order for the sampled signal to be able to be reconstructed for the set of frequencies $u \in (-\sigma, \sigma + c)$.

1.5.3.2 The 1D Papoulis Generalized Sampling Expansion – An Example

Let us examine an example of a sampling scheme which uses up to first order derivatives. This implies that the sampling scheme may be illustrated as –

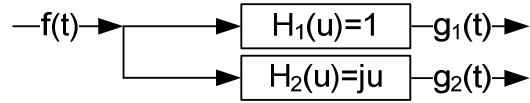


Figure 4 – Sampling with up to first order derivatives

The sampling scheme defines –

$$\begin{aligned} H_1(u) &= 1 & H_2(u) &= ju \\ g_1(t) &= f(t) & g_2(t) &= f'(t) \\ T_g &= 4\pi/\sigma & c &= \sigma \end{aligned} \quad (1.27)$$

From the theorem above, we deduce that $f(t)$ can be expressed in terms of the samples of $g_{1,2}(t)$.

The set of linear equations gives us –

$$\begin{aligned} Y_1(u, t) + juY_1(u, t) &= 1 \\ Y_1(u, t) + j(u + \sigma)Y_1(u, t) &= e^{j\sigma t} \end{aligned} \quad (1.28)$$

The determinant of the linear system is given by -

$$\begin{vmatrix} 1 & ju \\ 1 & j(u + \sigma) \end{vmatrix} = j\sigma \neq 0 \quad (1.29)$$

The solution to this set of equations is given by –

$$Y_1(u, t) = 1 - \frac{u}{\sigma} (e^{j\sigma t} - 1) \quad Y_2(u, t) = \frac{1}{j\sigma} (e^{j\sigma t} - 1) \quad (1.30)$$

The Inverse Fourier Transform of these interpolation functions are given by -

$$y_1(u,t) = \frac{4\sin^2(\sigma t/2)}{\sigma^2 t^2} \quad y_2(u,t) = \frac{4\sin^2(\sigma t/2)}{\sigma^2 t} \quad (1.31)$$

Which gives us the interpolation formula –

$$f(t) = \sum_{n=-\infty}^{\infty} \frac{4\sin^2\left(\sigma\left(t - \frac{4\pi n}{\sigma}\right)/2\right)}{\sigma^2\left(t - \frac{4\pi n}{\sigma}\right)^2} f\left(\frac{4\pi n}{\sigma}\right) + \frac{4\sin^2\left(\sigma\left(t - \frac{4\pi n}{\sigma}\right)/2\right)}{\sigma^2\left(t - \frac{4\pi n}{\sigma}\right)} f'\left(\frac{4\pi n}{\sigma}\right) \quad (1.32)$$

1.5.3.3 Proof for 2D signals

Let us define $f(x,y)$ as a (σ_x, σ_y) band limited function if

$$f \in L^2 \text{ and } F(u,v) = 0 \quad |u| \geq \sigma_x \text{ or } |v| \geq \sigma_y \quad (1.33)$$

We denote the Fourier Transform of $f(x,y)$ by $F(u,v)$.

We now attempt to show that $f(x,y)$ can be expressed in terms of the samples

$g_k(nT_g^x, pT_g^y)$ of m 2D linear functionals $g_k(x,y)$ of $f(x,y)$ each of which samples at a slower rate –

$$\begin{aligned} T_g^x &= mT = 2\pi m / \sigma_x & c_x &= 2\sigma_x / m \\ T_g^y &= mT = 2\pi m / \sigma_y & c_y &= 2\sigma_y / m \end{aligned} \quad (1.34)$$

Let us assume we are given m linear systems with transfer functions –

$$H_k(u,v) \quad k \in [1, \dots, m] \quad (1.35)$$

These systems are all fed by the (σ_x, σ_y) band limited function $f(x,y)$

Each $g_k(x,y)$ is given by –

$$g_k(x,y) = \int_{-\sigma_x}^{\sigma_x} \int_{-\sigma_y}^{\sigma_y} F(u,v) H_k(u,v) e^{jux} e^{jvy} du dv \quad (1.36)$$

We shall attempt to express $f(x, y)$ in terms of the samples $g_k(nT_g^x, pT_g^y)$ of these functions.

i.e. – we wish to find $y_k(x, y)$ such that –

$$\begin{aligned} f(x, y) &= \sum_{n=-\infty}^{\infty} \sum_{p=-\infty}^{\infty} \left[g_1(nT_g^x, pT_g^y) y_1(x - nT_g^x, y - pT_g^y) + \dots + g_m(nT_g^x, pT_g^y) y_m(x - nT_g^x, y - pT_g^y) \right] = \\ &= \sum_{n=-\infty}^{\infty} \sum_{p=-\infty}^{\infty} \sum_{k=1}^m g_k(nT_g^x, pT_g^y) y_k(x - nT_g^x, y - pT_g^y) \end{aligned} \quad (1.37)$$

We begin by forming the following set of equations –

$$\begin{aligned} H_1(u, v) Y_1(u, v, x, y) + \dots + H_m(u, v) Y_m(u, v, x, y) &= 1 \\ H_1(u + c_x, v + c_y) Y_1(u, v, x, y) + \dots + H_m(u + c_x, v + c_y) Y_m(u, v, x, y) &= e^{j c_x x} e^{j c_y y} \\ H_1(u + 2c_x, v + 2c_y) Y_1(u, v, x, y) + \dots + H_m(u + 2c_x, v + 2c_y) Y_m(u, v, x, y) &= e^{j 2 c_x x} e^{j 2 c_y y} \\ \vdots & \\ H_m(u + (m-1)c_x, v + (m-1)c_y) Y_1(u, v, x, y) + \dots + \\ H_m(u + (m-1)c_x, v + (m-1)c_y) Y_m(u, v, x, y) &= e^{j(m-1)c_x x} e^{j(m-1)c_y y} \end{aligned} \quad (1.38)$$

Where –

$$y_k(x, y) = \frac{1}{c_x c_y} \int_{-\sigma_x}^{-\sigma_x + c_x} \int_{-\sigma_y}^{-\sigma_y + c_y} Y_k(u, v, x, y) e^{j u x} e^{j v y} dudv \quad (1.39)$$

The coefficients of the linear system of equations (1.39) $H_k(u + lc_x, v + lc_y)$ are independent of x, y , and the right side consists of periodic functions of x, y with a period of T_g^x and T_g^y .

Hence, the solutions $Y_k(u, v, x, y)$ must be periodic –

$$Y_k(u, v, x, y) = Y_k(u, v, x + T_g^x, y) = Y_k(u, v, x, y + T_g^y) = Y_k(u, v, x + T_g^x, y + T_g^y) \quad (1.40)$$

Using (1.39) and (1.40) we may write –

$$\begin{aligned} y_k(x - nT_g^x, y - pT_g^y) &= \frac{1}{c_x c_y} \int_{-\sigma_x}^{-\sigma_x + c_x} \int_{-\sigma_y}^{-\sigma_y + c_y} Y_k(u, v, x - nT_g^x, y - pT_g^y) e^{ju(x - nT_g^x)} e^{jv(y - pT_g^y)} dudv = \\ &= \frac{1}{c_x c_y} \int_{-\sigma_x}^{-\sigma_x + c_x} \int_{-\sigma_y}^{-\sigma_y + c_y} Y_k(u, v, x, y) e^{j u x} e^{-jnT_g^x u} e^{j v y} e^{-jpT_g^y v} dudv \end{aligned} \quad (1.41)$$

We notice that (1.41) implies that $y_k(x - nT_g, y - pT_g)$ is the $n^{\text{th}}, p^{\text{th}}$ Fourier series coefficient of the function $Y_k(u, v, x, y)e^{jux}e^{jvy}$ in the interval $(-\sigma_x, -\sigma_x + c_x) \times (-\sigma_y, -\sigma_y + c_y)$. Hence –

$$Y_k(u, v, x, y)e^{jux}e^{jvy} = \sum_{n=-\infty}^{\infty} \sum_{p=-\infty}^{\infty} y_k(x - nT_g^x, y - pT_g^y)e^{jnT_g^x u} e^{jpT_g^y v} \\ (u, v) \in (-\sigma_x, -\sigma_x + c_x) \times (-\sigma_y, -\sigma_y + c_y) \quad (1.42)$$

By multiplying the first equation in (1.39) by $e^{jux}e^{jvy}$ we have –

$$H_1(u, v)e^{jux}e^{jvy}Y_1(u, v, x, y) + \dots + H_m(u, v)e^{jux}e^{jvy}Y_m(u, v, x, y) = e^{jux}e^{jvy} \quad (1.43)$$

Plugging (1.42) into (1.43) we yield –

$$H_1(u, v) \sum_{n=-\infty}^{\infty} \sum_{p=-\infty}^{\infty} y_1(x - nT_g^x, y - pT_g^y)e^{jnT_g^x u} e^{jpT_g^y v} + \dots \\ + H_m(u, v) \sum_{n=-\infty}^{\infty} \sum_{p=-\infty}^{\infty} y_m(x - nT_g^x, y - pT_g^y)e^{jnT_g^x u} e^{jpT_g^y v} = e^{jux}e^{jvy} \quad (1.44)$$

which is true for every $(u, v) \in (-\sigma_x, -\sigma_x + c_x) \times (-\sigma_y, -\sigma_y + c_y)$.

We now multiply the second equation in (1.38) by $e^{jux}e^{jvy}$ and similarly yield –

$$H_1(u + c_x, v + c_y) \sum_{n=-\infty}^{\infty} \sum_{p=-\infty}^{\infty} y_1(x - nT_g^x, y - pT_g^y)e^{jnT_g^x(u+c_x)} e^{jpT_g^y(v+c_y)} + \dots \\ + H_m(u + c_x, v + c_y) \sum_{n=-\infty}^{\infty} \sum_{p=-\infty}^{\infty} y_m(x - nT_g^x, y - pT_g^y)e^{jnT_g^x(u+c_x)} e^{jpT_g^y(v+c_y)} = e^{j(u+c_x)x} e^{j(v+c_y)y} \quad (1.45)$$

Which is also true for every $(u, v) \in (-\sigma_x, -\sigma_x + c_x) \times (-\sigma_y, -\sigma_y + c_y)$. However, due to the fact that $e^{jnT_g^x(u+c_x)} e^{jpT_g^y(v+c_y)} = e^{jnT_g^x u} e^{jpT_g^y v}$ we may write (1.45) as –

$$H_1(u, v) \sum_{n=-\infty}^{\infty} \sum_{p=-\infty}^{\infty} y_1(x - nT_g^x, y - pT_g^y)e^{jnT_g^x u} e^{jpT_g^y v} + \dots \\ + H_m(u, v) \sum_{n=-\infty}^{\infty} \sum_{p=-\infty}^{\infty} y_m(x - nT_g^x, y - pT_g^y)e^{jnT_g^x u} e^{jpT_g^y v} = e^{jux}e^{jvy} \quad (1.46)$$

which is also true for every $(u, v) \in (-\sigma_x + c_x, -\sigma_x + 2c_x) \times (-\sigma_y + c_y, -\sigma_y + 2c_y)$.

In the same manner we may prove that (1.44) holds for every $(u, v) \in (-\sigma_x, \sigma_x) \times (-\sigma_y, \sigma_y)$.

Note that in order to tile the entire plane we must examine some extra equations, which do not appear in (1.38), of the form –

$$\begin{aligned} H_1(u + c_x, v) & \sum_{n=-\infty}^{\infty} \sum_{p=-\infty}^{\infty} y_1(x - nT_g^x, y - pT_g^y) e^{jnT_g^x(u+c_x)} e^{jpT_g^y v} + \dots \\ & + H_m(u + c_x, v) \sum_{n=-\infty}^{\infty} \sum_{p=-\infty}^{\infty} y_m(x - nT_g^x, y - pT_g^y) e^{jnT_g^x(u+c_x)} e^{jpT_g^y v} = e^{j(u+c_x)x} e^{jvy} \end{aligned} \quad (1.47)$$

which, by the same reasoning is equal to –

$$\begin{aligned} H_1(u, v) & \sum_{n=-\infty}^{\infty} \sum_{p=-\infty}^{\infty} y_1(x - nT_g^x, y - pT_g^y) e^{jnT_g^x u} e^{jpT_g^y v} + \dots \\ & + H_m(u, v) \sum_{n=-\infty}^{\infty} \sum_{p=-\infty}^{\infty} y_m(x - nT_g^x, y - pT_g^y) e^{jnT_g^x u} e^{jpT_g^y v} = e^{jux} e^{jvy} \end{aligned} \quad (1.48)$$

which is true for every $(u, v) \in (-\sigma_x + c_x, -\sigma_x + 2c_x) \times (-\sigma_y, -\sigma_y + c_y)$.

Finally, we multiply by $F(u, v)$ and integrate according to u, v . In other words we calculate the inverse Fourier transform -

$$\begin{aligned} \int_{-\sigma_x}^{\sigma_x} \int_{-\sigma_y}^{\sigma_y} F(u, v) & \left(H_1(u, v) \sum_{n=-\infty}^{\infty} \sum_{p=-\infty}^{\infty} y_1(x - nT_g^x, y - pT_g^y) e^{jnT_g^x u} e^{jpT_g^y v} + \dots + \right. \\ & \left. + H_m(u, v) \sum_{n=-\infty}^{\infty} \sum_{p=-\infty}^{\infty} y_m(x - nT_g^x, y - pT_g^y) e^{jnT_g^x u} e^{jpT_g^y v} \right) = \\ & = \int_{-\sigma_x}^{\sigma_x} \int_{-\sigma_y}^{\sigma_y} F(u, v) e^{jux} e^{jvy} du dv \end{aligned} \quad (1.49)$$

By using (1.36) we may write -

$$\begin{aligned} f(x, y) = \sum_{n=-\infty}^{\infty} g_1(nT_g^x, pT_g^y) y_1(x - nT_g^x, y - pT_g^y) + \dots + \\ + \sum_{n=-\infty}^{\infty} g_m(nT_g^x, pT_g^y) y_m(x - nT_g^x, y - pT_g^y) \end{aligned} \quad (1.50)$$

Q.E.D.

2 Coverage

2.1 Coverage of detecting Rain

In this section we discuss the problem of *detecting* rain by an arbitrary set of lines. Attempting to reconstruct rain maps using the data which was obtained from the Commercial Wireless Networks (CWN) requires an understanding of the processing which each RSL value undergoes. Such a processing clearly depends on the exact equipment which is used in the cellular network. As any digitally stored data dictates, the RSL value undergoes quantization. RSL values are often saved after being quantized to a resolution of 1dB but a quantization of 0.1dB may also be commonly found. The effects of the atmosphere and weather on the performance of a mm-wave communication link have been analysed by Frey[14]. It has been found that the attenuation due to heavy rain at frequencies below 1 GHz is negligible. In fact, the rain induced attenuations are in the order of the quantization and hence may probably not be measured properly. However, at frequencies above 15GHz, the attenuation as a function of the rain rate is large enough to be measured. Figure 5 shows the rain induced attenuation as a function of the mm wave frequency. One may easily notice that at frequencies of around 20GHz, the attenuations go beyond the quantization magnitude. This is what enables a proper measurement of various rain rates, using the CWN. It must be stressed that this plot depicts the attenuations per km. Thus, longer links will cause larger attenuations for a constant rain rate which further eases the RSL quantization requirements.

Backhaul operating frequencies of cellular networks vary depending on the communication technology. These are usually in the range of 20 GHz for longer range links and may reach up to 40 GHz for short links where two antennas are closer one to its pair. This in turn means that we may indeed use the logged backhaul RSL samples in order to measure the rain rates. Figure 6 shows the link lengths as a function of their frequencies, in an Israeli cellular provider network. This plot includes 3515 links and shows both directions of transmission, in blue and in red. The plot shows that transmission and reception frequencies rise as the link distance decreases. The plot also reveals the fact that common discrete frequencies are used within a specific cellular provider's network. This eases the management of frequencies between the various providers operating inside a certain country.

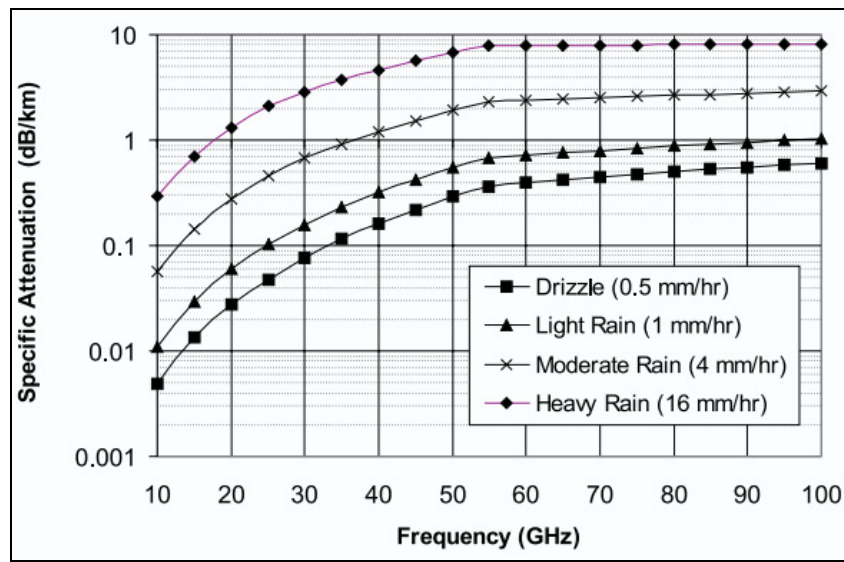


Figure 5 –Atmosphere and weather effects on performance of mm-wave communication link
[14]

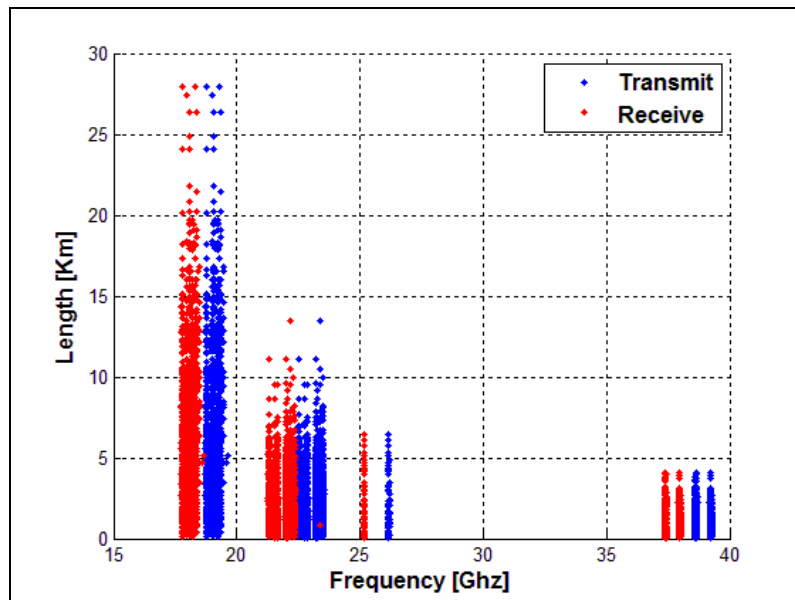


Figure 6 –The backhaul link lengths as a function of transmission frequencies.

By using equation (1.2) we may calculate the expected attenuation which is induced by a certain rain rate. Of course, this relation gives us the rain rate per unit distance (km). Hence, in order to know if a certain link will detect the rain we must consider its actual length. Moreover, we need to take into consideration the link's sensitivity. In other words, we must consider the

minimal rain rate which will cause a sensible attenuation. The lowest added attenuation which is sensible by a certain link is given by its quantization.

Now, for each link, assuming a specific cloud profile, we may calculate the minimal rain rate which such a link may detect. The cloud profile enables us to infer on the section of the cloud which intersects with the link, and by such, causes an added attenuation due to rain. This notion is depicted in Figure 7 in which cases (a) to (d) show a link which intersects with a cloud in a manner which will cause an added attenuation.

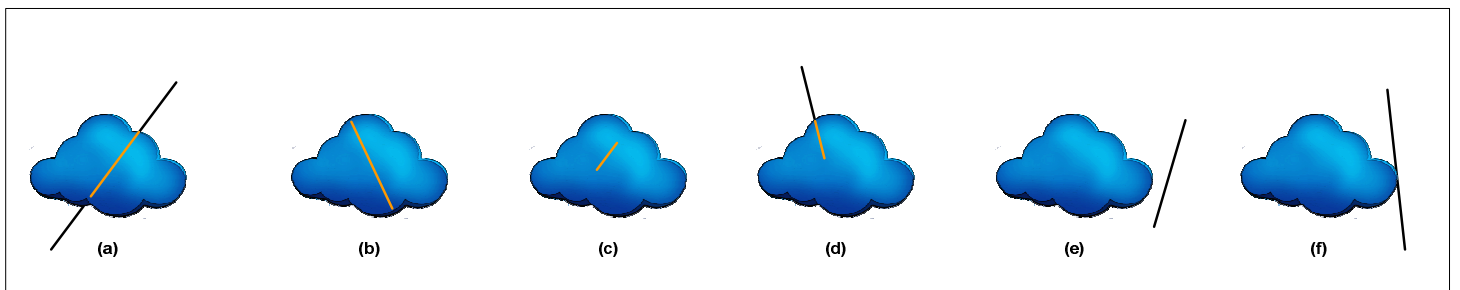


Figure 7 –Cloud intersecting with various links

Hence, once we know a cloud's profile and a link's length we may calculate the exact intersection length and use equation (1.2) and the link's quantization in order to calculate the minimal rain rate which is detectable by such a cloud. Denoting by L_{int} the section of the link which intersects with the cloud and by Q the link's quantization, the minimal rain rate which is detectable by such a link is given by –

$$R_{\min} = \left(\frac{Q}{aL_{\text{int}}} \right)^{1/b} \quad (2.1)$$

Assuming a cloud's profile is given by a generalized ellipse which is rotated by an angle of θ and centered at (x_c, y_c) -

$$\left(\frac{\cos \theta (x_c - x) + \sin \theta (y_c - y)}{\alpha} \right)^2 + \left(\frac{\sin \theta (x_c - x) - \cos \theta (y_c - y)}{\beta} \right)^2 = 1 \quad (2.2)$$

and the coordinates of a link's edges are given by $(x_1, y_1), (x_2, y_2)$ the equation which describes the link is given by –

$$y - y_1 = \frac{y_2 - y_1}{x_2 - x_1} (x - x_1)$$

$$\Rightarrow \begin{cases} y = mx + n \\ m = \frac{y_2 - y_1}{x_2 - x_1} \\ n = y_1 - mx_1 \end{cases} \quad (2.3)$$

The problem of determining the length of L_{int} reduces to solving a quadratic equation –

$$\left(\frac{\cos \theta (x_c - x) + \sin \theta \left(y_c - \left(\frac{y_2 - y_1}{x_2 - x_1} (x - x_1) + y_1 \right) \right)}{\alpha} \right)^2 + \dots$$

$$\left(\frac{\sin \theta (x_c - x) - \cos \theta \left(y_c - \left(\frac{y_2 - y_1}{x_2 - x_1} (x - x_1) + y_1 \right) \right)}{\beta} \right)^2 = 1 \quad (2.4)$$

Writing the equation above as a quadratic equation with coefficients A, B and C we may yield -

$$Ax^2 + Bx + C = 0$$

$$A = \beta^2 \cos^2 \theta + 2\beta^2 \cos \theta \sin \theta m + \beta^2 \sin^2 \theta m^2 +$$

$$a^2 \sin^2 \theta + 2a^2 \sin \theta \cos \theta m + a^2 \sin^2 \theta m^2$$

$$B = -2\beta^2 \cos^2 \theta x_c + 2\beta^2 \cos \theta \sin \theta (n - y_c - mx_c) + \beta^2 \sin^2 \theta (2mn - 2my_c) +$$

$$-2a^2 \sin^2 \theta x_c - 2a^2 \sin \theta \cos \theta (n - y_c - mx_c) + a^2 \cos^2 \theta (2mn - 2my_c) \quad (2.5)$$

$$C = \beta^2 x_c^2 \cos^2 \theta + 2\beta^2 \cos \theta \sin \theta m (-x_c n + x_c y_c) + \beta^2 \sin^2 \theta (n - y_c)^2 +$$

$$a^2 x_c^2 \sin^2 \theta - 2a^2 \cos \theta \sin \theta m (-x_c n + x_c y_c) + a^2 \cos^2 \theta (n - y_c)^2 +$$

$$-a^2 \beta^2$$

If the equation above has two solutions this implies that the line intersects with cloud in a manner which resembles either case (a) and (b) in Figure 7, if there is only one solution to the equation then the line intersects with cloud in a manner which resembles case (f) in Figure 7 and finally, if there is no solution to the equation then line intersects with cloud in a manner which resembles case (e) in Figure 7. Solutions to the inequality enable us to reveal cases (c) and (d). An understanding regarding which of these six cases we have in hand may be achieved by evaluating the discriminant of the quadratic equation.

The choice of the rain attenuation power law coefficients a and b should be set according to the link's operative frequency. Most reconstruction, detection or estimation algorithms make use of values suggested by Olsen, Rogers and Hodge [23] or Crane [7]. Table 2 shows common power law coefficients which are used for converting RSL attenuations per km to rain rate, as given by [7]. These coefficients are suitable for temperate maritime climate regions.

| Frequency | Multiplier a | Exponent b |
|-----------|----------------|--------------|
| 1 GHz | 0.00015 | 0.95 |
| 4 GHz | 0.0008 | 1.17 |
| 5 GHz | 0.00138 | 1.24 |
| 6 GHz | 0.0025 | 1.28 |
| 7.5 GHz | 0.00482 | 1.25 |
| 10 GHz | 0.0125 | 1.18 |
| 12.5 GHz | 0.0228 | 1.145 |
| 15 GHz | 0.0357 | 1.12 |
| 17.5 GHz | 0.0524 | 1.105 |
| 20 GHz | 0.0699 | 1.1 |
| 25 GHz | 0.113 | 1.09 |
| 30 GHz | 0.170 | 1.075 |
| 35 GHz | 0.242 | 1.04 |
| 40 GHz | 0.325 | 0.99 |
| 50 GHz | 0.485 | 0.9 |

Table 2 – Power Law Coefficients

In many hydrological applications, the actual interesting figure is the exact areas where a predetermined rain rate may or may not be detected. We may think of this as the inverse problem to the one discussed above.

Generating such maps requires evaluating exactly where the previous detection map which states the minimal detectable rain rate is indeed above the desired detectable rain rate.

3 Reconstruction

3.1 Reconstruction of a Sampled Function

3.1.1 Solution Overview

I address the problem of the *ability* to reliably reconstruct a two dimensional function (an image) being sampled by sums or projections along lines. I do not restrict in any manner the line types. Figure 8 depicts an example of such a sampling scheme. On the left hand side of this figure we see the underlying sampled image and its samples, in the case of the "classical" point sampling scheme; a *regular grid* of delta functions. Reconstruction from such a sampling scheme requires the usage of these point evaluations of the underlying function. On the right hand side of this figure we see the same underlying sampled image and its sampling scheme which is represented by the lines. One may easily notice that the lengths and angles of the lines are arbitrary, as the distances between the lines are.

Our solution to the question regarding the ability to reconstruct a two dimensional function which is sampled by the suggested sampling scheme involves employing a series of three separate operations which will be described in the following sections. These three stages consist of firstly solving a problem of sampling with a regular grid (equally spaced locations with lines) but with arbitrary types of lines. In the second and third stages we display the problem of a non-regular grid as one with missing samples. Essentially these three stages enable displaying this sampling scheme as a case of uniform sampling with missing samples [1][10][11][12]. Each sample is one which has been sampled by a linear functional. This functional is the mathematical representation of the line along which the projection has occurred. By considering these lines as linear functionals we enable the usage of the Generalized Sampling Expansion which was devised by Papoulis [24].

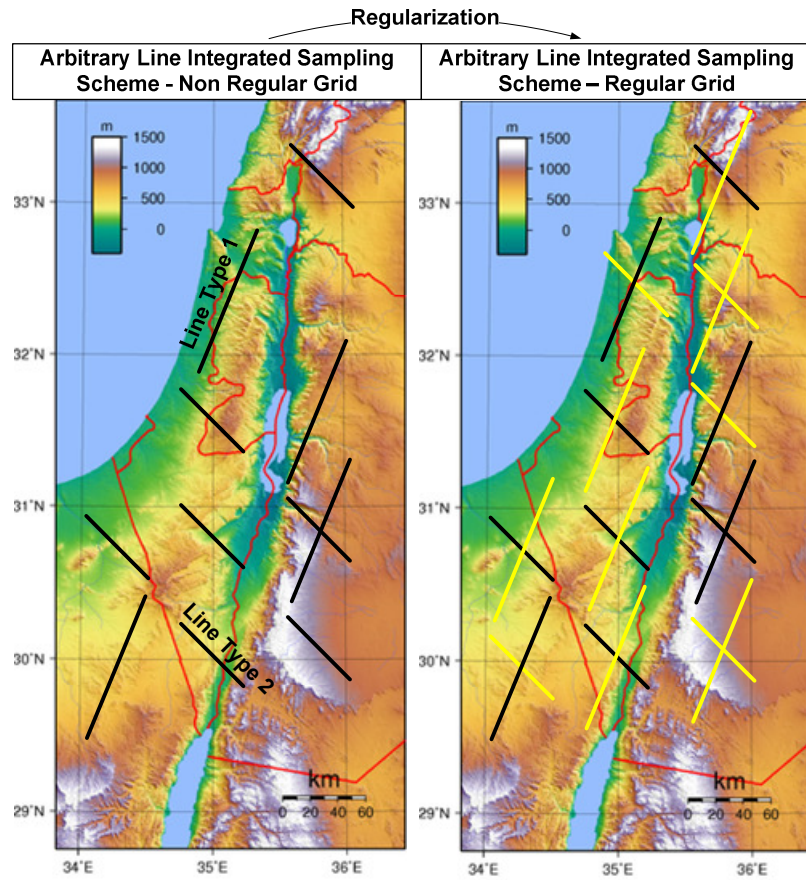


Figure 8 – The "Classical" Sampling vs. the Arbitrary Line Projections Sampling

3.1.2 Sampling with a single line type

I now show why sampling with a single type of line cannot be used in order to properly reconstruct a signal. In essence, the problem of aliasing may be alleviated by sampling fast enough. However, a discrete set of frequencies cannot be properly reconstructed when sampling with integration along a single type of line.

Sampling a 1D function with a line of length W may be thought of as a convolution with a Poisson comb after integrating –

$$f_I(t) = \sum_{n=-\infty}^{\infty} \left(\int_{t-nW/2}^{t+nW/2} f(t') dt' \right) \delta(t - nT) \quad (3.1)$$

We make use of the Fourier integration property –

$$\mathcal{F} \left\{ \int_{-\infty}^t f(t') dt' \right\} = \frac{F(u)}{iu} + \pi F(0) \delta(u) \quad (3.2)$$

We add a phase property to it and yield –

$$\mathcal{F} \left\{ \int_{-\infty}^{t+\alpha} f(t') dt' \right\} = \mathcal{F} \left\{ \int_{-\infty}^t f(t' - \alpha) dt' \right\} = e^{-i\alpha u} \left(\frac{F(u)}{iu} + \pi F(0) \delta(u) \right) \quad (3.3)$$

We may now apply a Fourier transform on equation (3.1)

$$\mathcal{F} \left\{ \sum_{n=-\infty}^{\infty} \left(\int_{t-nW/2}^{t+nW/2} f(t') dt' \right) \delta(t - nT) \right\} = \left\{ \sum_{n=-\infty}^{\infty} \mathcal{F} \left(\int_{t-nW/2}^{t+nW/2} f(t') dt' \right) \delta(t - nT) \right\} \quad (3.4)$$

Making use of the Poisson comb properties we yield –

$$\mathcal{F} \left\{ \sum_{n=-\infty}^{\infty} \left(\int_{t-nW/2}^{t+nW/2} f(t') dt' \right) \delta(t - nT) \right\} = \mathcal{F} \left(\int_{t-nW/2}^{t+nW/2} f(t') dt' \right) * \sum_{n=-\infty}^{\infty} \delta(u - nu_s) \quad (3.5)$$

Making use of the integration property we yield –

$$\begin{aligned} \mathcal{F} \left(\int_{t-nW/2}^{t+nW/2} f(t') dt' \right) * \sum_{n=-\infty}^{\infty} \delta(u - nu_s) &= F(u) \left(\frac{e^{iu} - e^{-iu}}{iu} \right) * \sum_{n=-\infty}^{\infty} \delta(u - nu_s) = \\ &= \sum_{n=-\infty}^{\infty} F(u - nu_s) \text{sinc}(u - nu_s) \end{aligned} \quad (3.6)$$

Finally, we see that first and foremost, in order to reconstruct $F(u)$ we must divide the outcome by the $\text{sinc}(.)$ which values may be zero.

Moreover, a sampling frequency in which no aliasing occurs doesn't exist due to the infinite support of the $\text{sinc}(.)$ unless $f(t)$ is band-limited.

3.1.3 Usage of the Papoulis Generalized Sampling Expansion for our solution

After having described the basic notion of the GSE, I now attempt to represent the Arbitrary Line Projections sampling scheme as a case of sampling with linear functionals. These functionals will represent our line projections.

Let us assume we are given a rather simple case of geometry of lines. A case where a two dimensional function was sampled by numerous arbitrary types of lines (two types in this example/figure). These lines may be of arbitrary angles and lengths. However, these lines are located on a regular grid. Such a simple case is depicted in Figure 9.

The Arbitrary Line Integrated Sampling Scheme

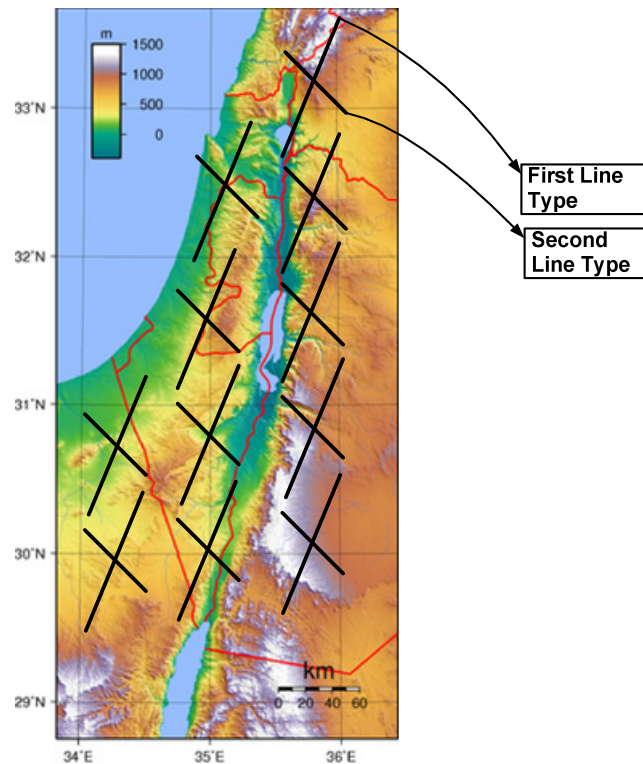


Figure 9 – Sampling scheme with projections on arbitrary lines with a regular grid

In such a case, we may employ the GSE by using two types of sampling functionals. One which will represent our first line type and the second to represent the second line type.

In general, a linear functional which represents a line projection is given by –

$$f_{W,\theta}(x,y) = \begin{cases} 1, & -0.5W \cos \theta \leq x \leq 0.5W \cos \theta \\ & y = x \tan \theta \\ 0, & \text{else} \end{cases} \quad (3.7)$$

$$F_{W,\theta}(u,v) = W \cdot \frac{\sin((u \cos \theta + v \sin \theta)W/2)}{(u \cos \theta + v \sin \theta)W/2}$$

In a case with only two lines the GSE set of linear equations is given by –

$$\begin{pmatrix} H_1(u, v) & H_2(u, v) & 1 \\ H_1(u + c_x, v + c_y) & H_2(u + c_x, v + c_y) & e^{jc_x u} e^{jc_y v} \end{pmatrix} = \begin{pmatrix} \frac{\sin((\cos \theta_1 u + \sin \theta_1 v) W_1 / 2)}{(\cos \theta_1 u + \sin \theta_1 v) W_1 / 2} & \frac{\sin((\cos \theta_2 u + \sin \theta_2 v) W_2 / 2)}{(\cos \theta_2 u + \sin \theta_2 v) W_2 / 2} & 1 \\ \frac{\sin((\cos \theta_1(u + c_x) + \sin \theta_1(v + c_y)) W_1 / 2)}{(\cos \theta_1(u + c_x) + \sin \theta_1(v + c_y)) W_1 / 2} & \frac{\sin((\cos \theta_2(u + c_x) + \sin \theta_2(v + c_y)) W_2 / 2)}{(\cos \theta_2(u + c_x) + \sin \theta_2(v + c_y)) W_2 / 2} & e^{jc_x u} e^{jc_y v} \end{pmatrix} \quad (3.8)$$

Validating that they indeed form a valid set of sampling functionals requires evaluating the following determinant

$$\left| \begin{array}{cc} \frac{\sin((\cos \theta_1 u + \sin \theta_1 v) W_1 / 2)}{(\cos \theta_1 u + \sin \theta_1 v) W_1 / 2} & \frac{\sin((\cos \theta_2 u + \sin \theta_2 v) W_2 / 2)}{(\cos \theta_2 u + \sin \theta_2 v) W_2 / 2} \\ \frac{\sin((\cos \theta_1(u + c_x) + \sin \theta_1(v + c_y)) W_1 / 2)}{(\cos \theta_1(u + c_x) + \sin \theta_1(v + c_y)) W_1 / 2} & \frac{\sin((\cos \theta_2(u + c_x) + \sin \theta_2(v + c_y)) W_2 / 2)}{(\cos \theta_2(u + c_x) + \sin \theta_2(v + c_y)) W_2 / 2} \end{array} \right| \quad (3.9)$$

for the set of frequencies given by $(-\sigma_x, 0) \times (-\sigma_y, 0)$. σ_x and σ_y are given by the distances between the lines-

$$\sigma_x = \frac{1}{2\Delta_x} \quad \sigma_y = \frac{1}{2\Delta_y} \quad (3.10)$$

3.1.4 Usage of the Papoulis Generalized Sampling Expansion for our solution – An Example

We now apply the formalism above for two lines with two angles of $\pi/4$ and $3\pi/4$ and an equal length, as shown in Figure 10.

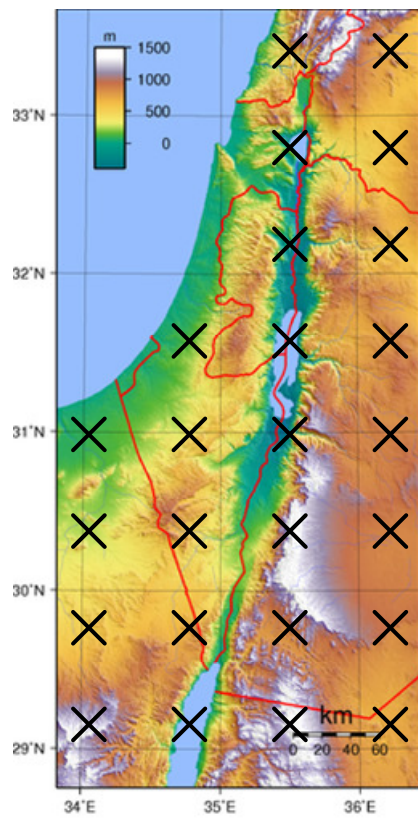


Figure 10 –GSE usage for two Lines with equal lengths and angles $\pi/4$ and $3\pi/4$

As suggested by equation (3.9) the system of equations for the Generalized Sampling Expansion for two angles of $\pi/4$ and $3\pi/4$ are given by -

$$\begin{vmatrix} \frac{\sin((\sqrt{2}u + \sqrt{2}v)W/2)}{(\sqrt{2}u + \sqrt{2}v)W/2} & \frac{\sin((-\sqrt{2}u + \sqrt{2}v)W/2)}{(-\sqrt{2}u + \sqrt{2}v)W/2} \\ \frac{\sin((\sqrt{2}(u + c_x) + \sqrt{2}(v + c_y))W/2)}{(\sqrt{2}(u + c_x) + \sqrt{2}(v + c_y))W/2} & \frac{\sin((-\sqrt{2}(u + c_x) + \sqrt{2}(v + c_y))W/2)}{(-\sqrt{2}(u + c_x) + \sqrt{2}(v + c_y))W/2} \end{vmatrix} \quad (3.11)$$

Numerically evaluating its determinant yields -

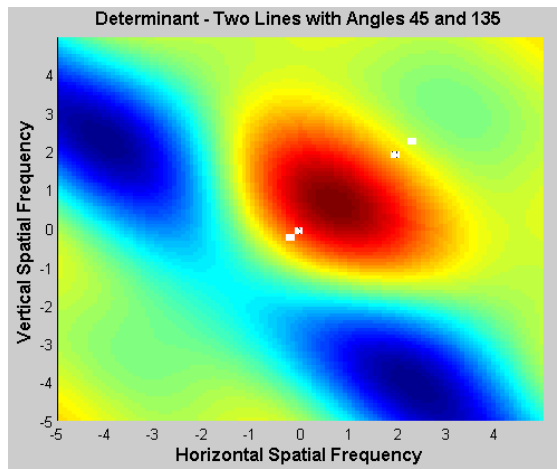


Figure 11 –GSE usage for two lines with equal lengths – determinant evaluation

Finally, now we know that these two lines can not form a proper sampling set and will yield non-reconstructable signals due to the frequencies for which the determinant evaluates to zero. We stress that the plot depicts the determinant evaluation for the set of frequencies $(-\sigma_x, \sigma_x) \times (-\sigma_y, \sigma_y)$ but the evaluation is required only for $(-\sigma_x, 0) \times (-\sigma_y, 0)$;

In section 3.2.2 which deals with the problem of synthesis (or how to choose a proper set of lines) we show why two different lengthed lines with an angle of 90 degrees between them may never be used for the purpose of sampling/reconstructing.

3.1.5 Coping with an irregular grid

I now attempt to relax the assumption we made in the previous section in which the lines are located on a regular grid. For this purpose we need a method of regularizing a non-regular grid on which the lines are located on. Figure 12 depicts this notion in which the newly added lines appear in yellow on the right hand side. These are samples which we do not have (missing samples) but which if appeared, we would have had a regular grid.

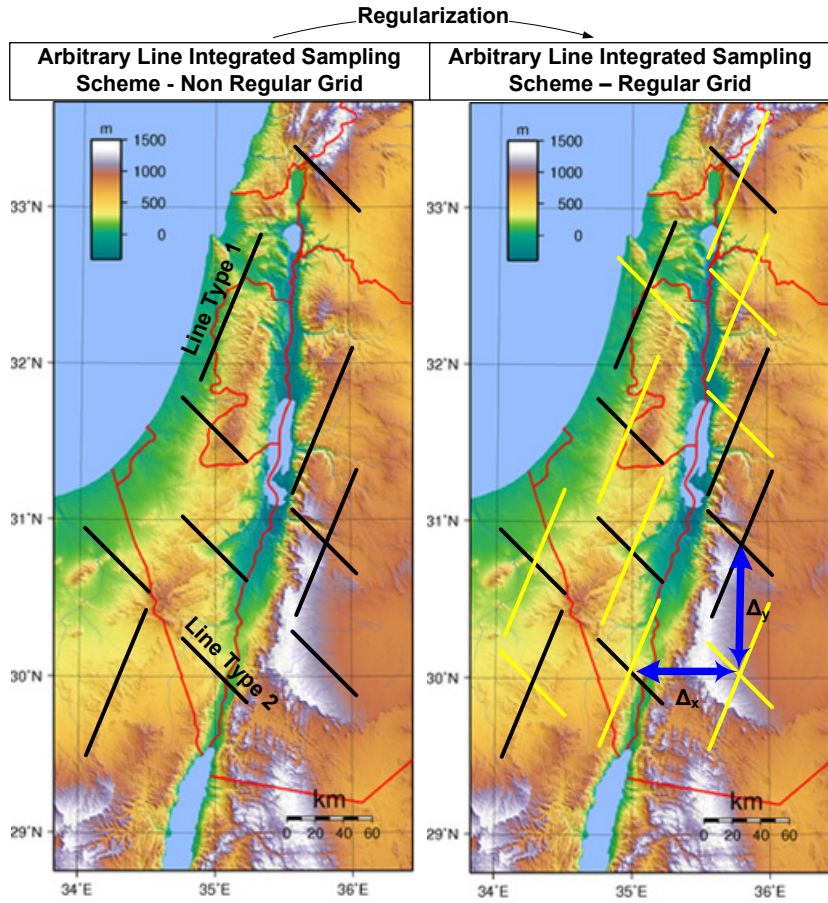


Figure 12 – The Regularization of the sampling Grid

We begin the regularization process with the identification of our linear sampling functionals. For this we are required to identify the number of different types of lines, where each type is characterized by its angle θ_k and its length W_k .

Hence, the identification process requires examining each pair of lines and checking whether $\theta_i = \theta_j$ and $W_i = W_j$ (for $i \neq j$). One may choose to ease the requirement of equivalence between two lines and define that two lines be treated as the same sampling functional if –

$$|\theta_i - \theta_j| \leq \Delta_\theta \text{ and } |W_i - W_j| \leq \Delta_W \quad (3.12)$$

To summarize, the pseudo code of the process of identifying the sampling functionals is shown below

```

NumberOfFunctionals=TotalNumberOfLines
For i=1 to TotalNumberOfLines-1
    For j= i+1 to TotalNumberOfLines
        If( |θi- θj|<Δθ & |Wi- Wj|<ΔW )
            NumberOfFunctionals = NumberOfFunctionals-1

```

Table 3 – Distinct Functional Identification Process

In the example of Figure 12 we show that after the regularization process, each of the three sampling functionals is placed in every location on the regular grid. Hence, once we know the number of sampling functionals we would like to locate each of these sampling functionals on the regularized grid sites. For the purpose of doing so we must determine the proper sampling grid on which to locate the sampling functionals. However, this problem doesn't necessarily have a unique solution. We chose to add a constraint which compels choosing the grid with the minimal amount of newly located lines on the grid (marked as yellow lines in Figure 12).

This suggests that we must find the *maximal* horizontal/vertical step sizes Δ_x, Δ_y between two nearby lines, which ensure that each existing line (marked as black lines in Figure 12) will fall on a valid grid site. The process of determining the grid step sizes begins with calculating the distances between the centres of nearby *existing* lines –

$$\delta_j^x \triangleq x_i - x_{i+1} \quad \delta_j^y \triangleq y_i - y_{i+1} \quad (3.13)$$

Having calculated the sets $\{\delta_j^x\}, \{\delta_j^y\}$ we must find their common divisor. Choosing our grid step sizes as one of their common divisors compels that existing lines fall on valid grid sites. Choosing the greatest common divisor is the choice which maximizes the values of Δ_x, Δ_y and by such minimizes the amount of newly located lines. To summarize, we choose the values of Δ_x, Δ_y as the Greatest common Divisor (GCD) of the sets $\{\delta_j^x\}, \{\delta_j^y\}$ -

$$\Delta_x = GCD(\{\delta_j^x\}) \quad \Delta_y = GCD(\{\delta_j^y\}) \quad (3.14)$$

We may choose to quantize the values of $\{\delta_j^x\}, \{\delta_j^y\}$ to certain accuracy in order to relax the requirement of finding the *maximal* horizontal/vertical step sizes Δ_x, Δ_y , as we did with Δ_θ, Δ_w . If we do not insert any such relaxations the regularization algorithm may yield a very dense grid. We denote the quantization value for Δ_x, Δ_y by Q_x, Q_y respectively. Inserting the relaxation on the values of $\{\delta_j^x\}, \{\delta_j^y\}$ yields –

$$\Delta_x = Q_x \cdot GCD \left\lfloor \frac{\{\delta_j^x\}}{Q_x} \right\rfloor \quad \Delta_y = Q_y \cdot GCD \left\lfloor \frac{\{\delta_j^y\}}{Q_y} \right\rfloor \quad (3.15)$$

where $\lfloor . \rfloor$ denotes the floor function.

E.g. for a quantization value of 1×10^{-3} we will yield the step sized up to a resolution of three figures after the decimal point.

We then draw a grid of points with spacings of Δ_x and Δ_y between one another, beginning with the most upper left existing line location. For each point on the grid we locate the linear sampling functionals.

We note that the $GCD(\cdot)$ of multiple values may be calculated by recursively calculating it on all of the entries -

$$\Delta x = GCD(\delta x_1, GCD(\delta x_2, GCD(\delta x_3, \dots))) \quad (3.16)$$

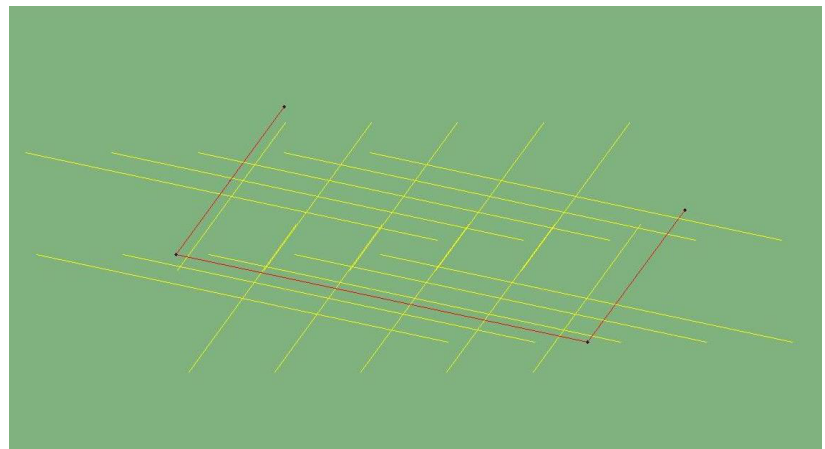
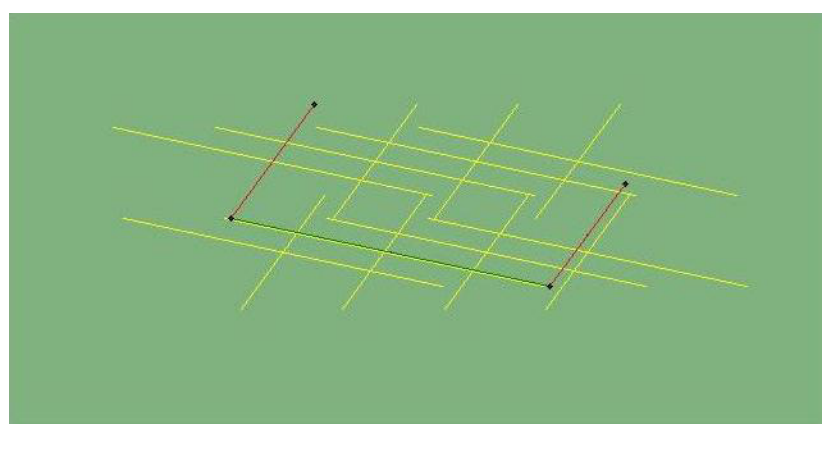
3.1.6 Coping with an irregular grid – An Example

Enabling a control over the precision of the regular grid which we attempt to fit, we would now like to understand which values yield better regularizations. When we state "better" we mean that the original existing lines are as close as possible to the ones of the regularization algorithm's output and we have a minimal amount of newly added lines.

The simulation depicted in Table 4 shows how varying the values of Q_x, Q_y changes the regularization results. In this simulation we used three different values of Q_x and set $Q_y = Q_x$. One may easily notice that smaller quantization values usually yields denser grids. However this isn't necessarily true for every grid regularization problem. This is due to the fact that the GCD

function isn't monotonous. This implies that choosing the optimal quantization values requires some trial and error.

However, it is always true that larger quantization values will reduce the accuracy and we notice that in the simulations with the higher quantization values, the initial red lines were fit to a yellow line which grows distantly apart from it.

| Q_x and Q_y | W_q | θ_q | Output Grid |
|-----------------------|---------------------|------------|--|
| 3.8×10^{-3} | 10×10^{-3} | $1/\pi$ |  |
| 2.9×10^{-3} | 10×10^{-3} | $1/\pi$ |  |
| 0.87×10^{-3} | 10×10^{-3} | $1/\pi$ | |

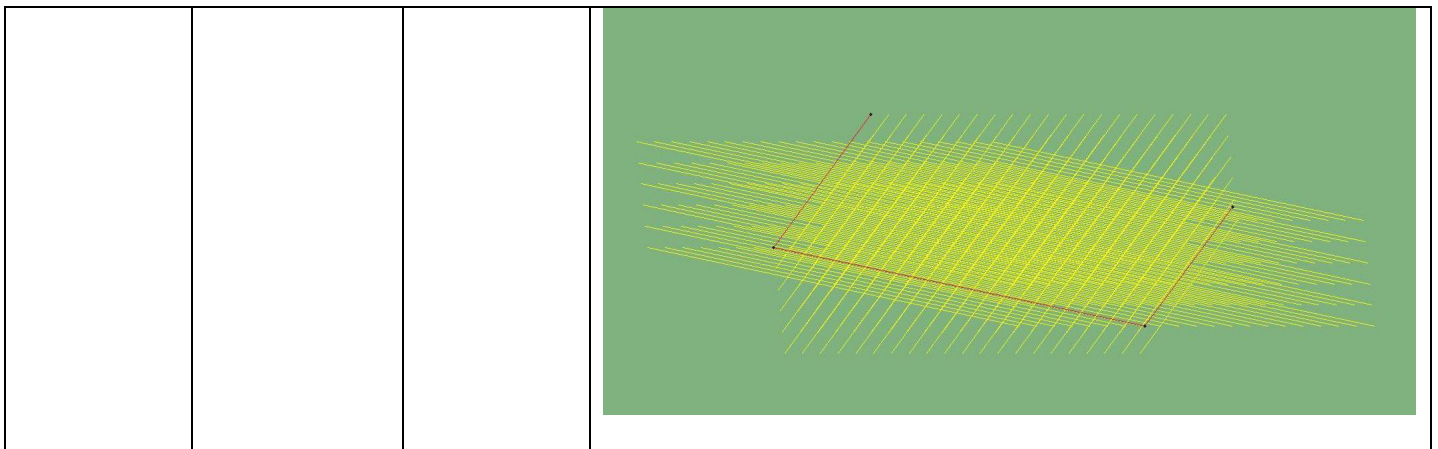


Table 4 – Evaluation of the Regularization Algorithm

3.1.7 Missing Samples

3.1.7.1 Missing Samples in the classical sampling scheme

In order to better clarify how we cope with the newly added lines which we are missing we first solve the inverse problem for the classical sampling scheme [10][11][12] with a train of delta functions.

Let us consider $f(t)$ as a σ band limited function if –

$$f \in L^2 \text{ and } F(u) = 0 \quad |u| \geq \sigma \quad (3.17)$$

which is sampled at a rate of $1/T$ such that $\sigma < \frac{1}{2T}$. By the Shannon reconstruction formula we

know that we may relate $f(t)$ to its samples by –

$$f(t) = 2\sigma T \sum_{k=-\infty}^{\infty} f(kT) \operatorname{sinc}[2\sigma(t - kT)] \quad (3.18)$$

Let us denote the by $S = \{i_1, i_2, i_3, \dots, i_n\}$ a finite set of integers which correspond to the

locations of the unknown/missing samples of $f(t)$.

Setting $t = i_j T$ $j \in \{1, 2, \dots, n\}$ we may write –

$$\begin{aligned}
f(i_j T) &= 2\sigma T \sum_{k=-\infty}^{\infty} f(kT) \text{sinc}\left[2\sigma(i_j T - kT)\right] = \\
&= 2\sigma T \sum_{k \notin S} f(kT) \text{sinc}\left[2\sigma(i_j T - kT)\right] + 2\sigma T \sum_{k=1}^n f(kT) \text{sinc}\left[2\sigma(i_j T - i_k T)\right]
\end{aligned} \tag{3.19}$$

We may write this set of n equations as –

$$\mathbf{f} = \mathbf{h} + \mathbf{Af} \tag{3.20}$$

where \mathbf{f} is the column vector of unknown samples

$$\mathbf{f}(j) = f(i_j T) \quad j \in \{1, 2, \dots, n\} \tag{3.21}$$

\mathbf{h} is the column vector composed of the known samples

$$\mathbf{h}(j) = 2\sigma T \sum_{k \notin S} f(kT) \text{sinc}\left[2\sigma(i_j T - kT)\right] \quad j \in \{1, 2, \dots, n\} \tag{3.22}$$

and \mathbf{A} is a matrix with the following entries –

$$A(j, k) = 2\sigma T \text{sinc}\left[2\sigma T(i_j - i_k)\right] \quad j, k \in \{1, 2, \dots, n\} \tag{3.23}$$

Finally, the vector of unknown samples \mathbf{f} may be found by solving the inverse problem –

$$\mathbf{f} = (\mathbf{I} - \mathbf{A})^{-1} \mathbf{h} \tag{3.24}$$

This also implies that the vector of unknown samples \mathbf{f} may be calculated if the following determinant is non zero.

$$|\mathbf{I} - \mathbf{A}| \neq 0 \tag{3.25}$$

Our desire is to apply a similar formalism for our purpose, the problem of missing projective samples which are one of the added samples from the regularization phase.

3.1.7.2 Missing Samples in the Arbitrary Line Projections sampling scheme

After applying the regularization process described in section 3.1.5, we are left with a fully regular grid where each grid site consists of our linear sampling functionals. However, our

original sampling scheme didn't consist of the newly located lines (the yellow ones in Table 4). I now formalize the problem as a problem of missing samples.

Following a similar formalism as described in section 3.1.7.1, we address the case of missing samples for the case of the Arbitrary Line Projections sampling scheme.

Let us define $f(x, y)$ as a (σ_x, σ_y) band limited function if

$$f \in L^2 \text{ and } F(u, v) = 0 \quad |u| \geq \sigma_x \text{ or } |v| \geq \sigma_y \quad (3.26)$$

which is sampled at a rate of $1/T_x$ $1/T_y$ such that $\sigma_x < \frac{1}{2T_x}$ $\sigma_y < \frac{1}{2T_y}$. Without loss of

generality, we may relate $f(x, y)$ to its samples by equation (1.50) –

$$\begin{aligned} f(x, y) &= \sum_{p=-\infty}^{\infty} \sum_{q=-\infty}^{\infty} \left[g_1(pT_g^x, qT_g^y) y_1(x - pT_g^x, y - qT_g^y) + \dots + g_m(pT_g^x, qT_g^y) y_m(x - pT_g^x, y - qT_g^y) \right] = \\ &= \sum_{p=-\infty}^{\infty} \sum_{q=-\infty}^{\infty} \sum_{k=1}^m g_k(pT_g^x, qT_g^y) y_k(x - pT_g^x, y - qT_g^y) \end{aligned} \quad (3.27)$$

We recall that this reconstruction equation indicates that $f(x, y)$ was sampled by m linear functionals.

Let us denote the missing samples indices by the set –

$$S = \{(p, q, k = 1)_{11}, (p, q, k = 1)_{12}, \dots, (p, q, k = r)_{r1}, \dots, (p, q, k = m)_{ml}\} \quad (3.28)$$

Examining the equation above, we divide it to a sum of samples we have and missing ones –

$$f(x, y) = \sum_{\{p, q, k\} \notin S} g_k(pT_x, qT_y) y_k(x - pT_x, y - qT_y) + \sum_{\{p, q, k\} \in S} g_k(pT_x, qT_y) y_k(x - pT_x, y - qT_y) \quad (3.29)$$

The values $g_k(pT_x, qT_y)$ in which $\{p, q, k\} \notin S$ are samples which we had before the regularization of the grid. We would like to make sure that a reconstruction is possible without the missing samples $g_k(pT_x, qT_y)$ $\{p, q, k\} \in S$.

We notice that if we integrate the left hand side of (3.29) along the line with the angle θ_k and the length W_k which is located at $(x, y) = (pT_x, qT_y)$ we yield our missing sample which is exactly $g_k(pT_x, qT_y)$.

Applying this integration on the right hand side requires calculating the solution to the GSE linear system which is given in (1.39), which yields the functions $y_k(x, y)$. We may use (1.39) in order to complete the integration of the right hand side –

$$\int_{t \in (p', q', k')} y_k(x - pT_x, y - qT_y) dt = \frac{m}{2\sigma_u} \frac{m}{2\sigma_v} \int_{t \in (p', q', k')} \int_{-\sigma_u}^{-\sigma_u + \frac{2\sigma_u}{m}} \int_{-\sigma_v}^{\sigma_v + \frac{2\sigma_v}{m}} Y_k(u, v, x, y) e^{j(ux+vy)} du dv dt \quad (3.30)$$

Integrating along the line with the angle θ_k and length W_k which is located at

$(x, y) = (pT_x, qT_y)$ is denoted by $\int_{t \in (p', q', k')} y_k(.) dt$.

Let us denote the results of the integration by –

$$\int_{t \in (p', q', k')} y_k(x, y) dt \triangleq A_{k'kpq'} \quad (3.31)$$

where the indices (p', q', k') are the appropriate indices given to the missing sample in S . e.g. – if we were to integrate the fourth functional along a line which corresponds to the missing sample $(1, 2, 3)_{35}$ we would yield A_{3412} .

After integration along the k' sampling functional we yield equations of the form -

$$g_{k'}(pT_x, qT_y) = \sum_{\{p, q, k\} \notin S} g_k(pT_x, qT_y) A_{k'kpq} + \sum_{\{p, q, k\} \in S} g_k(pT_x, qT_y) A_{k'kpq} \quad (3.32)$$

where the sum over $\{p, q, k\} \notin S$ may be fully evaluated since $g_k(pT_x, qT_y)$ in which $\{p, q, k\} \notin S$ are samples which we had before the regularization of the grid. Hence, we may write (3.32) as –

$$g_{k'}(pT_x, qT_y) = h_{k'} + \sum_{\{p, q, k\} \in S} g_k(pT_x, qT_y) A_{k'kpq} \quad (3.33)$$

This is a set of linear equations which solution yields the missing samples $g_{k'}(pT_x, qT_y) \{p, q, k\} \in S$. Writing this in matrix form gives us –

$$\begin{aligned}\vec{g}_1 &= h_1 + \sum_k \vec{g}_k \mathbf{A}_{1k} \\ &\vdots \\ \vec{g}_k &= h_k + \sum_k \vec{g}_k \mathbf{A}_{kk}\end{aligned}\tag{3.34}$$

Where the elements of the matrix \mathbf{A}_{kk} are $A_{k'kpq}$.

Defining the vectors –

$$\vec{g} = (\vec{g}_1, \dots, \vec{g}_k)^T\tag{3.35}$$

and

$$\vec{h} = (\vec{h}_1, \dots, \vec{h}_k)^T\tag{3.36}$$

enable displaying the set of equations in (3.34) as the *augmented matrix* –

$$\mathbf{M}\vec{g} = \vec{h}\tag{3.37}$$

Where \mathbf{M} is called the *augmented matrix* and is given by –

$$\mathbf{M} = \left(\begin{array}{c|c|c|c|c} \mathbf{I} - \mathbf{A}_{11} & -\mathbf{A}_{12} & -\mathbf{A}_{13} & \cdots & -\mathbf{A}_{1m} \\ \hline -\mathbf{A}_{21} & \mathbf{I} - \mathbf{A}_{22} & \cdots & \cdots & -\mathbf{A}_{2m} \\ \hline -\mathbf{A}_{31} & \vdots & \mathbf{I} - \mathbf{A}_{33} & \ddots & -\mathbf{A}_{3m} \\ \hline \vdots & \vdots & \ddots & \ddots & \vdots \\ \hline -\mathbf{A}_{m1} & -\mathbf{A}_{m2} & -\mathbf{A}_{m3} & \cdots & \mathbf{I} - \mathbf{A}_{mm} \end{array} \right)\tag{3.38}$$

If the augmented matrices' determinant is non-zero we may restore the missing samples by using the ones we have. This is by virtue of the fact that the function has been over-sampled.

3.1.8 Missing Samples - An Example

I now apply the missing samples formalism which we devised in the previous section on the following regularized grid -

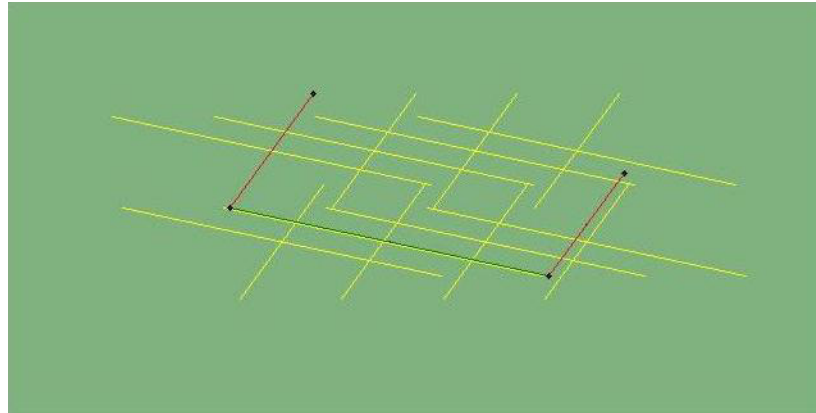


Figure 13 – Missing Samples Example

In this example we have two types of sampling functionals from which we have two samples of the first one and only one sample of the second one.

Due to the fact that we have two sampling functionals, we may write the reconstruction formula as (note: on the following section we denoted $f_1(\cdot) \triangleq g_1(\cdot), f_2(\cdot) \triangleq g_2(\cdot)$)-

$$f(x, y) = \sum_{m,n} f_1(m, n) y_1(x-m, y-n) + f_2(m, n) y_2(x-m, y-n) \quad (3.39)$$

And in explicit form –

$$\begin{aligned} f(x, y) = & f_1(1,1) y_1(x-1, y-1) + f_2(1,1) y_2(x-1, y-1) + \\ & f_1(1,2) y_1(x-1, y-2) + f_2(1,2) y_2(x-1, y-2) + \\ & f_1(2,1) y_1(x-2, y-1) + f_2(2,1) y_2(x-2, y-1) + \\ & f_1(2,2) y_1(x-2, y-2) + f_2(2,2) y_2(x-2, y-2) + \\ & f_1(3,1) y_1(x-3, y-1) + f_2(3,1) y_2(x-3, y-1) + \\ & f_1(3,2) y_1(x-3, y-2) + f_2(3,2) y_2(x-3, y-2) + \\ & f_1(4,1) y_1(x-4, y-1) + f_2(4,1) y_2(x-4, y-1) + \\ & f_1(4,2) y_1(x-4, y-2) + f_2(4,2) y_2(x-4, y-2) \end{aligned} \quad (3.40)$$

We now explicitly write the values of the function at each sample location –

Table 5 – Missing Samples an Example

The samples we have are $f_1(2,2), f_2(1,1), f_2(4,2)$ as the red lines in Figure 13 suggests. We write the equations above as a linear system which divides between the known samples and the unknown samples – $\vec{f} = \vec{h} + A_1 \vec{f}_1 + A_2 \vec{f}_2$

$$\begin{aligned}
& \begin{pmatrix} f(1,1) \\ f(1,2) \\ f(2,1) \\ f(2,2) \\ f(3,1) \\ f(3,2) \\ f(4,1) \\ f(4,2) \end{pmatrix} = \begin{pmatrix} f_1(2,2)y_1(1-2,1-2) + f_2(1,1)y_2(1-1,1-1) + f_2(4,2)y_2(1-4,1-2) \\ f_1(2,2)y_1(1-2,2-2) + f_2(1,1)y_2(1-1,2-1) + f_2(4,2)y_2(1-4,2-2) \\ f_1(2,2)y_1(2-2,1-2) + f_2(1,1)y_2(2-1,1-1) + f_2(4,2)y_2(2-4,1-2) \\ f_1(2,2)y_1(2-2,2-2) + f_2(1,1)y_2(2-1,2-1) + f_2(4,2)y_2(2-4,2-2) \\ f_1(2,2)y_1(3-2,1-2) + f_2(1,1)y_2(3-1,1-1) + f_2(4,2)y_2(3-4,1-2) \\ f_1(2,2)y_1(3-2,2-2) + f_2(1,1)y_2(3-1,2-1) + f_2(4,2)y_2(3-4,2-2) \\ f_1(2,2)y_1(4-2,1-2) + f_2(1,1)y_2(4-1,1-1) + f_2(4,2)y_2(4-4,1-2) \\ f_1(2,2)y_1(4-2,2-2) + f_2(1,1)y_2(4-1,2-1) + f_2(4,2)y_2(4-4,2-2) \end{pmatrix} + \\
& \quad \begin{pmatrix} y_1(1-1,1-1) & y_1(1-1,1-2) & y_1(1-2,1-1) & y_1(1-3,1-1) & y_1(1-3,1-2) & y_1(1-4,1-1) & y_1(1-4,1-2) \\ y_1(1-1,2-1) & y_1(1-1,2-2) & y_1(1-2,2-1) & y_1(1-3,2-1) & y_1(1-3,2-2) & y_1(1-4,2-1) & y_1(1-4,2-2) \\ y_1(2-1,1-1) & y_1(2-1,1-2) & y_1(2-2,1-1) & y_1(2-3,1-1) & y_1(2-3,1-2) & y_1(2-4,1-1) & y_1(2-4,1-2) \\ y_1(2-1,2-1) & y_1(2-1,2-2) & y_1(2-2,2-1) & y_1(2-3,2-1) & y_1(2-3,2-2) & y_1(2-4,2-1) & y_1(2-4,2-2) \\ y_1(3-1,1-1) & y_1(3-1,1-2) & y_1(3-2,1-1) & y_1(3-3,1-1) & y_1(3-3,1-2) & y_1(3-4,1-1) & y_1(3-4,1-2) \\ y_1(3-1,2-1) & y_1(3-1,2-2) & y_1(3-2,2-1) & y_1(3-3,2-1) & y_1(3-3,2-2) & y_1(3-4,2-1) & y_1(3-4,2-2) \\ y_1(4-1,1-1) & y_1(4-1,1-2) & y_1(4-2,1-1) & y_1(4-3,1-1) & y_1(4-3,1-2) & y_1(4-4,1-1) & y_1(4-4,1-2) \\ y_1(4-1,2-1) & y_1(4-1,2-2) & y_1(4-2,2-1) & y_1(4-3,2-1) & y_1(4-3,2-2) & y_1(4-4,2-1) & y_1(4-4,2-2) \end{pmatrix} \begin{pmatrix} f_1(1,1) \\ f_1(1,2) \\ f_1(2,1) \\ f_1(3,1) \\ f_1(3,2) \\ f_1(4,1) \\ f_1(4,2) \end{pmatrix} + \\
& \quad + \begin{pmatrix} y_2(1-1,1-2) & y_2(1-2,1-1) & y_2(1-2,1-2) & y_2(1-3,1-1) & y_2(1-3,1-2) & y_2(1-4,1-1) \\ y_2(1-1,2-2) & y_2(1-2,2-1) & y_2(1-2,2-2) & y_2(1-3,2-1) & y_2(1-3,2-2) & y_2(1-4,2-1) \\ y_2(2-1,1-2) & y_2(2-2,1-1) & y_2(2-2,1-2) & y_2(2-3,1-1) & y_2(2-3,1-2) & y_2(2-4,1-1) \\ y_2(2-1,2-2) & y_2(2-2,2-1) & y_2(2-2,2-2) & y_2(2-3,2-1) & y_2(2-3,2-2) & y_2(2-4,2-1) \\ y_2(3-1,1-2) & y_2(3-2,1-1) & y_2(3-2,1-2) & y_2(3-3,1-1) & y_2(3-3,1-2) & y_2(3-4,1-1) \\ y_2(3-1,2-2) & y_2(3-2,2-1) & y_2(3-2,2-2) & y_2(3-3,2-1) & y_2(3-3,2-2) & y_2(3-4,2-1) \\ y_2(4-1,1-2) & y_2(4-2,1-2) & y_2(4-2,1-1) & y_2(4-3,1-1) & y_2(4-3,1-2) & y_2(4-4,1-1) \\ y_2(4-1,2-2) & y_2(4-2,2-2) & y_2(4-2,2-1) & y_2(4-3,2-1) & y_2(4-3,2-2) & y_2(4-4,2-1) \end{pmatrix} \begin{pmatrix} f_2(1,2) \\ f_2(2,1) \\ f_2(2,2) \\ f_2(3,1) \\ f_2(3,2) \\ f_2(4,1) \end{pmatrix} \quad (3.41)
\end{aligned}$$

We would like to find the samples \vec{f}_1 and \vec{f}_2 (which total in 13 missing samples as the yellow lines in Figure 13 suggests). For this purpose we write the equations above in this form but before plugging in the values of x and y .

This enables us to first integrate and then yield interesting results in the LHS of the system of equations.

The equations which we yield by integrating the equation along the first type of functional are-

$$\begin{pmatrix} f_1(1,1) \\ f_1(1,2) \\ f_1(2,1) \\ f_1(2,2) \\ f_1(3,1) \\ f_1(3,2) \\ f_1(4,1) \\ f_1(4,2) \end{pmatrix} = \begin{pmatrix} f_i(2,2)A_{1122} + f_2(1,1)A_{1211} + f_2(4,2)A_{1242} \\ f_i(2,2)A_{1122} + f_2(1,1)A_{1211} + f_2(4,2)A_{1242} \end{pmatrix} + \begin{pmatrix} A_{1111} & A_{1122} & A_{1121} & A_{1131} & A_{1132} & A_{1141} & A_{1142} \\ A_{1111} & A_{1122} & A_{1121} & A_{1131} & A_{1132} & A_{1141} & A_{1142} \\ A_{1111} & A_{1122} & A_{1121} & A_{1131} & A_{1132} & A_{1141} & A_{1142} \\ A_{1111} & A_{1122} & A_{1121} & A_{1131} & A_{1132} & A_{1141} & A_{1142} \\ A_{1111} & A_{1122} & A_{1121} & A_{1131} & A_{1132} & A_{1141} & A_{1142} \\ A_{1111} & A_{1122} & A_{1121} & A_{1131} & A_{1132} & A_{1141} & A_{1142} \\ A_{1111} & A_{1122} & A_{1121} & A_{1131} & A_{1132} & A_{1141} & A_{1142} \\ A_{1111} & A_{1122} & A_{1121} & A_{1131} & A_{1132} & A_{1141} & A_{1142} \end{pmatrix} \begin{pmatrix} f_i(1,1) \\ f_i(1,2) \\ f_i(2,1) \\ f_i(3,1) \\ f_i(3,2) \\ f_i(4,1) \\ f_i(4,2) \end{pmatrix} + \\
+ \begin{pmatrix} A_{1212} & A_{1221} & A_{1222} & A_{1231} & A_{1232} & A_{1241} \\ A_{1212} & A_{1221} & A_{1222} & A_{1231} & A_{1232} & A_{1241} \\ A_{1212} & A_{1221} & A_{1222} & A_{1231} & A_{1232} & A_{1241} \\ A_{1212} & A_{1221} & A_{1222} & A_{1231} & A_{1232} & A_{1241} \\ A_{1212} & A_{1221} & A_{1222} & A_{1231} & A_{1232} & A_{1241} \\ A_{1212} & A_{1221} & A_{1222} & A_{1231} & A_{1232} & A_{1241} \\ A_{1212} & A_{1221} & A_{1222} & A_{1231} & A_{1232} & A_{1241} \\ A_{1212} & A_{1221} & A_{1222} & A_{1231} & A_{1232} & A_{1241} \end{pmatrix} \begin{pmatrix} f_2(1,2) \\ f_2(2,1) \\ f_2(2,2) \\ f_2(3,1) \\ f_2(3,2) \\ f_2(4,1) \\ f_2(4,2) \end{pmatrix} \quad (3.42)$$

The equations which we yield by integrating the equations along the second type of functional are of similar form and are given by -

$$\begin{aligned}
& \begin{pmatrix} f_2(1,1) \\ f_2(1,2) \\ f_2(2,1) \\ f_2(2,2) \\ f_2(3,1) \\ f_2(3,2) \\ f_2(4,1) \\ f_2(4,2) \end{pmatrix} = \begin{pmatrix} f_1(2,2)A_{2122} + f_2(1,1)A_{2211} + f_2(4,2)A_{2242} \\ f_1(2,2)A_{2122} + f_2(1,1)A_{2211} + f_2(4,2)A_{2242} \end{pmatrix} + \\
& \quad + \begin{pmatrix} A_{2111} & A_{2112} & A_{2121} & A_{2131} & A_{2132} & A_{2141} & A_{2142} \\ A_{2111} & A_{2112} & A_{2121} & A_{2131} & A_{2132} & A_{2141} & A_{2142} \\ A_{2111} & A_{2112} & A_{2121} & A_{2131} & A_{2132} & A_{2141} & A_{2142} \\ A_{2111} & A_{2112} & A_{2121} & A_{2131} & A_{2132} & A_{2141} & A_{2142} \\ A_{2111} & A_{2112} & A_{2121} & A_{2131} & A_{2132} & A_{2141} & A_{2142} \\ A_{2111} & A_{2112} & A_{2121} & A_{2131} & A_{2132} & A_{2141} & A_{2142} \\ A_{2111} & A_{2112} & A_{2121} & A_{2131} & A_{2132} & A_{2141} & A_{2142} \\ A_{2111} & A_{2112} & A_{2121} & A_{2131} & A_{2132} & A_{2141} & A_{2142} \end{pmatrix} \begin{pmatrix} f_1(1,1) \\ f_1(1,2) \\ f_1(2,1) \\ f_1(3,1) \\ f_1(3,2) \\ f_1(4,1) \\ f_1(4,2) \end{pmatrix} \\
& \quad + \\
& \quad + \begin{pmatrix} A_{2212} & A_{2221} & A_{2222} & A_{2231} & A_{2232} & A_{2241} \\ A_{2212} & A_{2221} & A_{2222} & A_{2231} & A_{2232} & A_{2241} \\ A_{2212} & A_{2221} & A_{2222} & A_{2231} & A_{2232} & A_{2241} \\ A_{2212} & A_{2221} & A_{2222} & A_{2231} & A_{2232} & A_{2241} \\ A_{2212} & A_{2221} & A_{2222} & A_{2231} & A_{2232} & A_{2241} \\ A_{2212} & A_{2221} & A_{2222} & A_{2231} & A_{2232} & A_{2241} \\ A_{2212} & A_{2221} & A_{2222} & A_{2231} & A_{2232} & A_{2241} \end{pmatrix} \begin{pmatrix} f_2(1,2) \\ f_2(2,1) \\ f_2(2,2) \\ f_2(3,1) \\ f_2(3,2) \\ f_2(4,1) \\ f_2(4,2) \end{pmatrix} \quad (3.43)
\end{aligned}$$

From these equations we can generate a system of equations which will enable us to reveal whether we may reconstruct the signal by checking the determinant of this system. The new system of equations will be built by choosing a subset of equations out of the ones we showed above. We choose only those equations which have a missing sample appearing on the RHS. This will give us exactly 13 equations.

This in fact is the process which yields the augmented matrix which in this case is –

$$\mathbf{M} \begin{pmatrix} f_1 \\ f_2 \end{pmatrix} = \begin{pmatrix} h_1 \\ h_2 \end{pmatrix} \quad \mathbf{M} = \left(\begin{array}{c|c} \mathbf{I} - \mathbf{A}_{11} & -\mathbf{A}_{12} \\ \hline -\mathbf{A}_{21} & \mathbf{I} - \mathbf{A}_{22} \end{array} \right) \quad (3.44)$$

The dimensions of the matrices \mathbf{A}_{ij} are determined by the amount of missing samples from each sampling functional. In this example their dimensions are given by –

$$[\mathbf{A}_{11}] = 7 \times 7, [\mathbf{A}_{12}] = 7 \times 6, [\mathbf{A}_{21}] = 6 \times 7, [\mathbf{A}_{22}] = 6 \times 6 \quad (3.45)$$

Due to the fact that we have 7 missing samples from the first sampling functional and 6 from the second. A numerical calculation of the determinant of \mathbf{M} may prove that it is identically

zero, a case in which we cannot reconstruct the missing samples from the ones we have. This is a sensible result due to the fact that we are missing a very large amount of samples.

3.1.9 Integrating the 3 Phases

In sections 3.1.3, 3.1.5 and 3.1.7 I have described a procedure with which one may test if a concrete realization of the Arbitrary Line Projections sampling scheme renders a reconstructable function. These tests involve the following stages –

1. Identify the linear sampling functionals after choosing Δ_θ, Δ_w
2. Calculate the GSE determinant using these functionals and ensure it is non-zero for every frequency in $\psi = [-\sigma_u, -\sigma_u + c_u] \times [-\sigma_v, -\sigma_v + c_v]$
3. Regularize the non-regular grid using the sampling functionals.
4. Identify the missing samples and calculate the augmented matrix \mathbf{M}
5. Ensure the determinant of \mathbf{M} is non-zero
6. **If all of the tests above have passed we proclaim the sampled function to be reconstructable**

3.1.10 Computational Complexity of the Solution

3.1.10.1 Definitions and Notations

As stated in section 3.1.9, applying our solution to the problem of identifying sampling schemes which yield reconstructable functions involve three phases. These are; identifying the sampling functionals and regularizing the grid, calculating the GSE matrix and evaluating its determinant and finally, calculating the augmented matrix and ensuring that it is non singular by evaluating its determinant.

Let us use the following notations for the sake of developing analytical terms which determine our computational complexity -

| Term | Explanation |
|-------------------------------|---|
| m | Number of distinct sampling functionals |
| n | Number of samples |
| ρ | Ratio of missing samples |
| $f_j \ j \in \{1, \dots, n\}$ | The j^{th} sample |

| | |
|---------------------------------|---|
| $f_j^x \ j \in \{1, \dots, n\}$ | The j^{th} sample x coordinate |
| $f_j^y \ j \in \{1, \dots, n\}$ | The j^{th} sample y coordinate |
| k | The amount of samples including missing ones (after regularization) |
| Δ_{GSE} | The step size for evaluating the GSE determinant |
| Δ_M | The integration step size for constructing the augmented matrix |

Table 6 – Computational Complexity Terms

3.1.10.2 Complexity of Coping with an irregular grid

The identification of distinct sampling functionals requires checking whether pairs of samples were projected along similar sampling functionals, as suggested in Table 3. This implies that calculating m requires a number of operations which is proportional to –

$$O(n^2) \quad (3.46)$$

Calculating the amount of missing samples requires calculating regularizing the grid, which requires calculating the GCD from n samples. The complexity of calculating the GCD, using Euclid's algorithm is known to be $O\left(\left(\max_i \{\lceil \log_2 a \rceil, \lceil \log_2 b \rceil\}\right)^3\right)$ where a and b are a pair of numbers. In our case, we apply a recursive GCD with the coordinates of our n samples. Hence, the complexity of the regularization phase is –

$$O\left(\left(\max_i \{\lceil \log_2 f_i^x \rceil\}\right)^3\right) \quad (3.47)$$

3.1.10.3 Complexity of the Generalized Sampling Expansion Usage

The GSE matrix dimensions' is $m \times m$. The most straightforward method to calculate a matrices determinant employs the LU decomposition which is known to have a complexity of –

$$O(m^3) \quad (3.48)$$

Let us recall that employing the GSE expansion assumes that $f(x, y)$ is a (σ_x, σ_y) band limited function as defined in (1.33). We must then evaluate its determinant for a set of frequencies in the range which is given by –

$$(u, v) \in (-\sigma_x, -\sigma_x + 2\sigma_x / m) \times (-\sigma_y, -\sigma_y + 2\sigma_y / m) \quad (3.49)$$

Defining the evaluation step size by Δ_{GSE} we have to evaluate the GSE determinant a following number of times –

$$\left(\frac{2\sigma_x}{m\Delta_{GSE}} \cdot \frac{2\sigma_y}{m\Delta_{GSE}} \right) = \frac{4\sigma_x\sigma_y}{(m\Delta_{GSE})^2} \quad (3.50)$$

Considering this together with the complexity of the *LU* decomposition algorithm, gives us the total complexity which is required for evaluating the GSE determinant –

$$O\left(\max\left\{m^3, \frac{1}{(m\Delta_{GSE})^2}\right\}\right) \quad (3.51)$$

3.1.10.4 Complexity of coping with Missing Samples

The last phase which we must employ is the evaluation of the augmented matrices determinant. We assume that once we know the amount and locations of the missing samples, they endure the following relation –

$$k = \frac{n}{\rho} \quad (3.52)$$

This also means that the amount of missing samples is given by-

$$k - n = n \frac{(1-\rho)}{\rho} \quad (3.53)$$

We must then construct a matrix of which dimensions are $(k-n) \times (k-n)$ and evaluate its determinant which yields a complexity of –

$$O((k-n)^3) = O\left(n^3 \frac{(1-\rho)^3}{\rho^3}\right) \quad (3.54)$$

We must calculate $(k-n)^2$ integrals each of which requires three integrations, as suggested in section 3.1.7. We define the integration units as follows –

$$du = \frac{\sigma_x}{\Delta_{GSE}} \quad dv = \frac{\sigma_y}{\Delta_{GSE}} \quad dt = \frac{1}{\Delta_M} \quad (3.55)$$

This implies that the integration along a single missing sample requires –

$$O\left(\left(\frac{1}{m}du\right)\cdot\left(\frac{1}{m}dv\right)\cdot dt\right) = O\left(\frac{4\sigma_x\sigma_y}{\Delta_M(m\Delta_{GSE})^2}\right) \quad (3.56)$$

Finally, the phase of coping with the missing samples is of a complexity of –

$$O\left(\max\left\{\left(k-n\right)^3, \frac{\left(k-n\right)^2}{\Delta_M(m\Delta_{GSE})^2}\right\}\right) \quad (3.57)$$

3.2 Non Reconstructable Geometries

In the following section we discuss different choices of sampling functionals which cannot yield reconstructable functions. Such a prior knowledge on the sampling sets which always yield a reconstructable or non reconstructable function may clearly decrease the complexity of solving the questions regarding the reconstructability, as suggested in section 3.1.10.

3.2.1 Two Equally lengthed Sampling Functionals with Different Angles

Lemma:

No two lines with different angles but with equal lengths will always yield a non reconstructable function in the case of equal horizontal and vertical sampling rates

Proof:

Without loss of generality we choose $\theta_1 = 0$. A different angle is simple a rotation of the axis.

The GSE determinant which must be evaluated is given by –

$$\begin{vmatrix} H_1(u, v) & H_2(u, v) \\ H_1(u + c_x, v + c_y) & H_2(u + c_x, v + c_y) \end{vmatrix} = \begin{vmatrix} \frac{\sin(u)}{u} & \frac{\sin((\cos \theta_2 u + \sin \theta_2 v) + (\cos \theta_2 u + \sin \theta_2 v))}{(\cos \theta_2 u + \sin \theta_2 v)} \\ \frac{\sin((u + c_x))}{((u + c_x))} & \frac{\sin((\cos \theta_2 (u + c_x) + \sin \theta_2 v) + (\cos \theta_2 (u + c_x) + \sin \theta_2 v)))}{(\cos \theta_2 (u + c_x) + \sin \theta_2 v) + (\cos \theta_2 (u + c_x) + \sin \theta_2 v))} \end{vmatrix} \quad (3.58)$$

We evaluate this determinant and yield –

$$\frac{\sin(u)}{u} \frac{\sin((\cos \theta_2 (u + c_x) + \sin \theta_2 v) + (\cos \theta_2 (u + c_x) + \sin \theta_2 v)))}{(\cos \theta_2 (u + c_x) + \sin \theta_2 v) + (\cos \theta_2 (u + c_x) + \sin \theta_2 v))} - \frac{\sin((u + c_x))}{((u + c_x))} \frac{\sin((\cos \theta_2 u + \sin \theta_2 v) + (\cos \theta_2 u + \sin \theta_2 v))}{(\cos \theta_2 u + \sin \theta_2 v)} \quad (3.59)$$

Requiring that this sampling set yields a non reconstructable sampling set means that we can find a set of frequencies which plugging them into the determinant nullifies it. And indeed, choosing,

$$u = v = -\frac{\sigma}{2} \quad (u, v) \in \psi \quad (3.60)$$

Gives us the following -

$$\frac{\sin\left(-\frac{\sigma}{2}\right) \sin\left(\left(\cos \theta_2\left(\frac{-\sigma}{2}+\sigma\right)+\sin \theta_2\left(-\frac{\sigma}{2}+\sigma\right)\right)\right)}{-\frac{\sigma}{2}} - \frac{\sin\left(\left(-\frac{\sigma}{2}+\sigma\right)\right) \sin\left(\left(\cos \theta_2 \frac{-\sigma}{2}+\sin \theta_2 \frac{-\sigma}{2}\right)\right)}{\left(\left(-\frac{\sigma}{2}+\sigma\right)\right)} = 0 \quad (3.61)$$

Manipulating these equations gives –

$$\frac{-\sin\left(\frac{\sigma}{2}\right) \sin\left(\left(\cos \theta_2\left(\frac{\sigma}{2}\right)+\sin \theta_2\left(\frac{\sigma}{2}\right)\right)\right)}{-\frac{\sigma}{2}} - \frac{\sin\left(\frac{\sigma}{2}\right) \sin\left(\left(\cos \theta_2\left(\frac{-\sigma}{2}\right)+\sin \theta_2\left(\frac{-\sigma}{2}\right)\right)\right)}{\left(\frac{\sigma}{2}\right)} = 0 \quad (3.62)$$

$$\frac{\sin\left(\left(\cos \theta_2\left(\frac{\sigma}{2}\right)+\sin \theta_2\left(\frac{\sigma}{2}\right)\right)\right)}{\left(\cos \theta_2\left(\frac{\sigma}{2}\right)+\sin \theta_2\left(\frac{\sigma}{2}\right)\right)} - \frac{-\sin\left(\left(\cos \theta_2\left(\frac{\sigma}{2}\right)+\sin \theta_2\left(\frac{\sigma}{2}\right)\right)\right)}{-\left(\cos \theta_2\left(\frac{\sigma}{2}\right)+\sin \theta_2\left(\frac{\sigma}{2}\right)\right)} = 0 \quad (3.63)$$

$$\frac{\sin\left(\left(\cos\theta_2\left(\frac{\sigma}{2}\right) + \sin\theta_2\left(\frac{\sigma}{2}\right)\right)\right)}{\left(\cos\theta_2\left(\frac{\sigma}{2}\right) + \sin\theta_2\left(\frac{\sigma}{2}\right)\right)} - \frac{\sin\left(\left(\cos\theta_2\left(\frac{\sigma}{2}\right) + \sin\theta_2\left(\frac{\sigma}{2}\right)\right)\right)}{\left(\cos\theta_2\left(\frac{\sigma}{2}\right) + \sin\theta_2\left(\frac{\sigma}{2}\right)\right)} = 0 \quad (3.64)$$

This proves that for a sampling set which is composed of two lines with similar length but with different angles, no reconstruction of a band limited function can be achieved.

3.2.2 Two Different lengthed Sampling Functionals with 90 deg apart

Lemma:

No two lines with different lengths but with an angle of 90° between them will always yield a non reconstructable function

Proof:

Without loss of generality we choose $\theta_1 = 0$. A different angle is simply a rotation of the axis.

The GSE determinant which must be evaluated is given by –

$$\begin{vmatrix} \frac{\sin(uW_1/2)}{uW_1/2} & \frac{\sin(vW_2/2)}{vW_2/2} \\ \frac{\sin((u+c_x)W_1/2)}{(u+c_x)W_1/2} & \frac{\sin((v+c_y)W_2/2)}{(v+c_y)W_2/2} \end{vmatrix} = \frac{\sin(uW_1/2)}{uW_1/2} \frac{\sin((v+c_y)W_2/2)}{(v+c_y)W_2/2} - \frac{\sin(vW_2/2)}{vW_2/2} \frac{\sin((u+c_x)W_1/2)}{(u+c_x)W_1/2} \quad (3.65)$$

We evaluate this determinant and yield –

$$\frac{\sin(uW_1/2)}{u} \frac{\sin((v+c_y)W_2/2)}{(v+c_y)} - \frac{\sin(vW_2/2)}{v} \frac{\sin((u+c_x)W_1/2)}{(u+c_x)} \quad (3.66)$$

Requiring that this sampling set yields a non reconstructable sampling set means that we can find a set of frequencies which plugging them into the determinant nullifies it. And indeed, choosing,

$$u = -\frac{\sigma_x}{2}, v = -\frac{\sigma_y}{2} \quad (u, v) \in \psi \quad (3.67)$$

Gives us the following -

$$\frac{\sin\left(-\frac{\sigma_x}{2}W_1/2\right)\sin\left(\left(-\frac{\sigma_y}{2}+\sigma_y\right)W_2/2\right)}{-\frac{\sigma_x}{2}} - \frac{\sin\left(-\frac{\sigma_y}{2}W_2/2\right)\sin\left(\left(-\frac{\sigma_x}{2}+\sigma_x\right)W_1/2\right)}{-\frac{\sigma_y}{2}} \quad (3.68)$$

Manipulating these equations gives –

$$\frac{\sin\left(\frac{\sigma_x}{2}W_1/2\right)\sin\left(\left(\frac{\sigma_y}{2}\right)W_2/2\right)}{\frac{\sigma_x}{2}} - \frac{\sin\left(\frac{\sigma_y}{2}W_2/2\right)\sin\left(\left(\frac{\sigma_x}{2}\right)W_1/2\right)}{\frac{\sigma_y}{2}} = 0 \quad (3.69)$$

This proves that for a sampling set which is composed of two lines with different lengths but with an angle of 90° apart, no reconstruction of a band limited function can be achieved.

4 Application

4.1 Coverage

The following figures depict the results of an implementation of a tool which receives link coordinates, quantization values and lengths at its input and generates coverage maps. The tool enables setting the generalized ellipse's parameters as the cloud profile. It also enables choosing the power law coefficients.

We applied the simulations below on a set of links from the Israeli cellular service provider named Cellcom. These included a set of 3515 links. We chose the power law coefficients as $a = 0.15$ $b = 1.09$ due to the fact that the links operate at frequencies ranging at around $27Ghz$.

We also simulated threshold maps as discussed in the previous section.

One may easily notice that the cloud's profile vastly affects the size of the areas which are *undetectable* or *out of coverage*. This tool gives an insight on the locations where rain gauges or other rain monitoring equipment must be added in order to achieve a flawless system. We discuss this issue more in depth in following section.

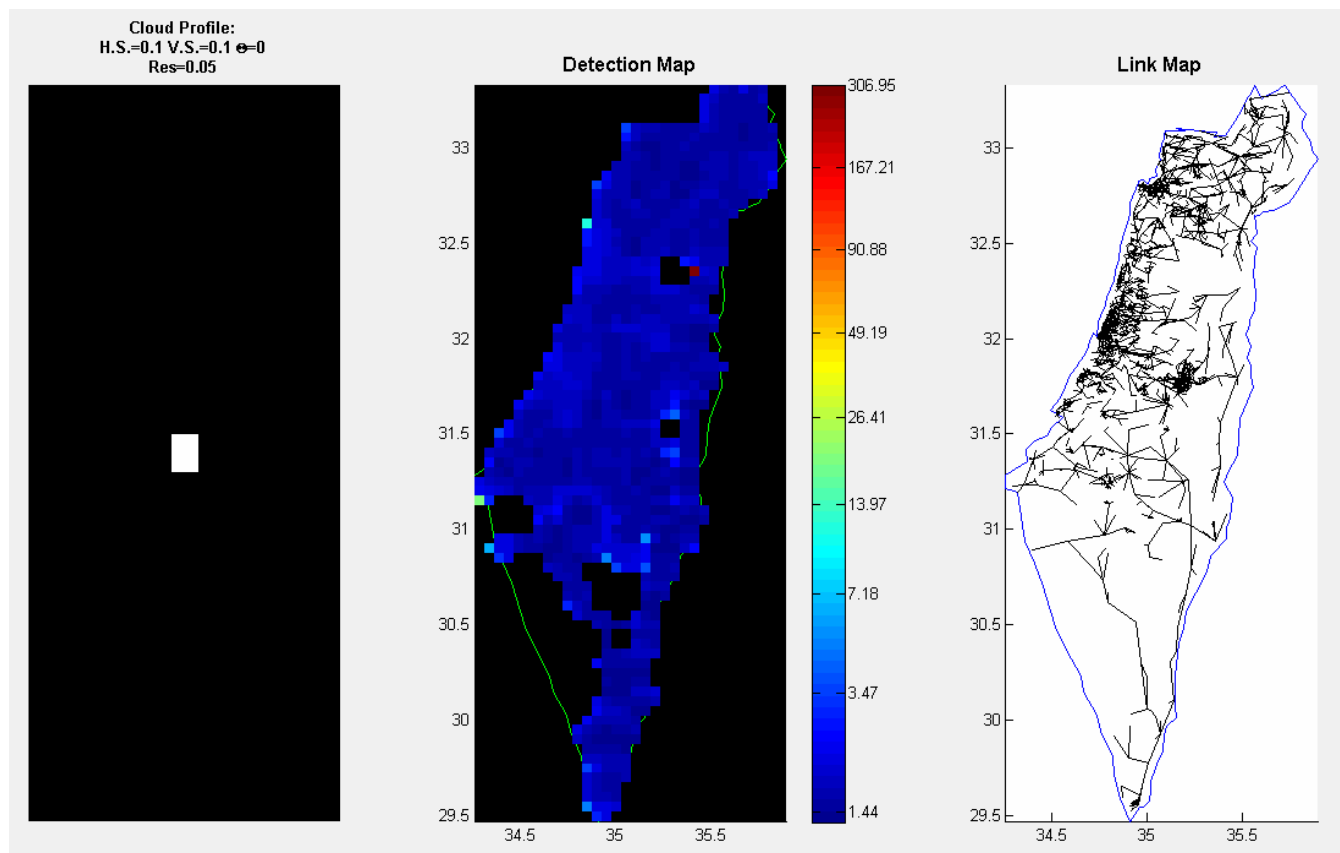


Figure 14 –Coverage Map I

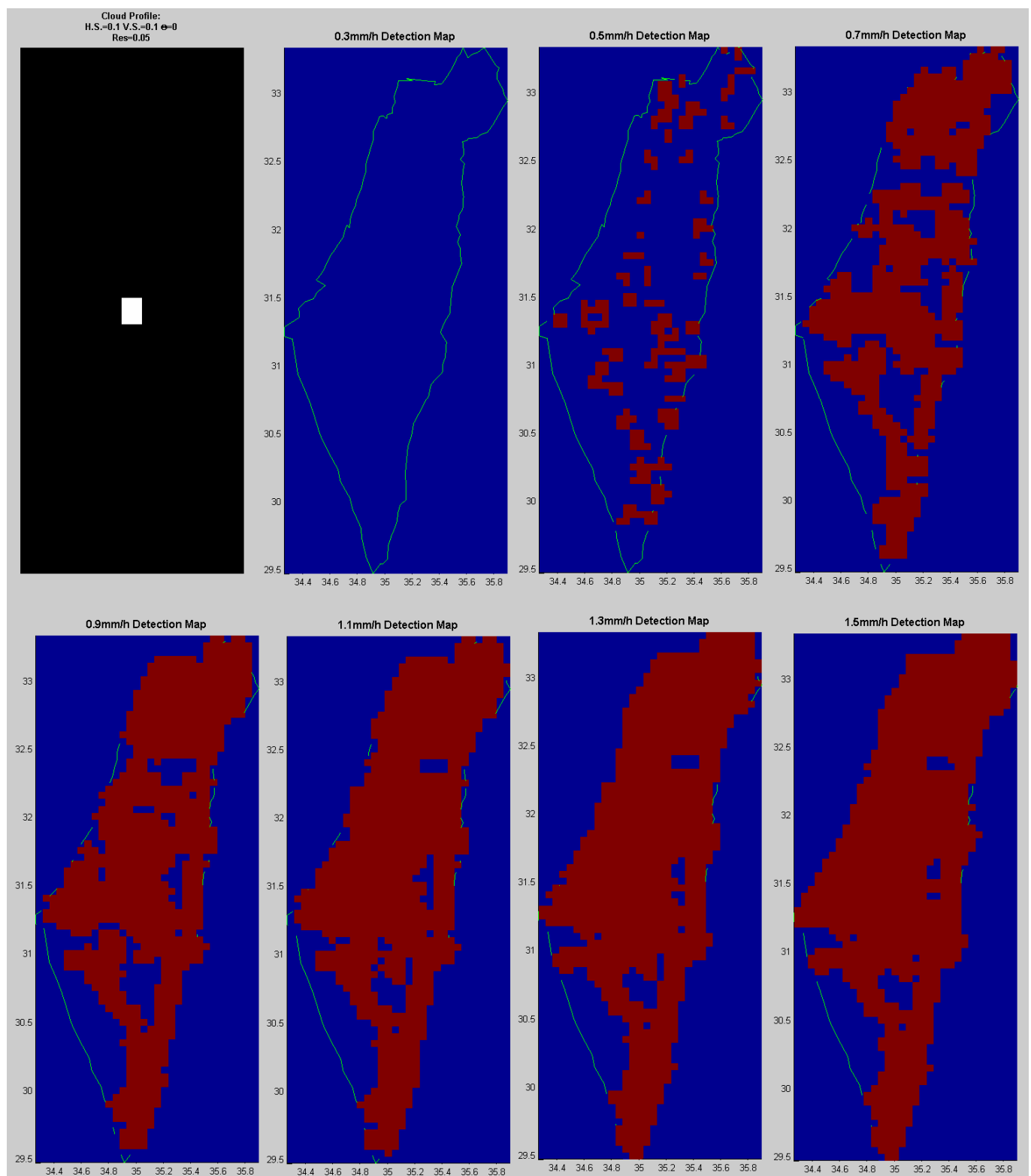


Figure 15 – Coverage Threshold Map I

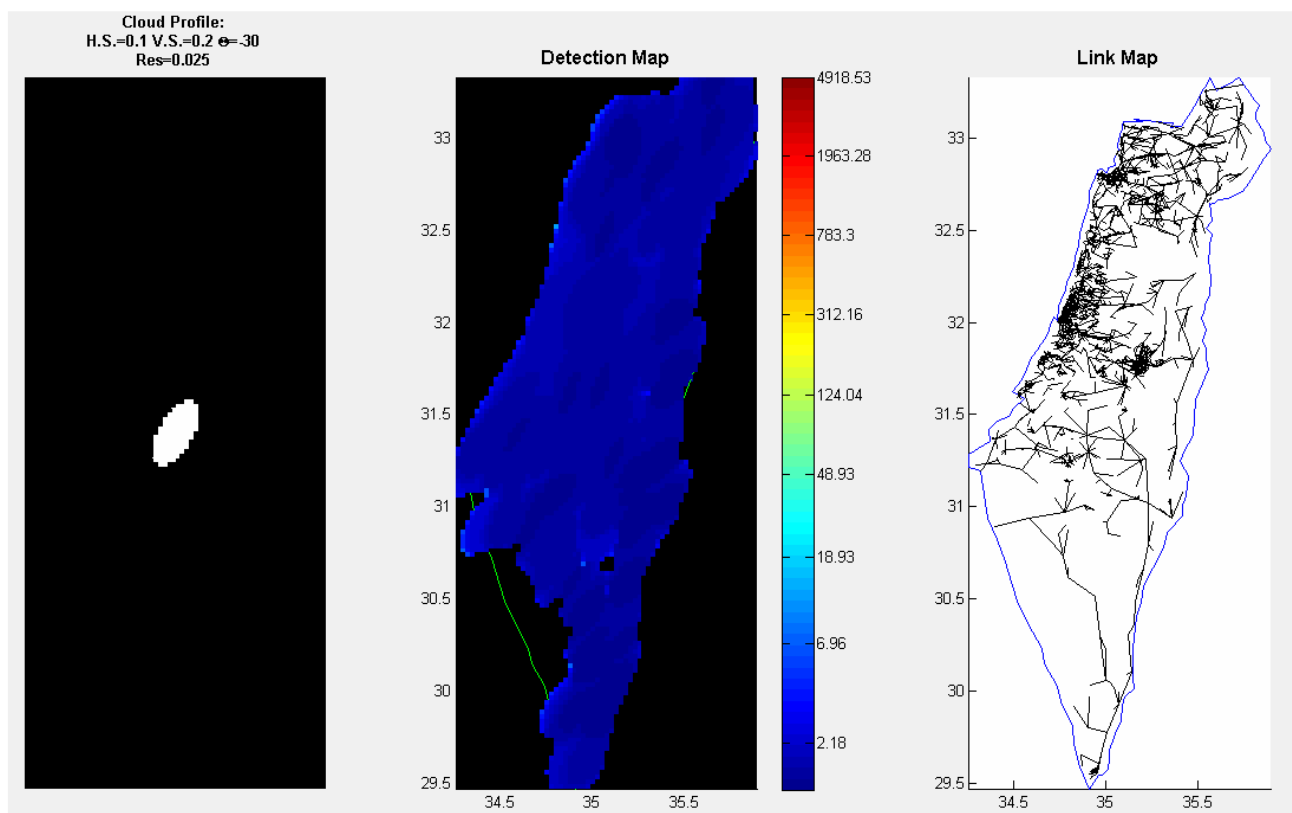


Figure 16 – Coverage Map II

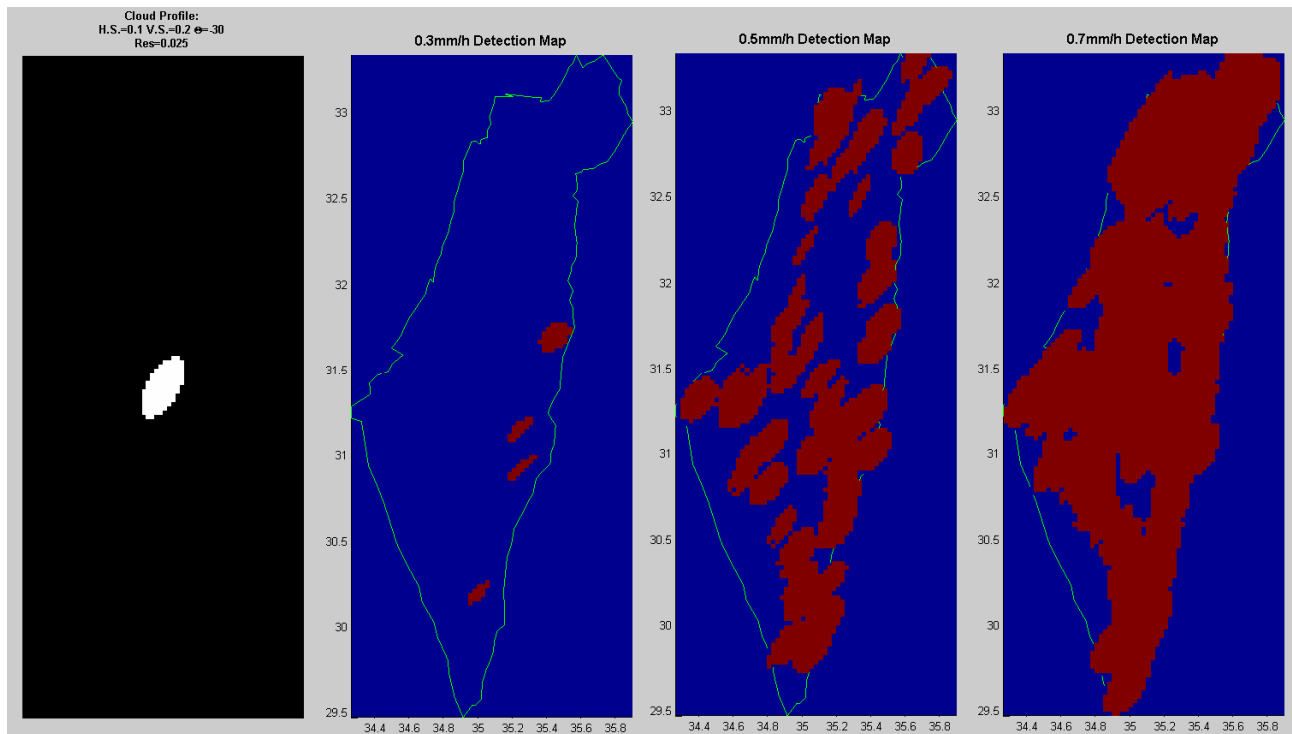


Figure 17 – Coverage Threshold Map II

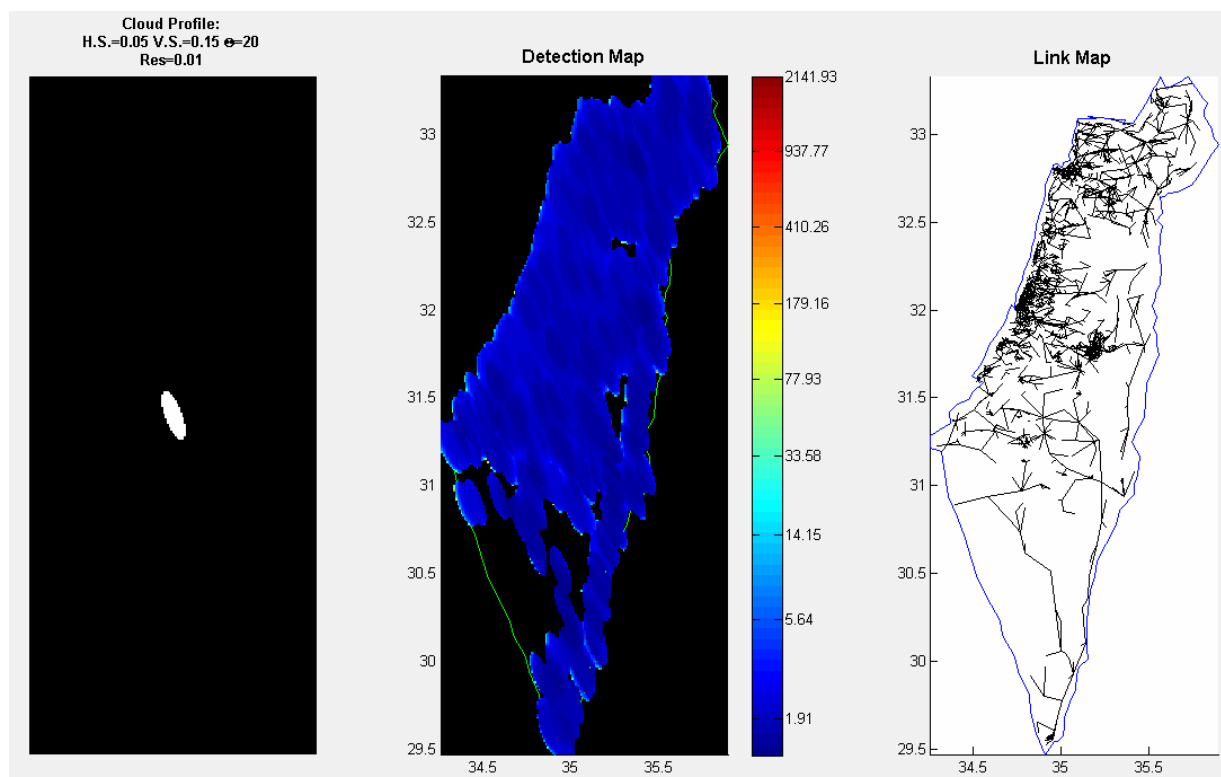


Figure 18 – Coverage Map III

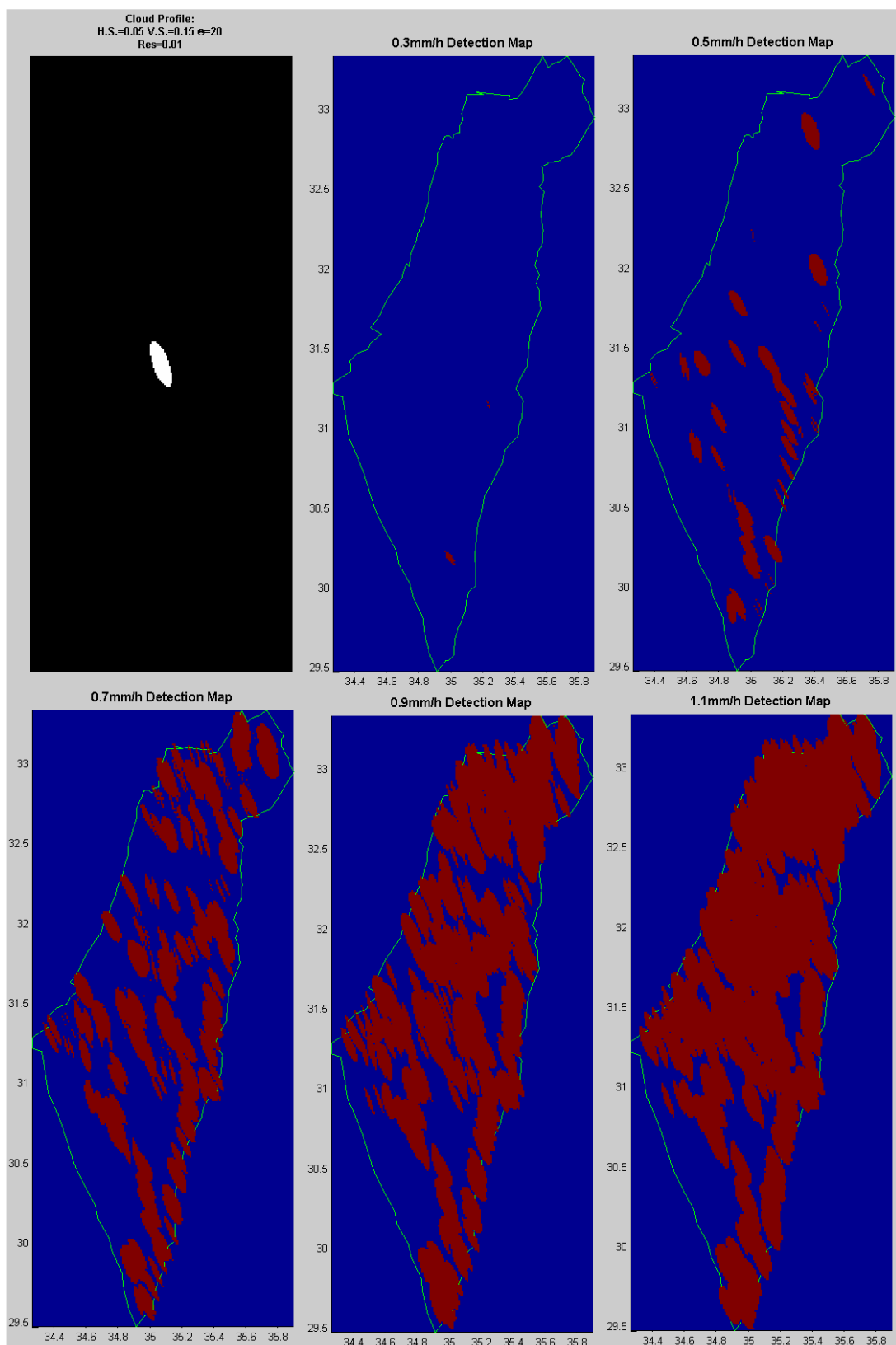


Figure 19 – Coverage Threshold Map III

4.1.1 Sensitivity to Network Parameters

The problem of constructing a rain map via CWN as discussed in section 2.1 involves choosing or determining the rain profile which is of interest. Given a set of links one may then apply the procedure which was presented in section 4.1 for the sake of locating the undetectable regions or areas out of coverage.

Once undetectable regions were located, one may choose to apply a number of actions in order to improve the detection coverage:

1. Increase the operational frequencies of the existing links. This in turn will yield a higher sensitivity of the links to the rain rate, as is depicted in Figure 5.
2. Increase the length of the existing links. This will assist in reaching the quantization level and will enable covering more areas. However this will assist only in cases where the cloud profile is larger than the existing links and where increasing the line length will cause an increase in the line intersection.
3. Decrease the quantization of the links and by such increase the links' sensitivity to detecting rain
4. Add links in areas which are out of coverage

In Figure 20 we simulate the effect of choosing a different operational frequency. The left figure depicts the minimal detected rain in case the links operate at a frequency of 5 GHz, the middle figure includes links operating at a frequency of 25 GHz and the right most figures includes links operating at a frequency of 40Ghz.

In Figure 21 we simulate the effect of choosing a different quantization. The left figure depicts the minimal detected rain in case the links operate at a quantization of 1dB and right figure includes links operating at a quantization of 0.1dB.

In Figure 22 and Figure 23 we show the thresholded maps of Figure 20 and Figure 21 respectively.

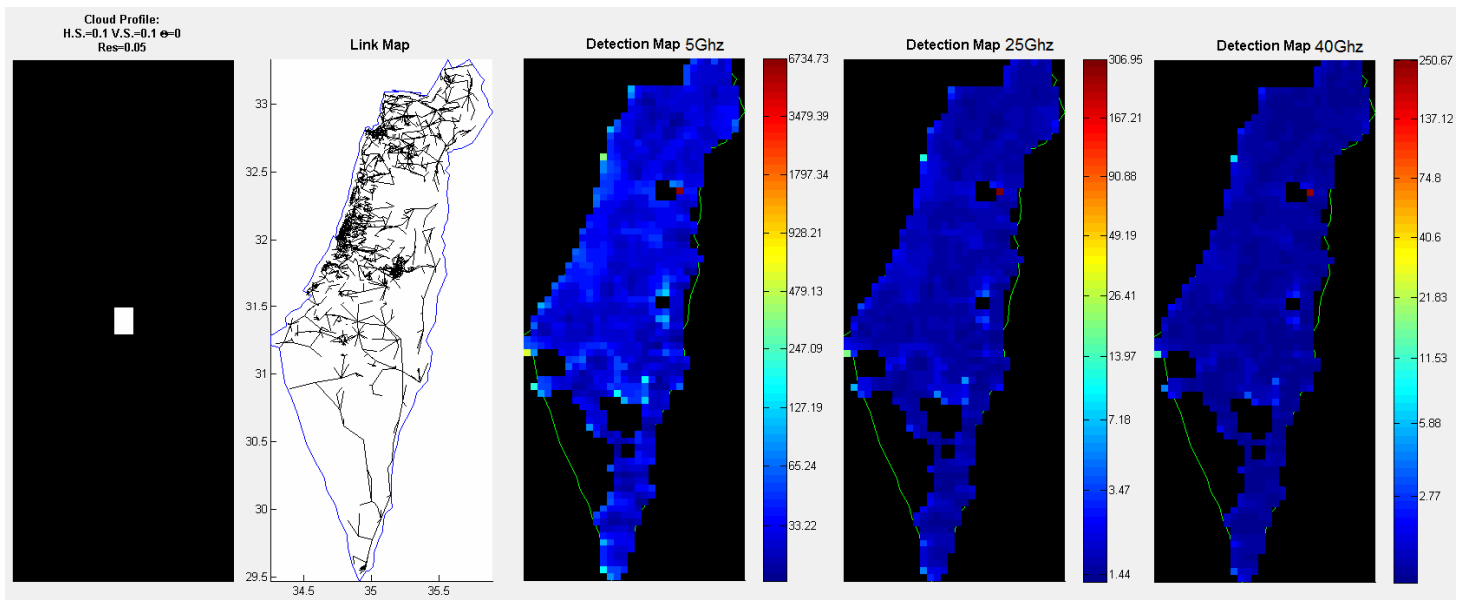


Figure 20 – Improving the Coverage – Links Operational Frequency

Figure 20 clearly shows the fact that as the operational frequency increases, so does the sensitivity to the rain rate.

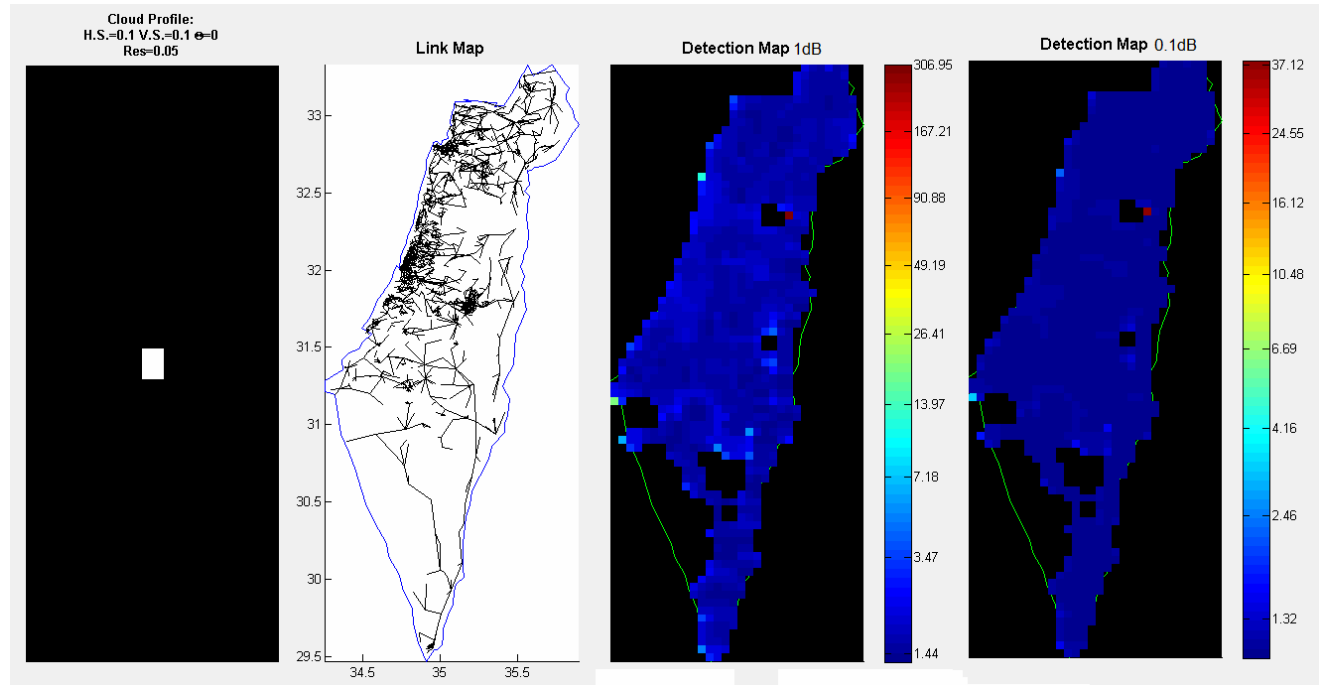


Figure 21 – Improving the Coverage – Links Operational Quantization

Figure 21 clearly shows the fact that as the quantization decreases, the sensitivity to the rain rate increases.

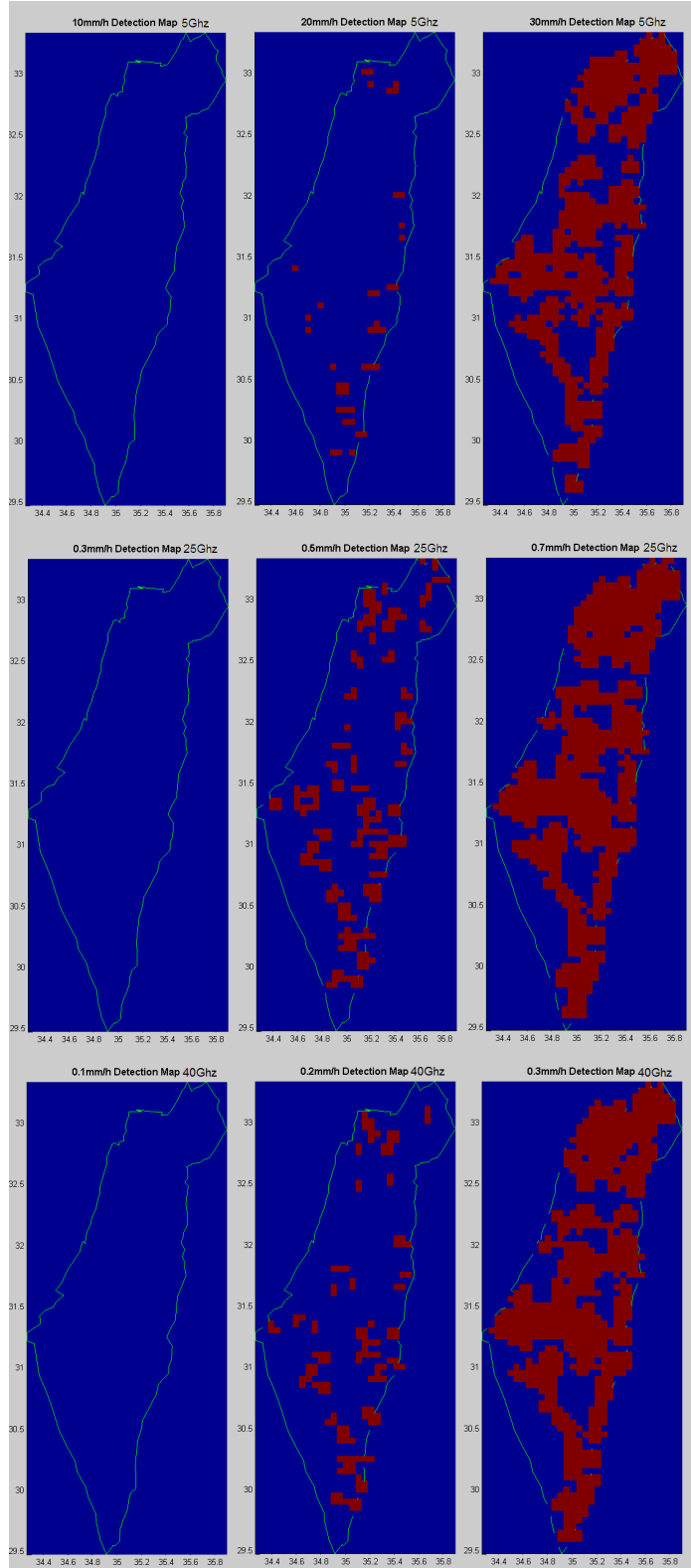


Figure 22 – Improving the Coverage – Links Quantization Tresholded

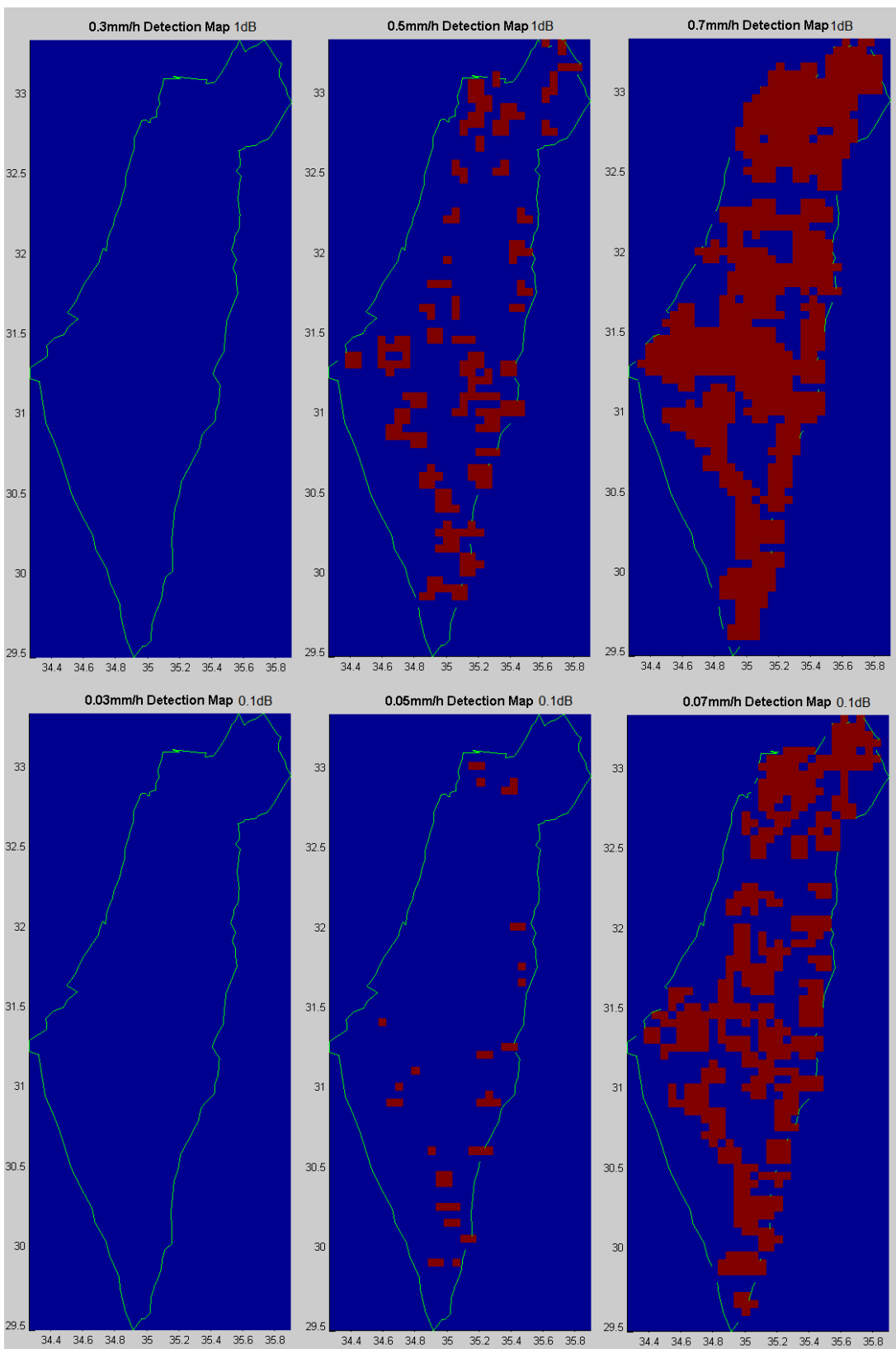


Figure 23 – Improving the Coverage – Links Quantization Tresholded

4.2 Reconstructability

4.2.1 Example 1

Let us consider the set of wireless links around the area in Israel named Ramot-Menashe. We examine a set of links in that area and find the links depicted in Figure 24.

One may easily identify that in this case there are two different types of sampling functionals despite the fact that we have three links (two of the links are similar in length and angle). We apply the regularization procedure described above and yield the regularized grid of sampling functions as depicted in Figure 24 on the right hand side.

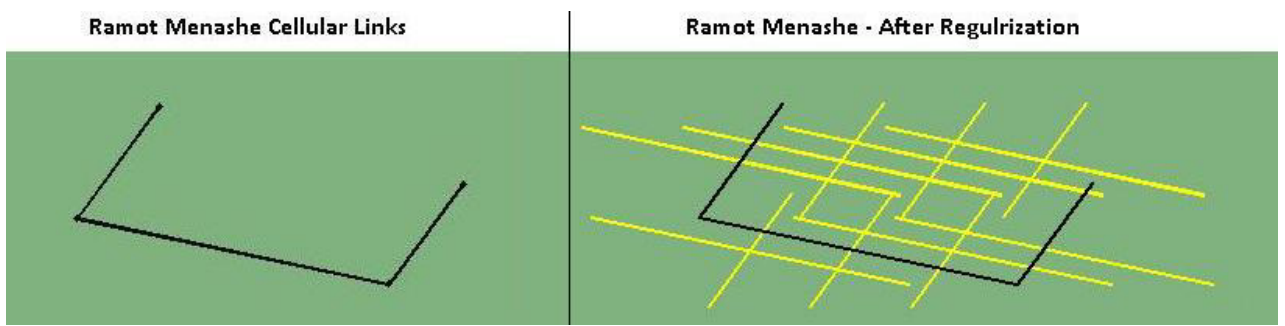


Figure 24 – The Microwave Links in Ramot-Menashe

Once the two sampling functionals have been determined we may calculate the GSE determinant which is given by the following –

$$\begin{vmatrix} W_1 \frac{\sin((u \cos \theta_1 + v \sin \theta_1)W_1 / 2)}{(u \cos \theta_1 + v \sin \theta_1)W_1 / 2} & W_2 \frac{\sin((u \cos \theta_2 + v \sin \theta_2)W_2 / 2)}{(u \cos \theta_2 + v \sin \theta_2)W_2 / 2} \\ W_1 \frac{\sin(((u + \sigma_u) \cos \theta_1 + (v + \sigma_v) \sin \theta_1)W_1 / 2)}{((u + \sigma_u) \cos \theta_1 + (v + \sigma_v) \sin \theta_1)W_1 / 2} & W_2 \frac{\sin(((u + \sigma_u) \cos \theta_2 + (v + \sigma_v) \sin \theta_2)W_2 / 2)}{((u + \sigma_u) \cos \theta_2 + (v + \sigma_v) \sin \theta_2)W_2 / 2} \end{vmatrix} \quad (4.1)$$

where σ_u, σ_v are related to the grid distances Δ_x, Δ_y by $2\Delta_x = \sigma_u^{-1}$ and similarly for σ_v .

Numerically evaluating this determinant for the set of required frequencies ψ proves that it is non-zero and that usage of these two sampling functionals may enable a reliable reconstruction.

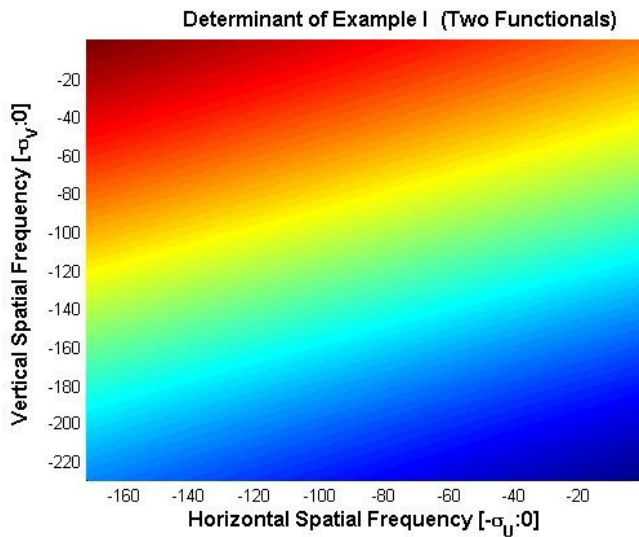


Figure 25 – The GSE determinant - example I

We now commence with the test process. We are now left with the evaluation of the augmented matrix determinant. The missing samples are those marked in yellow in Figure 24. Let us denote by g_1 the longer sampling functional and by g_2 the shorter sampling functional. i.e. – we are missing the following samples –

$$\begin{aligned} & g_1(1,1), g_1(1,2), g_1(1,3), g_1(1,4), g_1(2,1), g_1(2,3), g_1(2,4) \\ & g_2(1,2), g_2(1,3), g_2(1,4), g_2(2,1), g_2(2,2), g_2(2,3) \end{aligned} \quad (4.2)$$

We now must construct the augmented matrix. This is actually, the exact case which we explicitly solved in section 3.1.8. This process yielded the following structure for the augmented matrix.

$$\mathbf{M} \begin{pmatrix} g_1 \\ g_2 \end{pmatrix} = \begin{pmatrix} h_1 \\ h_2 \end{pmatrix} \quad \mathbf{M} = \left(\begin{array}{c|c} \mathbf{I} - \mathbf{A}_{11} & -\mathbf{A}_{12} \\ \hline -\mathbf{A}_{21} & \mathbf{I} - \mathbf{A}_{22} \end{array} \right) \quad (4.3)$$

Calculating the determinant of \mathbf{M} proves that it is singular and thus we cannot reconstruct the missing samples from the ones we have. This is a sensible result due to the fact that we are missing a very large amount of samples.

4.2.2 Example 2

Let us consider another set of lines as given in Figure 26. One may easily identify that in this case there are three different types of sampling functionals. We apply the regularization procedure described above and yield the regularized grid of sampling functions as depicted in Figure 26 on the right hand side.

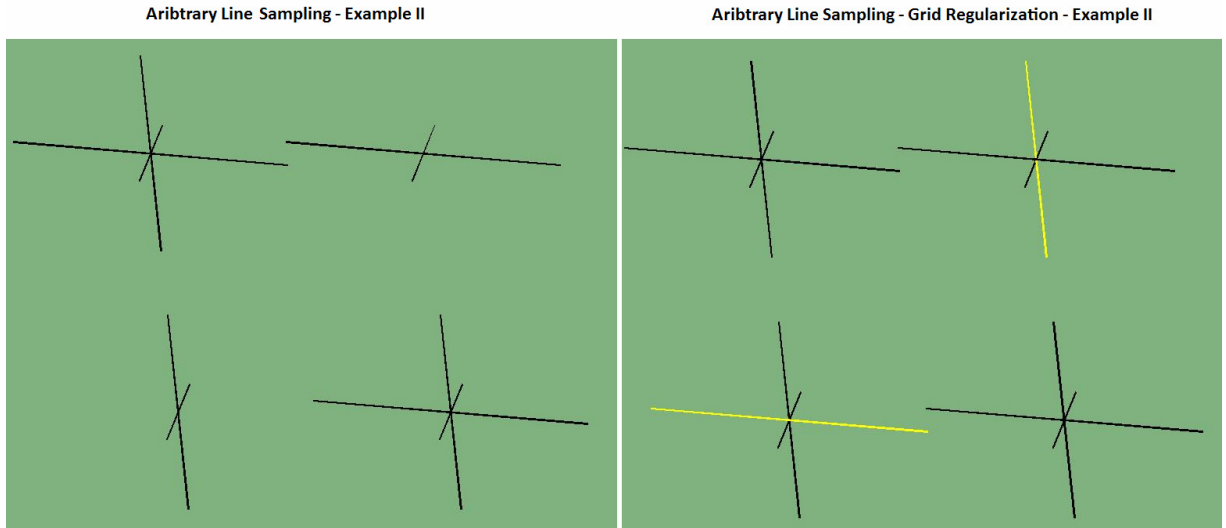


Figure 26 – The Arbitrary Lines – Example II

Once the three sampling functionals have been determined we may calculate the GSE determinant which is given by the following –

$$\left| \begin{array}{ccc} W_1 \frac{\sin\left((u \cos \theta_1 + v \sin \theta_1)\frac{W_1}{2}\right)}{(u \cos \theta_1 + v \sin \theta_1)\frac{W_1}{2}} & W_2 \frac{\sin\left((u \cos \theta_2 + v \sin \theta_2)\frac{W_2}{2}\right)}{(u \cos \theta_2 + v \sin \theta_2)\frac{W_2}{2}} & W_3 \frac{\sin\left((u \cos \theta_3 + v \sin \theta_3)\frac{W_3}{2}\right)}{(u \cos \theta_3 + v \sin \theta_3)\frac{W_3}{2}} \\ W_1 \frac{\sin\left(\left(u + \frac{2\sigma_u}{3}\right) \cos \theta_1 + \left(v + \frac{2\sigma_v}{3}\right) \sin \theta_1\right) \frac{W_1}{2}}{\left(\left(u + \frac{2\sigma_u}{3}\right) \cos \theta_1 + \left(v + \frac{2\sigma_v}{3}\right) \sin \theta_1\right) \frac{W_1}{2}} & W_2 \frac{\sin\left(\left(u + \frac{2\sigma_u}{3}\right) \cos \theta_2 + \left(v + \frac{2\sigma_v}{3}\right) \sin \theta_2\right) \frac{W_2}{2}}{\left(\left(u + \frac{2\sigma_u}{3}\right) \cos \theta_2 + \left(v + \frac{2\sigma_v}{3}\right) \sin \theta_2\right) \frac{W_2}{2}} & W_3 \frac{\sin\left(\left(u + \frac{2\sigma_u}{3}\right) \cos \theta_3 + \left(v + \frac{2\sigma_v}{3}\right) \sin \theta_3\right) \frac{W_3}{2}}{\left(\left(u + \frac{2\sigma_u}{3}\right) \cos \theta_3 + \left(v + \frac{2\sigma_v}{3}\right) \sin \theta_3\right) \frac{W_3}{2}} \\ W_1 \frac{\sin\left(\left(u + \frac{4\sigma_u}{3}\right) \cos \theta_1 + \left(v + \frac{4\sigma_v}{3}\right) \sin \theta_1\right) \frac{W_1}{2}}{\left(\left(u + \frac{4\sigma_u}{3}\right) \cos \theta_1 + \left(v + \frac{4\sigma_v}{3}\right) \sin \theta_1\right) \frac{W_1}{2}} & W_2 \frac{\sin\left(\left(u + \frac{4\sigma_u}{3}\right) \cos \theta_2 + \left(v + \frac{4\sigma_v}{3}\right) \sin \theta_2\right) \frac{W_2}{2}}{\left(\left(u + \frac{4\sigma_u}{3}\right) \cos \theta_2 + \left(v + \frac{4\sigma_v}{3}\right) \sin \theta_2\right) \frac{W_2}{2}} & W_3 \frac{\sin\left(\left(u + \frac{4\sigma_u}{3}\right) \cos \theta_3 + \left(v + \frac{4\sigma_v}{3}\right) \sin \theta_3\right) \frac{W_3}{2}}{\left(\left(u + \frac{4\sigma_u}{3}\right) \cos \theta_3 + \left(v + \frac{4\sigma_v}{3}\right) \sin \theta_3\right) \frac{W_3}{2}} \end{array} \right| \quad (4.4)$$

Similarly to the first example, σ_u, σ_v are related to the grid distances Δ_x, Δ_y by $2\Delta_x = \sigma_u^{-1}$ and $2\Delta_y = \sigma_v^{-1}$. Numerically evaluating this determinant for the set of required frequencies $\psi = [-\sigma_u, -\sigma_u/3] \times [-\sigma_v, -\sigma_v/3]$ proves that it is non-zero and that using these three sampling

functionals may yield a reliable reconstruction. The numerical evaluation of the determinant appears in Figure 27.

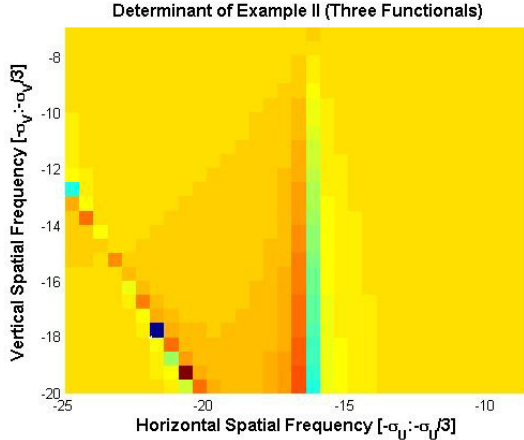


Figure 27 – The Arbitrary Lines – Example II – The GSE Determinant

We are now left with the evaluation of the augmented matrix determinant. The missing samples are those marked in yellow in Figure 26. Let us denote the sampling functionals of which we have missing samples g_1 and g_2 (meaning g_3 doesn't have any missing samples). This in turn means that we are missing the samples $g_1(2,1)$ and $g_2(1,2)$. We now must construct the augmented matrix –

$$\begin{aligned} g_1(2,1) &= h_1 + g_1(2,1) A_{1111} + g_2(1,2) A_{1211} \\ g_2(1,2) &= h_2 + g_1(2,1) A_{2111} + g_2(1,2) A_{2211} \end{aligned} \quad (4.5)$$

Writing this in matrix form we have –

$$\mathbf{M} = \begin{pmatrix} 1 - s_{1111} & s_{1211} \\ s_{2111} & 1 - s_{2211} \end{pmatrix} \quad (4.6)$$

However, numerically calculating the determinant of \mathbf{M} proves that it is singular and thus we cannot reconstruct the missing samples from the ones we have. This is due to the fact that when we apply the GSE theorem we define –

$$\begin{aligned} T_x &= 3T_{Nyq,x} \\ T_y &= 3T_{Nyq,y} \end{aligned} \quad (4.7)$$

The value of 3 represents three sampling functionals, and it means that we may sample 3 times *slower* and still reconstruct samples functions up to the same original Nyquist frequency. This also means that we *aren't over-sampling*. We are sampling with the slowest sample rate required in order to reconstruct a function to its Nyquist frequency. If we recalculate \mathbf{M} using a faster sampling rate of-

$$\begin{aligned} T_x &= 2T_{Nyq,x} \\ T_y &= 2T_{Nyq,y} \end{aligned} \quad (4.8)$$

we find that $|\mathbf{M}| \neq 0$. This means that using the samples we have, we may now reconstruct the two missing samples.

4.2.3 Example 3

We now consider the case of links which was suggested by Giuli [15] as depicted in Figure 28. In their article, Giuli *et al* showed cases of rain events which their links are able of reconstructing properly. These rain events are shown in Figure 29.

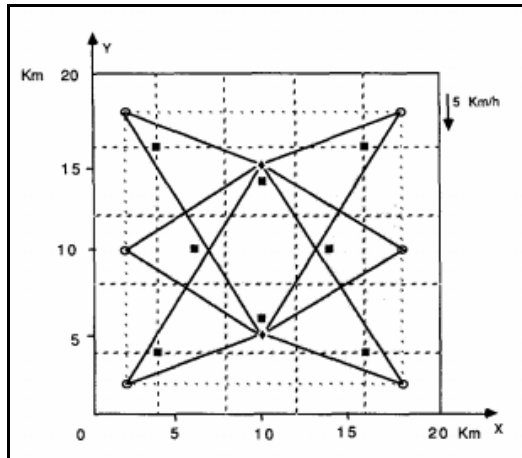


Figure 28 – The Giuli Links [15]

Using our method we show that errors can indeed occur if Giuli's set of links is used for rain events with a high spatial frequency. Moreover, visually considering the rain events which they simulated easily shows the very low spatial frequency nature of the chosen events. Giuli *et al* chose to simulate rain events with a decay rate of $\sim 4 \text{ mm/hr}^{-1} \text{ km}^{-2}$ in a cell size of 15 km^2 , a very low spatial frequency, which isn't very prone to errors.

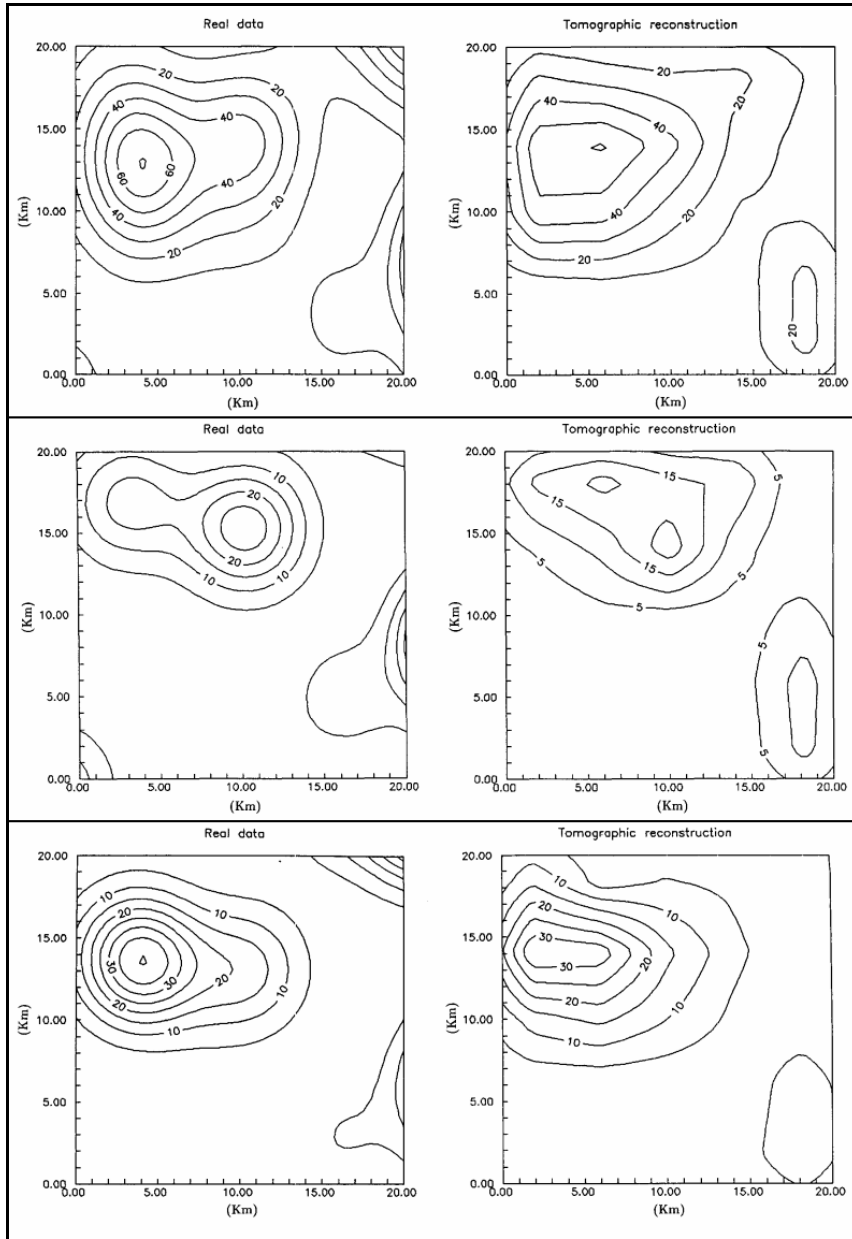


Figure 29 – The Giuli Rain Events [15]

Let us consider another set of lines as given in Figure 30. One may identify that in this case there are eight different types of sampling functionals. However, in our simulation we chose to quantize the angles in a manner which yields only 4 distinct line types. We apply the regularization procedure described in the previous sections and yield the regularized grid of sampling functions as depicted in Figure 30 on the right hand side.

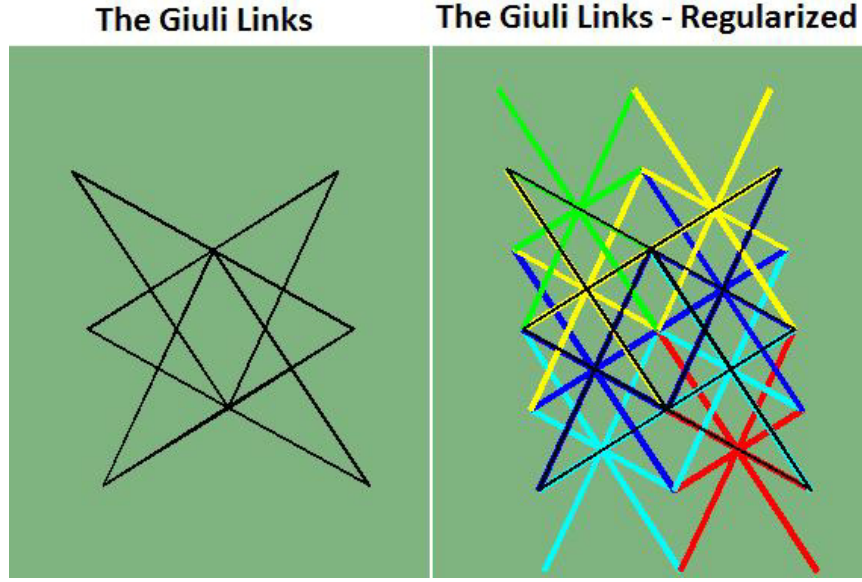


Figure 30 – The Giuli Lines Regularized– Example III

Once the three sampling functionals have been determined we may calculate the GSE determinant which is given by the following –

$$\begin{vmatrix} W_1 \frac{\sin\left((u \cos \theta_1 + v \sin \theta_1)\frac{W_1}{2}\right)}{(u \cos \theta_1 + v \sin \theta_1)\frac{W_1}{2}} & W_2 \frac{\sin\left((u \cos \theta_2 + v \sin \theta_2)\frac{W_2}{2}\right)}{(u \cos \theta_2 + v \sin \theta_2)\frac{W_2}{2}} & W_3 \frac{\sin\left((u \cos \theta_3 + v \sin \theta_3)\frac{W_3}{2}\right)}{(u \cos \theta_3 + v \sin \theta_3)\frac{W_3}{2}} & W_4 \frac{\sin\left((u \cos \theta_4 + v \sin \theta_4)\frac{W_4}{2}\right)}{(u \cos \theta_4 + v \sin \theta_4)\frac{W_4}{2}} \\ W_1 \frac{\sin\left(\left(u + \frac{2\sigma_u}{4}\right)\cos \theta_1 + \left(v + \frac{2\sigma_v}{4}\right)\sin \theta_1\right)\frac{W_1}{2}}{\left(\left(u + \frac{2\sigma_u}{4}\right)\cos \theta_1 + \left(v + \frac{2\sigma_v}{4}\right)\sin \theta_1\right)\frac{W_1}{2}} & \vdots & \vdots & \vdots \\ W_1 \frac{\sin\left(\left(u + \frac{2\sigma_u}{4}\right)\cos \theta_1 + \left(v + \frac{2\sigma_v}{4}\right)\sin \theta_1\right)\frac{W_1}{2}}{\left(\left(u + \frac{2\sigma_u}{4}\right)\cos \theta_1 + \left(v + \frac{2\sigma_v}{4}\right)\sin \theta_1\right)\frac{W_1}{2}} & \vdots & \ddots & \vdots \\ W_1 \frac{\sin\left(\left(u + \frac{6\sigma_u}{4}\right)\cos \theta_1 + \left(v + \frac{6\sigma_v}{3}\right)\sin \theta_1\right)\frac{W_1}{2}}{\left(\left(u + \frac{6\sigma_u}{3}\right)\cos \theta_1 + \left(v + \frac{6\sigma_v}{3}\right)\sin \theta_1\right)\frac{W_1}{2}} & \dots & \dots & \sin\left(\left(u + \frac{6\sigma_u}{4}\right)\cos \theta_4 + \left(v + \frac{6\sigma_v}{3}\right)\sin \theta_4\right)\frac{W_4}{2} \\ W_1 \frac{\sin\left(\left(u + \frac{6\sigma_u}{3}\right)\cos \theta_1 + \left(v + \frac{6\sigma_v}{3}\right)\sin \theta_1\right)\frac{W_1}{2}}{\left(\left(u + \frac{6\sigma_u}{3}\right)\cos \theta_1 + \left(v + \frac{6\sigma_v}{3}\right)\sin \theta_1\right)\frac{W_1}{2}} & & & \left(\left(u + \frac{6\sigma_u}{3}\right)\cos \theta_4 + \left(v + \frac{6\sigma_v}{3}\right)\sin \theta_4\right)\frac{W_4}{2} \end{vmatrix} \quad (4.9)$$

Similarly to the first example, σ_u, σ_v are related to the grid distances Δ_x, Δ_y by $2\Delta_x = \sigma_u^{-1}$ and $2\Delta_y = \sigma_v^{-1}$. Numerically evaluating this determinant for the set of required frequencies $\psi = [-\sigma_u, -\sigma_u/4] \times [-\sigma_v, -\sigma_v/4]$ proves that there is a set of frequencies for which no reliable reconstruction can be made. The numerical evaluation of the determinant appears in Figure 31.

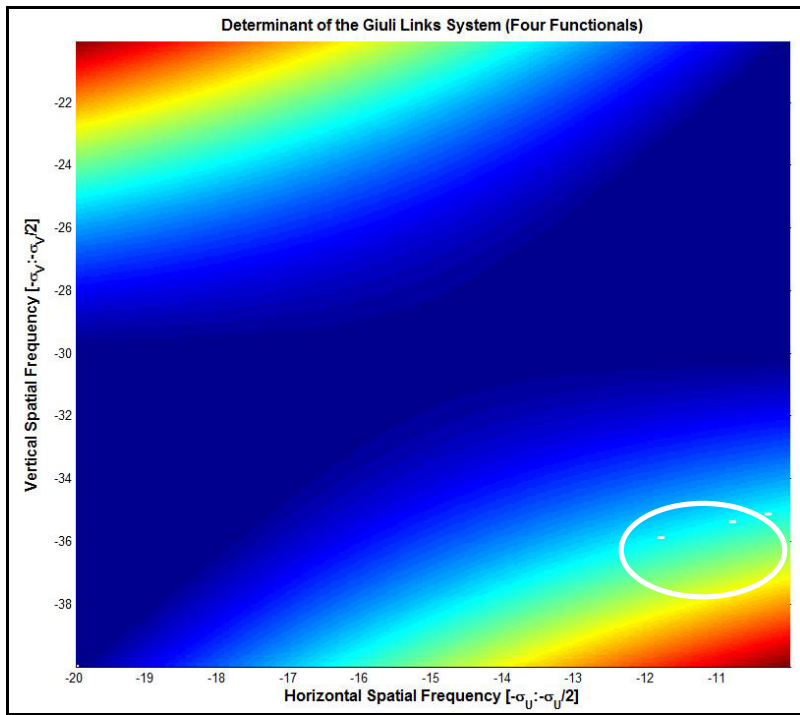


Figure 31 – The Giuli Lines – Example III – The GSE Determinant

4.2.4 Example 4

The purpose of this example, as opposed to the previous examples is to present the weaknesses of our suggested solution. Our procedure for stating when a set of lines composes a proper set which will ensure the ability to reconstruct a sampled function isn't a two-directional procedure. In other words, it is a sufficient but not necessary condition. One may find a set of lines which our procedure states as insufficient for the sampling and reconstruction task however, intuition states that due to their nature they seem sufficient indeed.

The example below shows that the intuition may work well by considering links of urban vs. rural areas in Israel. Clearly, as we move from an urban through a semi-urban to a rural area, the density of links decreases. This notion is also depicted by the histograms in Figure 2 where one may notice how the spread changes as we move from the central and urban area of Israel outside towards the sub-urban areas. In the most rural area of Israel, the centre of the Negev, the links of which direction is from north to south are usually very long. Being a rather rural area, these links serve a very small amount of population and hence, the CWN engineers attempt to minimize their amount. However, due to the fact that Israel is very long and narrow, the links from east to west have a length which may easily be found in urban or sub-urban areas too.

This nature of links causes the regularization process to return a very large amount of missing samples. This in turn, clearly causes the sampling set to be an insufficient set for the task of sampling and reconstruction. However, in urban areas where a very dense set of lines is present, the regularization process may also yield a very large amount of missing samples. This is because in such an area, a very large amount of distinct links are extant. This is most probably the most prominent weakness of our procedure.

In the figure below we operated our procedure on three areas of Israel, two urban areas and one rural area. We chose quantization values Δ_θ and Δ_w which yielded only four types of distinct lines. This is of course a very crude approximation of the line types and it yields a very inexact approximation of the existing links. However, it also greatly assists in decreasing the amount of missing samples. This is because more of the existing links are quantized to one of the distinct types.

Our intuition was that the two urban areas would yield a reconstructable set and that the rural one would yield an improper sampling set. However, as is seen in Figure 32, our suggested procedure states that one of the two urban areas is an insufficient sampling set. In Figure 32 we see the map of Israel links with three rectangles which surround the areas and links on which we operated our suggested procedure. The rectangles which are colored blue were found to be a sufficient set for the reconstruction task whereas the red rectangles which are colored red were found to be an insufficient set for the reconstruction task.

This result is what emphasizes that the central weakness of our procedure is its attempt to regularize a highly irregular grid. We believe that a treatment of the reconstructability problem may be better treated within a framework of "irregular sampling". Moreover, such a large amount of missing samples, which is usually the output of the regularization algorithm, may yield a singular augmented matrix \mathbf{M} simply due to numerical instabilities (and not due to a true singularity). We discuss this future direction in section 5.

In general we find it tough to state precisely what are common maximal spatial frequencies which are reconstructable in urban, sub-urban or rural areas due to the nature of our regularization process which may yield many missing samples for slightly different sampling realizations.

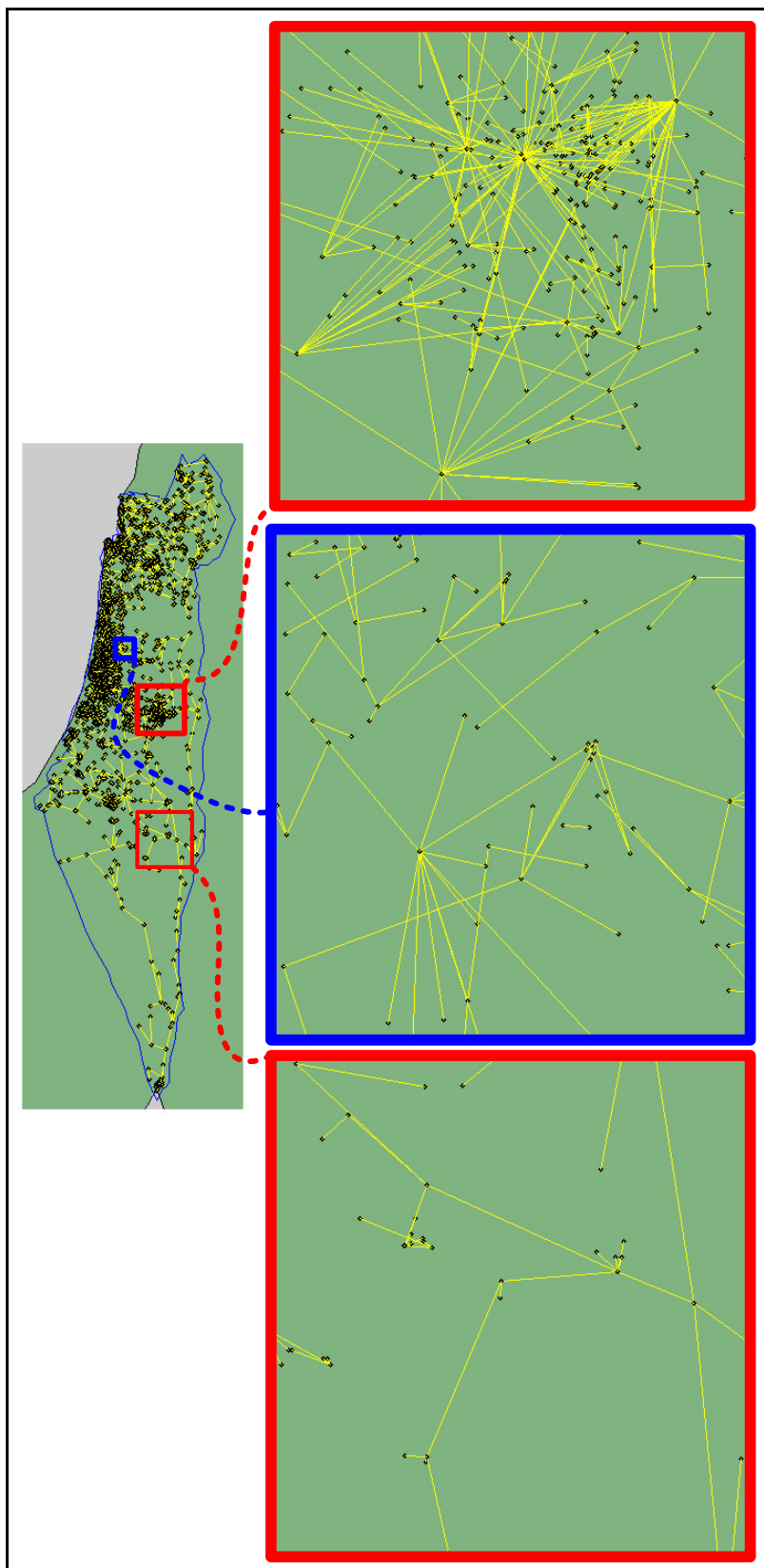


Figure 32 – Israel Links – Example III

5 Discussion

5.1 A Discussion on our Simplifications and Future Directions

In the preceding sections we discussed a few methods for determining when and where a set of lines may function properly in the task of generating coverage or reconstructability maps. The coverage maps, as mentioned above, are maps which state the locations which a level of rain above a sensitivity threshold may be detected. For the purpose of this problem we simulated a cloud which "scans" the map of lines in the country of Israel. For each line and cloud intersection we solved an equation which returns the minimal detectable rain rate. However, we have clearly simplified the problem immensely by assuming the cloud is a compact geometrical shape with a closed analytical form. Moreover, we have also assumed that within this closed geometrical shape, the rain rate is constant. These two assumptions may be easily relaxed for the task when the problem of generating coverage maps is treated in a brute force manner via a simulator. Any cloud profile with any rain rate within its form may be chosen and simulated for.

We find the relaxation of the cloud profile to be a future extension direction which is inevitable. By properly looking into the statistical properties of rain fronts, one may choose a cloud (or rain front) profile which is properly reasoned and provides coverage maps which any meteorological service can benefit from.

We have also presented a method for determining whether an arbitrary set of Projections along lines composes of a sampling scheme which yields a reconstructable function and to what frequency may a reliable reconstruction be held. This requires applying the Papoulis GSE, regularizing a non-regular grid with missing samples by the method described above, and finally, calculating what we have defined as the augmented matrix and testing for its singularity.

We would like to state that for the case of two types of lines, there are certain angles between the lines which yield a non reconstructable function. An obvious example is the case where there is an angle of 90° between the lines. The arguments of the sinc functions in the GSE determinant are then exactly equal for any $v = 0$ and thus yield a determinant which is equal to zero.

We have also found that no sampling scheme with only two lines and at least one missing sample may be reconstructed. This is due to the fact that sampling with only one type of line is equivalent to multiplying our spectrum with a sinc function which has numerous nulls in the

frequency domain. Hence, the fact that we have missing samples leaves us with some samples which contain missing data due to these sinc nulls.

We find the first future research which should be treated properly is relaxing the requirement to regularize an irregular grid. The need to regularize the grid causes the need to evaluate determinants of very large matrices (in the part of determining the ability to cope with missing samples). We have also found cases in which a great number of lines covers a sampled area and which, despite one's intuition, our procedure states is a sampling set which yields a non-reconstructable function. This is the strongest reason proving that the regularization process must be relaxed and treated otherwise. We stress that the procedure shown above provides a sufficient but not necessary condition for the reconstructability. We believe that this problem may somehow be treated within the framework of irregular sampling but this direction hasn't been fully pursued.

Also, we haven't explored the questions regarding the exact dependencies between the GSE matrix singularity and the lengths and angles of the sampling lines. It seems that an answer to which types of lines yield singular matrices and exactly why these lines cause the matrix's singularity may lead to insights dealing with a smart choice of these lines. Stressing yet again that more sampling lines in each sampling location yield a sampling grid which is $O(m^2)$ times less dense, motivates us to know exactly what types of lines to choose according to their lengths and angles. This in turn may enable the reduction of the sampling grid density (and reduce the sampling rate).

The method suggested here may also be generalized for different types of sampling functionals. One may want to combine between sampling both with line projections and point samples (rain gauges).

Usage of such a sampling scheme may greatly assist in reducing aliasing artefacts. This is due to both the low-pass nature of the local averaging due to the projections, and the added randomness which tends to reduces aliasing.

We would like to stress that this work dealt only with the answer to the question regarding “whether a reconstruction is feasible”. If the procedure shown above yields a positive answer, the framework showed here also hints on the method of reconstruction. Usage of the interpolation kernels as given in (1.39) may assist in reconstructing the sampled function. However, we currently leave the question of determining what to do in case a sampling scheme was found to be insufficient for reconstruction unanswered.

Obviously this answer requires finding the exact critical missing samples, and then considering the “optimal” locations to add samples (line projections) to. However, as in the Nyquist sampling theorem, these reconstruction kernels have infinite support and by such limit our ability to perfectly reconstruct the sampled signal.

We would also like to note that the solution to our problem only required evaluating the exact value of the reconstruction kernels at specific points and as such didn't require their determining their exact functional form. However, a reconstruction of a sampled function will clearly require the need to know their exact form.

Another direction which we have touched only minimally was the treatment of this problem in the framework of stochastic processes. We have shown a method to evaluate or calculate the exact autocorrelation function of the sampling process (see the appendix). In our solution to this problem we assumed a uniform distribution of distance perturbations between adjacent lines, a uniform distribution of the line angles and finally, an exponential distribution of the line lengths. These assumptions enabled calculating the autocorrelation function in this particular case. From this point it is summoned upon to test the autocorrelation function for a variety of input spectra in order to find exactly under what terms can the input spectra be properly reconstructed.

However, we emphasize that such an approach will only tell us if the average spectrum can be properly reconstructed. Employing the stochastic processes framework will never tell us if a concrete realization of a sampling set may be properly reconstructed. For an answer regarding a concrete specific sampling set one should follow an approach which resembles the approach which we have suggested here, the one which states when a set of lines indeed yields a reconstructable sampling set.

Another direction which we found interesting but which we haven't fully explored in this thesis is the assumption of sparsity of the rain signal. If one is able to properly justify such an assumption, and find the basis with which the rain signal is sparse, he would be able to use compressive sensing tools which enjoy the ability of not needing to assume that the sampled function is band limited. And indeed, local rain events intuitively don't seem to have a band limited nature due to their very local nature. Such a rain event may consist of a very strong rain in a very small local area. As such, the rain resembles a rectangular function which, as is known, doesn't have a limited bandwidth (its Fourier transform is a sinc function).

I list below the future directions as I see them:

- Generalize the cloud profile for the coverage problem
- Consider statistical properties of rain clouds for the coverage problem
- Relax the regularization requirement in the reconstructability problem
Consider non-uniform sampling for this purpose
- Provide necessary and sufficient condition to the reconstructability problem (as opposed to sufficient only)
- Analyze exactly where should a link be added for reaching reconstructability
- Extend the reconstructability problem to an actual reconstruction of a rain map

5.2 Adding Rain Gauges

After having treated the question regarding the reconstructability of a two dimensional function which is sampled by projections along lines with arbitrary geometry we may come across a set of microwave links which yield a non reconstructable function.

The problem of how to reconstruct rain maps from this set of microwave links is then left open. Even if we knew which missing link is the one which renders the reconstruction process impossible, it is rather obvious that we may not be able to add a microwave link in the required location. This is mostly due to the price of such a link and our ability to intervene with the cellular operator's link management task.

We would then like to add a cheaper rain monitoring device, a Rain Gauge.

Rain Gauges are most probably the first precipitation (rain) measurement tools ever to be used. A Rain Gauge is a receptacle which is designed to measure the amount of rain which reaches the surface by simply accumulating it. Being so, its measurements are usually thought of as *point samples*.

The main advantage of Rain Gauges in comparison to the alternative rain measurement systems is their low price and lack of any calibration process. However one must consider the difficulty in deploying a network of Rain Gauges which appropriately samples an area of interest. Moreover, acknowledging the spatial and temporal nature of precipitation one realizes the difficulty in properly sampling an area of interest using Rain Gauges alone.

5.2.1 Sampling with both Rain Gauges and Lines

The true beauty in the Papoulis Generalized Sampling Expansion is its ability to treat any type of sampling functional as long as they are linear (or linear time/space invariant). If we treat the rain gauge as a simple delta function we indeed yield a LSI sampling functional.

This enables us to repeat the entire formalism which we suggested above by simply adding another functional into the GSE phase.

Let us assume that the sampling set which we had is one which is composed of two types of lines and a rain gauge, as is depicted in Figure 33.

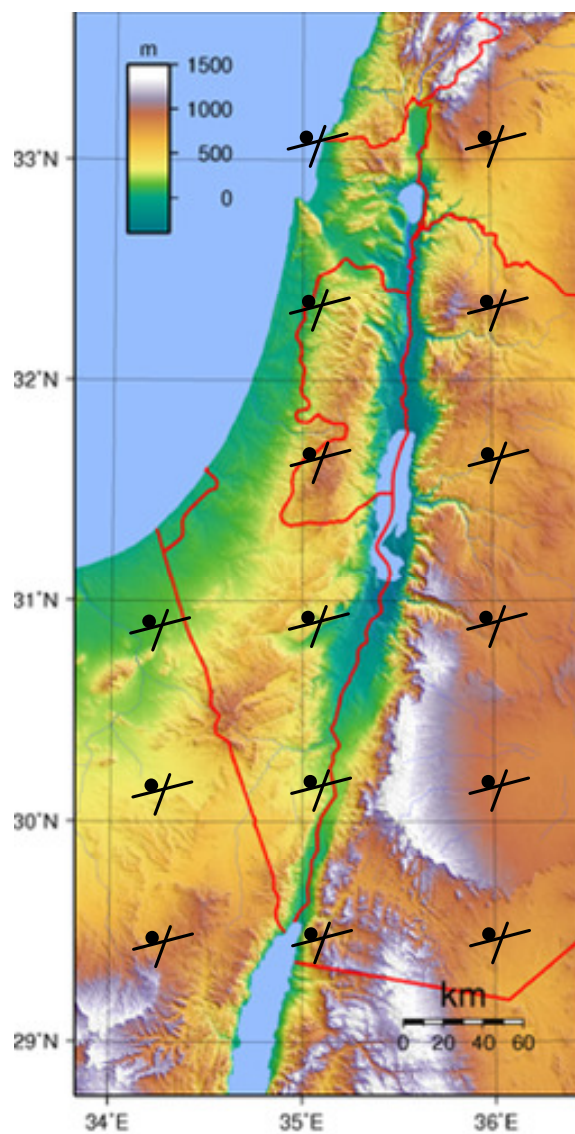


Figure 33 – Rain Gauge Sampling Scheme

We recall that the Fourier Transform of a shifted delta function is given by –

$$\delta(x + d_x, y + d_y) \underset{\mathcal{F}\{\cdot\}}{\Leftrightarrow} e^{\pm jd_x u} e^{\pm jd_y v} \quad (5.1)$$

In such a case, our sampling functionals are given by –

$$\begin{aligned} H_1(u, v) &= \frac{\sin((\cos \theta_1 u + \sin \theta_1 v))}{(\cos \theta_1 u + \sin \theta_1 v)} & H_2(u, v) &= \frac{\sin((\cos \theta_2 u + \sin \theta_2 v))}{(\cos \theta_2 u + \sin \theta_2 v)} \\ H_3(u, v) &= e^{\pm jd_x u} e^{\pm jd_y v} \end{aligned} \quad (5.2)$$

And as usual, the GSE matrix of the system of equations for such a sampling scheme is given by–

$$\begin{vmatrix} H_1(u, v) & H_2(u, v) & H_3(u, v) \\ H_1(u + c_x, v + c_y) & H_2(u + c_x, v + c_y) & H_3(u + c_x, v + c_y) \\ H_1(u + 2c_x, v + 2c_y) & H_2(u + 2c_x, v + 2c_y) & H_3(u + 2c_x, v + 2c_y) \end{vmatrix} \quad (5.3)$$

We must ensure that it is non-zero for the proper set of frequencies as required by the Papoulis GSE.

The problem of an irregular grid stays the same when adding a rain gauge. The only change is to the phase of determining a distinct set of sampling functionals. However, we ourselves added the rain gauge, so we are left with a set of distinct lines and our added delta function.

The phase of treating missing samples stays the same as the two suggested procedures in (3.14) and (3.16). For missing samples along a line, we employ the procedure suggested in section (3.16) which involves integrating along functionals of which missing samples exist.

For missing samples of rain gauges, we employ the procedure suggested in section (3.14) which involves no integration but simply constructing a set of linear equations and plugging them into the entire inverse problem set of linear equations.

We stress that we do not require an entire grid of rain gauges but rather a single rain gauge. The lack of a grid of rain gauges will be treated within the formalism of missing samples as previously shown.

5.3 Coverage of other than Rain

The approach to the coverage problem and the suggested tool may be generalized to any phenomenon which is sensitive to the length of the intersecting link and a cloud. We discuss here a different environmental phenomenon which may find an interest in such a tool.

State of the art fog observation methods include Transmissometers, Satellite systems, Scatter meters and even Human observers, all of which are expensive solutions.

Preliminary results concerning fog monitoring utilizing commercial microwave systems have been shown by David *et al* [8]. David applied the Rayleigh approximation in order to relate fog to attenuation per km-

$$\gamma = \Phi \cdot LWC \quad (5.4)$$

where γ [dB / km] is the attenuation, Φ is an attenuation coefficient which is temperature and frequency dependent and LWC is the liquid water content.

The attenuation coefficient suggested by David is based on the Rayleigh approximation (fog drops are generally less than 0.01 cm, small with respect to centimetre microwaves) and is given by –

$$\Phi = \chi f \quad (5.5)$$

Where χ is a known constant which depends on the dielectric permittivity of water and f is the link's frequency.

After the approximations, the resulting equation, relating between the water vapour and the measured attenuation is given by –

$$\gamma = \chi f L_{int} \cdot LWC \quad (5.6)$$

which implies that we may use the procedure suggested in section 2.1 for the sake of generating fog maps.

We would like to stress however, that other than rain, fog may be present in heights where the links may miss it. Hence, this technique isn't fully suited for the coverage of fog. Snow, Hail and/or Sleet on the other hand are environmental phenomena which are more suited for this

approach. Employing this approach requires a proper mathematical relation between the phenomenon's rate and its attenuation.

6 Appendix

6.1 Correlation Function of the Sampling Process

In this section we present a method of calculating the spectrum of the random process of sampling a function with *random* lines.

6.1.1 Modeling the Sampling Process

We begin with the manner by which we model the sampling process. Similar to deterministic sampling problem where the sampled function is multiplied by the Dirac comb we must multiply a function by a Dirac comb but after integration along a line –

$$\tilde{f}(x, y) = \sum_{n=-\infty}^{\infty} \sum_{m=-\infty}^{\infty} f_I(n\Delta x, m\Delta y) \delta(x - n\Delta x, y - m\Delta y) \quad (6.1)$$

The function $f_I(x, y)$ is the outcome of the integration along a line realization –

$$f_I(x, y) = \int_{L_{n,m}} f(x', y') dl \quad (6.2)$$

We parameterize the line by –

$$\begin{aligned} L_{n,m}: & x \in [-0.5W_{n,m} \cos \theta_{n,m} + n\Delta x + \delta x_n, 0.5W_{n,m} \cos \theta_{n,m} + n\Delta x + \delta x_n] \\ & y = \tan \theta_{n,m} (x - n\Delta x - \delta x_n) + (m\Delta y + \delta y_m) \end{aligned} \quad (6.3)$$

Where $W_{n,m}$ and $\theta_{n,m}$ are its respective length and angle and $\delta x_n, \delta y_m$ are random variables which generate the offset of the line from the regular sampling grid.

Due to the fact that the line function is equal to 1 only along the line and zero otherwise, we may write –

$$\tilde{f}(x, y) = \sum_{n=-\infty}^{\infty} \sum_{m=-\infty}^{\infty} \left(\iint_{\mathbb{R}^2} L_{n,m} f(x', y') ds \right) \delta(x - n\Delta x, y - m\Delta y) \quad (6.4)$$

$W_{n,m}, \theta_{n,m}$ and $\delta x_n, \delta y_m$ are random variables.

Our desire is to calculate the autocorrelation function of this sampling process.

We stress that this modeling doesn't consider missing links/samples.

6.1.2 Choice of the Random Variables Probability Distribution Functions

Enabling the completion of the calculation of the Autocorrelation function requires defining or choosing the complementary probability distribution functions. Analysing Figure 2 we see that a choice of a uniform distribution for the link angles seems like a reasonable choice assuming we are in an urban area –

$$\theta_{n,m} \sim U[-\pi, \pi] \quad (6.5)$$

However, if a sub-urban or rural area is considered, a more complex functional description must be employed for the angles' probability distribution function.

A choice of an exponential distribution for the link lengths seems proper assuming we are in an urban area –

$$p_{w_{n,m}}(x) = \lambda e^{-\lambda(x-W_M)} \quad (6.6)$$

The parameter W_M enables shifting the function in order to set the minimal length with non-zero probability. Choice of the decay rate parameter λ may be done by many ways. We chose to estimate it by considering the maximum likelihood estimation (MLE) of the parameter. We assume the line lengths are I.I.D.

The MLE of λ is then given by –

$$\begin{aligned} P(x_i | \lambda) &= \lambda e^{-\lambda(x_i - W_M)} \\ \Rightarrow P(\vec{x} | \lambda) &= \prod_{i=1}^N \lambda e^{-\lambda(x_i - W_M)} = \lambda^N e^{-\lambda \left[\sum_{i=0}^N (x_i - W_M) \right]} \\ \hat{\lambda} &= \arg \max_{\lambda} P(\vec{x} | \lambda) = \arg \max_{\lambda} \log(P(\vec{x} | \lambda)) \\ \Rightarrow \frac{\partial \log(P(\vec{x} | \lambda))}{\partial \lambda} &= \frac{N}{\lambda} - \left(\sum_{i=0}^N (x_i - W_M) \right) = 0 \\ \Rightarrow \hat{\lambda} &= \frac{1}{\frac{1}{N} \sum_{i=0}^N (x_i - W_M)} \end{aligned} \quad (6.7)$$

Finally, a choice of a uniform distribution for the link distances is a valid choice assuming we are considering a small urban cell of links –

$$\delta x_n, \delta y_n \sim U[-\delta, \delta] \quad (6.8)$$

However, we limit the range of the links distances to be –

$$\delta \leq \max\left(\frac{\Delta x}{2}, \frac{\Delta y}{2}\right) \quad (6.9)$$

In order to prevent switches between line sites

6.1.3 The Sampling Process's Autocorrelation Function and Spectrum

Our desire is to calculate the autocorrelation function of the sampling process which we modelled in the previous section.

$$\mathbb{R} = E\{f_I(x, y) f_I(x + \tau, y + \sigma)\} \quad (6.10)$$

Writing this explicitly we yield –

$$\begin{aligned} & E \left\{ \sum_{n=-\infty}^{\infty} \sum_{m=-\infty}^{\infty} \left(\int_{L_{n,m}} f(x, y) dl \right) \delta(x - n\Delta x, y - m\Delta y) \sum_{n'=-\infty}^{\infty} \sum_{m'=-\infty}^{\infty} \left(\int_{L_{n',m'}} f(x, y) dl \right) \delta(x + \tau - n'\Delta x, y + \sigma - m'\Delta y) \right\} = \\ & E \left\{ \sum_{n=-\infty}^{\infty} \sum_{m=-\infty}^{\infty} \sum_{n'=-\infty}^{\infty} \sum_{m'=-\infty}^{\infty} \left(\iint_{\mathbb{R}^2} L_{n,m} f(x, y) ds \iint_{\mathbb{R}^2} L_{n',m'} f(x, y) ds \right) \delta(x - n\Delta x, y - m\Delta y) \delta(x + \tau - n'\Delta x, y + \sigma - m'\Delta y) \right\} = \\ & \left\{ \sum_{n=-\infty}^{\infty} \sum_{m=-\infty}^{\infty} \sum_{n'=-\infty}^{\infty} \sum_{m'=-\infty}^{\infty} E \left(\iint_{\mathbb{R}^2} L_{n,m} f(x, y) ds \iint_{\mathbb{R}^2} L_{n',m'} f(x, y) ds \right) \delta(x - n\Delta x, y - m\Delta y) \delta(x + \tau - n'\Delta x, y + \sigma - m'\Delta y) \right\} \end{aligned} \quad (6.11)$$

For the sake of simplicity we define –

$$E \left(\iint_{\mathbb{R}^2} L_{n,m} f(x, y) ds \iint_{\mathbb{R}^2} L_{n',m'} f(x, y) ds \right) \triangleq A_{n,m,n',m'} \quad (6.12)$$

Adopting the suggestions for the probability distribution functions which were suggested in the previous section enables calculating the values of $A_{n,m,n',m'}$ –

$$\begin{aligned}
A_{n,m,n',m'} &= \\
&\left[\int_{\delta_x} \frac{1}{\delta} \int_{\delta_y} \frac{1}{\delta} \int_W \lambda e^{-\lambda(W-W_M)} \int_{\theta} \frac{1}{2\pi} \left(\iint_{\mathbb{R}^2} L_{n,m} f(x, y) ds \right) d\theta dW d\delta_x d\delta_y \bullet \right] && \text{if } n \neq n' \text{ or } m \neq m' \\
&\left[\int_{\delta_x} \frac{1}{\delta} \int_{\delta_y} \frac{1}{\delta} \int_W \lambda e^{-\lambda(W-W_M)} \int_{\theta} \frac{1}{2\pi} \left(\iint_{\mathbb{R}^2} L_{n',m'} f(x, y) ds \right) d\theta dW d\delta_x d\delta_y \right] && = \\
&\left[\int_{\delta_x} \frac{1}{\delta} \int_{\delta_y} \frac{1}{\delta} \int_W \lambda e^{-\lambda(W-W_M)} \int_{\theta} \frac{1}{2\pi} \left(\iint_{\mathbb{R}^2} L_{n,m} f(x, y) ds \right)^2 d\theta dW d\delta_x d\delta_y \right] && \text{if } n = n' \text{ and } m = m' \quad (6.13) \\
&\left(\frac{\lambda}{2\pi\delta^2} \right)^2 \left[\int_W \lambda e^{-\lambda(W-W_M)} \int_{\Gamma_{n,m}} f(x, y) ds dW \right] \bullet \left[\int_W \lambda e^{-\lambda(W-W_M)} \int_{\Gamma_{n',m'}} f(x, y) ds dW \right] && \text{if } n \neq n' \text{ or } m \neq m' \\
&\frac{\lambda}{2\pi\delta^2} \left[\int_W \lambda e^{-\lambda(W-W_M)} \left[\int_{\Gamma_{n,m}} f(x, y) ds \right]^2 dW \right] && \text{if } n = n' \text{ and } m = m'
\end{aligned}$$

The definition of the integration area $\Gamma_{n,m}$ simplifies the description. The integration area is the result of the integration of $f(x, y)$ due to the uniformity of the angle and distances. The angle is uniform between $-\pi$ and π and the distances are uniform between $-\delta$ and δ .

This gives us an integration area which is the product of a circle which is shifter within a rectangle with an edge which length is equal to δ . This area is depicted in the figure below –

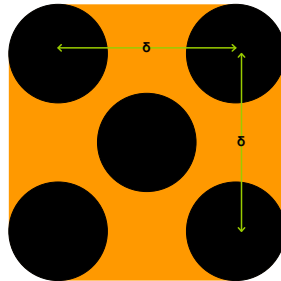


Figure 34 – The definition of the integration area $\Gamma_{n,m}$

We may write the autocorrelation function as –

$$\begin{aligned}
\mathbb{R} = E\{f_I(x, y) f_I(x + \tau, y + \sigma)\} = \\
\sum_{n=-\infty}^{\infty} \sum_{m=-\infty}^{\infty} \sum_{n'=-\infty}^{\infty} \sum_{m'=-\infty}^{\infty} \left\{ \left(\frac{\lambda}{2\pi\delta^2} \right)^2 \left[\int_W \lambda e^{-\lambda(W-W_M)} \int_{\Gamma_{n,m}} f(x', y') ds dW \right] \bullet \left[\int_W \lambda e^{-\lambda(W-W_M)} \int_{\Gamma_{n',m'}} f(x', y') ds dW \right] \bullet \right. \\
\left. \delta(x - n\Delta x, y - m\Delta y) \delta(x + \tau - n'\Delta x, y + \sigma - m'\Delta y) \right\} + \\
\sum_{n=-\infty}^{\infty} \sum_{m=-\infty}^{\infty} \left\{ \left[\frac{\lambda}{2\pi\delta^2} \left[\int_W \lambda e^{-\lambda(W-W_M)} \left[\int_{\Gamma_{n,m}} f(x', y') ds \right]^2 dW \right] - \left(\frac{\lambda}{2\pi\delta^2} \right)^2 \left[\int_W \lambda e^{-\lambda(W-W_M)} \int_{\Gamma_{n,m}} f(x', y') ds dW \right] \bullet \left[\int_W \lambda e^{-\lambda(W-W_M)} \int_{\Gamma_{n',m'}} f(x', y') ds dW \right] \right] \bullet \right. \\
\left. \delta(x - n\Delta x, y - m\Delta y) \delta(x + \tau - n\Delta x, y + \sigma - m\Delta y) \right\}
\end{aligned} \tag{6.14}$$

By defining the function $\Gamma(n, m)$ -

$$\Gamma(n, m) \triangleq \left(\frac{\lambda}{2\pi\delta^2} \right)^2 \int_W \lambda e^{-\lambda(W-W_M)} \int_{\Gamma_{n,m}} f(x', y') ds dW \tag{6.15}$$

We may write -

$$\begin{aligned}
\mathbb{R} = E\{f_I(x, y) f_I(x + \tau, y + \sigma)\} = \\
\sum_{n=-\infty}^{\infty} \sum_{m=-\infty}^{\infty} \sum_{n'=-\infty}^{\infty} \sum_{m'=-\infty}^{\infty} \left\{ \Gamma(n, m) \bullet \Gamma(n', m') \bullet \delta(x - n\Delta x, y - m\Delta y) \delta(x + \tau - n'\Delta x, y + \sigma - m'\Delta y) \right\} + \\
\sum_{n=-\infty}^{\infty} \sum_{m=-\infty}^{\infty} \left\{ \left[\frac{\lambda}{2\pi\delta^2} \left[\int_W \lambda e^{-\lambda(W-W_M)} \left[\int_{\Gamma_{n,m}} f(x', y') ds \right]^2 dW \right] - \Gamma^2(n, m) \right] \bullet \delta(x - n\Delta x, y - m\Delta y) \delta(x + \tau - n\Delta x, y + \sigma - m\Delta y) \right\}
\end{aligned} \tag{6.16}$$

Manipulating the delta functions gives us -

$$\begin{aligned}
\mathbb{R} = E\{f_I(x, y) f_I(x + \tau, y + \sigma)\} = \\
\sum_{n=-\infty}^{\infty} \sum_{m=-\infty}^{\infty} \sum_{n'=-\infty}^{\infty} \sum_{m'=-\infty}^{\infty} \left\{ \Gamma(n, m) \bullet \Gamma(n', m') \bullet \delta(\tau - (n' - n)\Delta x, \sigma - (m' - m)\Delta y) \right\} + \\
\sum_{n=-\infty}^{\infty} \sum_{m=-\infty}^{\infty} \left\{ \left[\frac{\lambda}{2\pi\delta^2} \left[\int_W \lambda e^{-\lambda(W-W_M)} \left[\int_{\Gamma_{n,m}} f(x', y') ds \right]^2 dW \right] - \Gamma^2(n, m) \right] \bullet \delta(\tau, \sigma) \right\}
\end{aligned} \tag{6.17}$$

We now notice that the second term has only a DC coefficient.

We write the sampling process as -

$$\begin{aligned}
\mathbb{R} = E\{f_I(x, y) f_I(x + \tau, y + \sigma)\} = \\
\sum_{n=-\infty}^{\infty} \sum_{m=-\infty}^{\infty} \sum_{n'=-\infty}^{\infty} \sum_{m'=-\infty}^{\infty} \left\{ \Gamma(n, m) \bullet \Gamma(n', m') \bullet \delta(\tau - (n' - n)\Delta x, \sigma - (m' - m)\Delta y) \right\} + DC \bullet \delta(\tau, \sigma)
\end{aligned} \tag{6.18}$$

Where -

$$DC \triangleq \sum_{n=-\infty}^{\infty} \sum_{m=-\infty}^{\infty} \left\{ \left[\frac{\lambda}{2\pi\delta^2} \left[\int_W \lambda e^{-\lambda(W-W_m)} \left[\int_{\Gamma_{n,m}} f(x',y') ds \right]^2 dW \right] - \Gamma^2(n,m) \right] \right\} \quad (6.19)$$

This shows us that the the equation above is simply a process of sampling a different function $\Gamma(n,m)$ with a different DC value. This means that we may easily determine when aliasing will occur by considering the spectrum of $\Gamma(n,m)$ with respect to the sampling rate.

7 References

- [1] - Aldroubi, A., & Gröchenig, K. (2001). Nonuniform sampling and reconstruction in shift-invariant spaces. *SIAM review*, 43(4), 585-620.
- [2] - Aldroubi and Grochenig. Non-uniform weighted average sampling and exact reconstruction in shift-invariant and wavelet spaces, *Appl. Comp. Harmonic. Anal.*, vol. 13, pp. 151-161, 2002.
- [3] - Atlas D, Ulbrich C, "Path and area integrated rainfall measurement by microwave attenuation in the 1–3 cm band" *J Appl Meteorol* 1977;16(12): 1322–31.
- [4] - Atlas D, Ulbrich C, "The physical basis for attenuation-rainfall relationships and the measurements of rainfall parameters by combined attenuation and radar methods", *J Rech Atmos* 1974;8:275–98.
- [5] - Balakrishnan, A. V. (1962). On the problem of time jitter in sampling. *Information Theory, IRE Transactions on*, 8(3), 226-236.
- [6] - Candes, E. J., & Tao, T. (2006). Near-optimal signal recovery from random projections: Universal encoding strategies?. *Information Theory, IEEE Transactions on*, 52(12), 5406-5425.
- [7] - Crane, Robert. "Prediction of attenuation by rain." *Communications, IEEE Transactions on* 28.9 (1980): 1717-1733.
- [8] - David, N., P. Alpert, and H. Messer. "Technical Note: Novel method for water vapor monitoring using wireless communication networks measurements." *Atmospheric Chemistry and Physics Discussions* 8.3 (2008): 11673-11684.
- [9] - De Marchi, S., Iske, A., & Sironi, A. Kernel-based Image Reconstruction from Scattered Radon Data by Positive Definite Functions.
- [10] - Dorabella M. S. Santos and Paulo J. S. G. Ferreira. "Reconstruction from Missing Function and Derivative Samples and Oversampled Filter Banks". *ICASSP 2004*, vol. III, Montreal, Canada, pp. 941-944.
- [11] - F. Marvasti, "Nonuniform Sampling: Theory and Practice", Kluwer Academic/ Plenum Publishers, New York, 2001

- [12] -Ferreira Paulo S.G, "Incomplete sampling series and the recovery of missing samples from oversampled band-limited signals", IEEE Trans. Signal Processing, vol. 40, no. 1, 1992, 225-227.
- [13] -Feuer, A., & Goodwin, G. C. (2005). Reconstruction of multidimensional bandlimited signals from nonuniform and generalized samples. Signal Processing, IEEE Transactions on, 53(11), 4273-4282.
- [14] -Frey, T. L. "The Effects of the Atmosphere and Weather on the Performance of a mm-Wave Communication Link." APPLIED MICROWAVE AND WIRELESS11 (1999): 76-81.
- [15] -Giuli, Dino, et al. "Tomographic reconstruction of rainfall fields through microwave attenuation measurements." Journal of applied meteorology 30.9 (1991): 1323-1340.
- [16] -Giuli, Dino, Luca Facheris, and Simone Tanelli. "Microwave tomographic inversion technique based on stochastic approach for rainfall fields monitoring."Geoscience and Remote Sensing, IEEE Transactions on 37.5 (1999): 2536-2555.
- [17] -<http://prswww.essex.ac.uk/mantissa/>
- [18] -Leijnse, H., R. Uijlenhoet, and J. N. M. Stricker. "Rainfall measurement using radio links from cellular communication networks." Water resources research43.3 (2007): W03201.
- [19] -Leneman, O. A. (1967). Correlation Function and Power Spectrum of Randomly Shaped Pulse Trains. Aerospace and Electronic Systems, IEEE Transactions on, (5), 774-778.
- [20] -Margolis, E., & Eldar, Y. C. (2008). Nonuniform sampling of periodic bandlimited signals. Signal Processing, IEEE Transactions on, 56(7), 2728-2745.
- [21] -Messer, Hagit, Artem Zinevich, and Pinhas Alpert. "Environmental monitoring by wireless communication networks." Science 312.5774 (2006): 713-713.
- [22] -Messer, Hagit. "Rainfall Monitoring Using Cellular Networks [In the Spotlight]."Signal Processing Magazine, IEEE 24.3 (2007): 144-142.
- [23] -Olsen, V. Rogers, and D. Hodge. "The aRb relation in the calculation of rain attenuation." Antennas and Propagation, IEEE Transactions on 26.2 (1978): 318-329.
- [24] -Papoulis, Athanasios. "Generalized sampling expansion." Circuits and Systems, IEEE Transactions on 24.11 (1977): 652-654.
- [25] -Radon, J. (2005). 1.1 Über die Bestimmung von Funktionen durch ihre Integralwerte längs gewisser Mannigfaltigkeiten. Classic Papers in Modern Diagnostic Radiology, 5.

- [26] -R.M. Young, "An Introduction to Nonharmonic Fourier Series", Academic Press, New York, 1980.
- [27] -Shannon, C. E. (1949). Communication in the presence of noise. Proceedings of the IRE, 37(1), 10-21.
- [28] -Sun, Q. (2006). Nonuniform average sampling and reconstruction of signals with finite rate of innovation. SIAM Journal on Mathematical Analysis, 38(5), 1389-1422.
- [29] -Sun, W., & Zhou, X. (2002). Reconstruction of band-limited signals from local averages. Information Theory, IEEE Transactions on, 48(11), 2955-2963.
- [30] -Unser, M. (2000). Sampling-50 years after Shannon. Proceedings of the IEEE, 88(4), 569-587.
- [31] -Zinevich, Artem, Pinhas Alpert, and Hagit Messer. "Estimation of rainfall fields using commercial microwave communication networks of variable density." Advances in Water Resources 31.11 (2008): 1470-1480.

8 תקציר

אותות הנוצרים מערכות מיקרוגל הינם למעשה מוצר מודולרי לאורך אותו קו בו עובר האות היהות והם תוצאת אינטראצייתו של האות את התופעת טبع אותו הוא חווה לאורך מסלולו. שיטה חדשנית אשר הוצאה ע"י Messer ב-2006 וע"י Leijnse ב-2007, אשר כללה שימוש בערכות סלולר ממחריות, העלה את האפשרות להשתמש בעורק המיקרוגל הסלוליuki הקיים לצורכי ניטור סביבתי. במלים אחרות, Messer הציעה את השימוש במידות קיימות מרשות סלולריות לצורך ניטור גשם.

במערכת אשר הוצאה ע"י Messer הגיאומטריה של עורקי התקשרות הינה שרירותית לחלוותן. מיקום עורקי התקשרות, משימה אשר מבוצעת ע"י טכני תקשורת, הינה משימה מורכבת. ביצוע משימה זו שואפת לאזן בין השאיפה למינימום של מספר שיחות הטלפון אשר הולכות לאיבוד בשל חוסר התקשרות תוך מקסימיזציה של המרחק בין עורקי התקשרות על מנת לעשות שימוש במספר קטן ככל הניתן של עורקים אלו (על מנת למזער עלויות). אופטמייזציה מסווג זה מניבה באופן לא מפתיע גיאומטריה שרירותית לחלוותן של פיזור מרחבו של עורקי התקשרות. בתזה זו אנו עוסקים בשתי שאלות מרכזיות אשר עלות כהוזאה מהטופולוגיה השרירותית אשר מתארת את פיזור העורקים. השאלה הראשונה היא שאלת הcisio. אנו עונבים על השאלה האם הדרישות להבטחת cisio אשר אפשר זיהוי ענן. ע"י הפעלת הגישה שלנו לפתרון בעיית הcisio אנו מסוגלים ליתר מפות cisio אשר מציגות את cisio המדויק של ארווי הגוף בישראל, תוך שימוש בשיטה החדשת המוצעת לניטור גשם.

השאלת השנייה אשר עליה ברצוננו לענות היא שאלת יכולת השחזר. אם ברצוננו לשחזר מפות גשם מדגימות של עורקי התקשרות, علينا בראש ובראשונה לענות על השאלה "האם פיזור נתון ניתן לשחזר מפה עצומות עורקי התקשרות, עלינו בראש ובראשונה לענות על השאלה "האם פיזור נתון ניתן לשחזר מפה גשם בצורה נcona?". בעובדה זו אנו פותרים את השאלה הנוגעת ליכולת לשחזר פונקציה דו ממדית, כדוגמת תמונה, אשר נדגמה ע"י היטלים קווים. ואמרנו היטלים קווים אנו מתקונים למקומות ערכי הפונקציה לאורכו של הקו. אנו לא מטילים כל אילוץ על הגיאומטריה של הקווים. הקווים יכולים להיות שונים זה מזה בזוויתם, אורכם ואף במרקם זה מזה.

תרומתנו היא פרוצדורה אשר קובעת האם סט נתון של עורקים מניב פונקציה אשר ניתן לשחזר אותה, ואם אכן ניתן, מהי התדריות המksamילית אשר ניתנת לשחזר ללא שגיאות. אנו מישמים את פתרונותינו לביעית הcisio ויכולת השחזר על עורקים של ספקית הסלולר הישראלית סלקום.

תודות 9

בראש ובראשונה אני רוצה להביע את תודתי **לפרופ' הגית מסר**. אני מאמין שהגית מצאה את הנקודה הסינגולרית היחידה המרכיבה את האיזון האופטימלי בין ההנחייה למטען חופש אקדמי. תפקודה הן כרועת צאן, אשר ידעהמתי להרחק אותך מכיווני מבוי סתום וכוקטור תמייה שהראה לי רק את הכוון הכללי ואפשר לי ללכת בדרך שלי תוך ביצוע טעויות שהכרחי שאעשה.

ברצוני להודות לחברים שלי מקבוצת המחקר של אוניברסיטת תל אביב על צבר רב של דיונים פוריים והצעות מרענןות. אני מודה לא הכר ליאוב ליברמן, דני צ'רקסקי, נעם דוד, עוז הראל, אלעד היימן, אורית אוסלנדר וyonatan austromacki. תודה שסבירתם בסובלנות את הרצאות האינסופיות שלי על תלאות המחקר שלי.

תודה מיוחדת **לארטיום זינביז'** שמשך אותו לכיוון שאלת המחקר שלי, שדה בין-תחומי המזאג היטב בין ניטור סביבתי ומתמטיקה שימושית.

לבסוף, אני רוצה להודות לחזי השני שלי, צפי, על היכולת הבלתי נלאית שלה לדחוף אותך לכיוון בו אגשים את החלומות שלי, הסובלנות שלה להשלים עם השעות האינסופיות בהן ישבי מול המחשב עם פח אשפה מלא בדף טויטה מקומטיהם.

צפי, תודה על היכולת לסבול את מה שהעכברי אותך, לקידוש המטרות שלי ובוקר על כך שפשות הייתה את.



הפקולטה להנדסה ע"ש איבי ואלדר פליישמן
בית הספר לתארים متקדמיים ע"ש זנדמן סליינר

**על יכולת הכספי והשחזר של פונקציות דו ממדיות
אשר נדגמו לאורך קוויים בעלי גיאומטריה שרירותית
עם יישום ליפוי שדות גשם**

חיבור זה הוגש כעבודה גמר לקראת התואר "מוסמך אוניברסיטה" בהנדסת חשמל ואלקטרוניקה

על ידי

עמרי סנדיין

העבודה נעשתה במחלקה להנדסת החשמל, מערכות
בנהניתה של פרופ' חגי מסר ירון

יולי, 2013



**על יכולת הכספי והשחזר של פונקציות דו ממדיות
אשר נדגמו לאורך קווים בעלי גיאומטריה שרירותית
עם יישום למשמעות גשם**

היבור זה הוגש כעבודת גמר לקראת התואר "מוסמך אוניברסיטה" בהנדסת חשמל ואלקטرونיקה

על ידי

עמרי סנדיין

יולי, 2013